Revealing the Molecular Mechanism of Atg11 and the Initiation of Selective Autophagy

Dissertation der Fakultät für Biologie
der Ludwig-Maximilians-Universität München

Nena Magdalena Matscheko

München, 2016

Diese Dissertation wurde angefertigt
unter der Leitung von Dr. Thomas Wollert
am Max Planck Institut für Biochemie

Erstgutachter: Prof. Dr. Stefan Jentsch
Zweitgutachter: Prof. Dr. Serena Schwenkert

Tag der Abgabe: 25.05.2016

Tag der mündlichen Prüfung: 21.10.2016

ERKLÄRUNG

Hiermit versichere ich an Eides statt, dass meine Dissertation selbständig und ohne unerlaubte Hilfsmittel angefertigt worden ist.
Die vorliegende Dissertation wurde weder ganz, noch teilweise, bei einer anderen Prüfungskommission vorgelegt.
Ich habe noch zu keinem früheren Zeitpunkt versucht, eine Dissertation einzureichen oder an einer Doktorprüfung teilzunehmen.

München, den 25.05.2016

Content

Summary

Cellular homeostasis and health requires the breakdown of surplus or damaged components by either the ubiquitin-proteasome system or by the lysosome. Transport of cytoplasmic material to the lysosome involves formation of a double-walled vesicle around the cargo at the phagophore assembly site (PAS) and its delivery to the lysosome, a pathway termed autophagy which is conserved from yeast to mammalian cells. Autophagy was long thought to only occur non-selectively during stress conditions; however, accumulating evidence shows that cargo is also chosen specifically and transported to the lysosome/vacuole via selective autophagy. Principally, the same autophagy-related (Atg) proteins contribute to autophagosome formation in both forms, including the initiator Atg1 kinase complex, and Atg9 for the delivery of membrane. However, selective autophagy requires specific cargo receptors and the scaffold protein Atg11 in addition to the core machinery. The present study explored the molecular function of Atg11 in yeast.

Initially, an in vitro approach was chosen for studying Atg11 function and interaction with core autophagy components. To this point, recombinant expression and purification of full length Atg11 was established. Purified Atg11 was employed firstly for excluding a proposed actin motor function of Atg11. Secondly, selective autophagy was reconstituted in vitro with recombinantly expressed cargo receptors and artificial membranes. Atg11 was found to be dispensable as adaptor for the interaction of Atg8-decorated membranes and the mitochondrial cargo receptor Atg32. Thirdly, a functional redundancy with the Atg1 kinase complex scaffold Atg17 suggested a role in initiation of selective autophagy. The function of Atg17 is to tether Atg9-vesicles at the PAS in non-selective autophagy. Here, in vivo studies showed that Atg11 and Atg17 are essential for selective and non-selective autophagy, respectively. Atg11 was found to interact with Atg9 and with Atg1 via Atg13 in vitro. The N-terminus of Atg11 harbors an Atg17-like domain and is sufficient for tethering of Atg9-proteoliposomes. The C-terminus of Atg11 inhibits the tethering activity of full length Atg11; however, interaction with the cargo receptor Atg32 restores tethering in vitro. Moreover, overexpression of Atg32 induces selective autophagy in vivo at the expense of reduced non-selective autophagy.

In summary, cargo-activated Atg11 was found to tether Atg9-proteoliposomes in vitro and initiate selective autophagy in vivo. Competition between Atg11 and Atg17 for Atg9 and controlled activation of their tethering activity allows regulation between selective and non-selective autophagy.

1 Introduction

Cellular homeostasis is crucial for the health of each individual cell and consequently for the health of a whole organism. A balance needs to be maintained between building up new components and degrading them if they become superfluous or damaged. Clearance of cellular components generally occurs via three distinct pathways: 1. ubiquitin-proteasome system (UPS) which targets endogenous proteins, marks them with ubiquitin and breaks them down after unfolding in the proteasome; 2. endocytosis-mediated degradation of extracellular cargo or plasma membrane proteins taken up by endocytic membrane vesicles; 3. lysosome-dependent degradation of intracellular components. Transport of cytoplasmic cargo to the lysosome requires its encapsulation in a membrane vesicle, a pathway termed autophagy (from greek auto = self and phagein = eating). Not only intracellular waste, including aggregated proteins or dysfunctional organelles, has to be cleared by autophagy. Also random cytosolic components are turned over in response to cytotoxic stress or starvation.

1.1 Membrane trafficking and GTPases

The budding of membrane from the donor compartment, the transport along the cytoskeleton, the targeting to the correct acceptor compartment and the final fusion with the destination membrane have to be tightly controlled. Master regulators of these processes are a family of proteins, the small GTPases. They are guanine nucleotide-dependent molecular switches, which change their activity depending on the association with either GTP or GDP. By recruiting diverse downstream effectors they are able to regulate numerous intracellular signaling pathways, including membrane trafficking.

GDP-bound GTPases are cytosolic and considered as inactive (reviewed in (Stenmark, 2009)). Only some rare exceptions fulfill an active role in the GDP-bound form. Association with a guanine nucleotide exchange factor (GEF) induces the release of the GDP and the recruitment of a GTP instead, generally activating the protein. The GTP-bound form is membrane-associated, where it recruits further effector proteins. Once the function is fulfilled, a GTPase-activator protein (GAP) accelerates the GTP hydrolysis by the GTPase subunit. Induction of a conformational shift of the GTPase results in the dissociation from the membrane. In summary, GEFs and GAPs are switching the cyclic activity of their GTPases on and off, respectively.

Different sub-families of GTPases regulate key steps of membrane trafficking. Assembly of coat proteins (COPI and COPII) on budding vesicles is mediated by Arf and Sar GTPases. However, the most abundant sub-family contains Rab/Ypt GTPases. Interaction with different effector proteins allows a small number of GTPases to regulate

cellular processes at many different levels. They promote vesicle scission by recruiting dynamins. Also vesicle uncoating has been shown to be mediated by Rabs. Transport of cargo vesicles along cytoskeletal tracks requires the interaction with motor proteins. Rabs have been found to recruit actin motors of the Myosin V family. Upon arrival at the destination, Rabs regulate tethering of the vesicle to the acceptor membrane, before they induce fusion by soluble N-ethylmaleimide-sensitive fusion attachment protein receptors (SNAREs) (Stenmark, 2009).

Membrane tethers are either a multi-subunit complex or a long coiled-coil protein. They are effectors of GTPases and regulated by them. Membrane tethers provide specificity to ensure delivery of vesicles to their correct destination compartment and promote SNARE -mediated fusion. Coiled-coil proteins acting as tethers are anchored to acceptor membranes via their C terminal domain. They can either interact with membrane-bound GTPases or insert a proprietary transmembrane domain directly into the membrane (Brocker et al., 2010). Their N terminal coiled-coil domains extend up to 200 nm from the membrane into the cytoplasm, facilitating the bridging between donor and acceptor membranes.

Membrane tethers can only juxtaposition vesicles. The actual fusion is catalyzed by SNARE proteins. Traditionally, SNAREs were grouped into vesicular (v-) and target (t-) SNAREs. A more recent classification uses structural properties to group SNAREs into Q- and R-SNAREs, depending on the respective amino acid they are contributing to the interaction interface. They are membrane-anchored with their C-terminus. Their structural hallmark is the subsequent highly conserved coiled-coil domain. During membrane fusion SNAREs anchored to opposite membranes form tight four-helix-bundles. The coiled-coils zip up the interaction interface and thereby move membranes into immediate contact until they can merge (Chen and Scheller, 2001). Different sets of SNAREs control the targeted fusion of membranes with their destination membrane, adding more specificity to the regulation by GTPases.

1.2 Autophagy

Autophagy is a transport pathway, which delivers cellular components to the lysosome (vacuole in yeast) for degradation. Three distinct forms of autophagy can be differentiated:

1. Chaperone-mediated autophagy (CMA) (reviewed in (Cuervo and Wong, 2014): Soluble proteins are captured by the cytosolic chaperone hsc70 and its co-chaperones and delivered to LAMP-2A, a transmembrane receptor and channel in the vacuolar

membrane. They are passed to the vacuolar lumen with the help of the luminal chaperone Lys-hsc70, where they are degraded. This form of autophagy is independent of vesicular transport and only able to degrade soluble proteins, comparable to the UPS.

2. Microautophagy (reviewed in (Li et al., 2012): Invaginations of the vacuolar membrane trap cytosolic material and pinch off into the vacuolar lumen, where they are degraded. Microautophagy is believed to maintain vacuolar size by delivering the limiting membrane to the lumen for degradation. It supports cell survival during nutrient starvation. Selective forms described so far include microautophagy of mitochondria, peroxisomes and the nucleus. The respective organelle needs to be in close proximity of the vacuole and is partly degraded after organelle fragmentation.

3. Macroautophagy: The focus of this investigation; from now on referred to as autophagy. Transport of cytoplasmic material destined for degradation in the vacuole occurs by encapsulation of this cargo in a double bilayer membrane. The initial cup-shaped membrane is called phagophore. It extends to engulf the cytoplasmic cargo completely. Sealing of the structure generates the double-membrane surrounded autophagosome. Though autophagy was originally believed to only recycle cytoplasmic material randomly (bulk / non-selective autophagy), it has now become clear that many different cargos are selectively targeted by the cell and physically linked to the autophagosomal membrane (selective autophagy). The source of the phagophore membrane, the process of phagophore formation and extension, up to fusion of the completed autophagosome with the lysosome, are still poorly understood. The tightly controlled multi-step pathway is orchestrated by the interaction of numerous proteins, termed Atg for AuTophaGy related, whose functions will be described in the following chapters.

1.3   The life cycle of an autophagosome

1.3.1   Initiation

Bulk autophagy recycles cytoplasm in response to a limited nutrient supply. Amino acid starvation leads to deactivation of the autophagy inhibitor Target of rapamycin (TOR) complex 1 (reviewed in (Loewith and Hall, 2011). The complex consists of Kog1, Lst8, Tco89, and either TOR1 or TOR2. TOR complex 2 shares some structural features but appears to be insensitive to changes in nutrient level, therefore the autophagy relevant complex is TOR complex 1. The first steps of autophagy include the TORC1-regulated recruitment of initiator-complexes to the site of autophagosome biogenesis, the phagophore assembly site (PAS).

1.3.1.1 Atg1 complex: regulating initiation

This complex of five proteins is regarded as initiator of phagophore assembly upon autophagy induction. The eponym of the complex is the kinase Atg1, which forms a subcomplex with Atg13. In addition, Atg17, Atg29 and Atg31 are components of the complex under starvation conditions (Nakatogawa et al., 2009). Also Atg11 has been found to interact with Atg1, as evidenced by yeast-2-hybrid (Y2H) studies (Kamada et al., 2000) and co-immunoprecipitation (co-IP) (Kim et al., 2001).

In normal conditions, yeast TOR kinase is hyperphosphorylating Atg13, thereby blocking its interaction with Atg1 (see Figure 1 a). In case of starvation conditions, limited amino acids are sensed by TOR, which is inactivated as a result. This inactivation leads to an association of dephosphorylated Atg13 with Atg1, and recruitment of the trimeric complex Atg17, Atg29 and Atg31 (see Figure 1 b). The crystal structure of the trimeric complex of *Lachancea thermotolerans* (Ragusa et al., 2012) revealed that the coiled-coil protein Atg17 forms highly elongated tail-to-tail dimers which adapt an S-shaped conformation. The binding site for Atg13 was identified in the N-terminus of Atg17 including cysteine 24, mediating the recruitment of the Atg1/Atg13 subcomplex (Kabeya et al., 2005). The C-terminal α-helix of Atg31 is interacting with the inner crescent of Atg17. Atg31 is constitutively bound by the N-terminus of Atg29. The C-terminus of Atg29 is largely unstructured and heavily phosphorylated in starvation conditions, whereas vegetative conditions result in no or only little phosphorylation (Mao et al., 2013a).

Being the scaffold for Atg1 kinase complex assembly, deletion of Atg17 should fully abrogate autophagy. However, though a strong reduction was indeed observed, Kabeya et al. observed small autophagosomes with half the size of a normal autophagosome, comparable to vesicles detected during vegetative growth of yeast cells (Baba et al., 1997). Apparently, Atg17 activity can be substituted to some extent by a homolog. Functional studies found that single deletions of Atg17 and Atg11 both reduce maturation of autophagic membrane, while the double knock out is entirely deficient in autophagy (Suzuki et al., 2007). A detailed investigation of a possible functional homology of the structurally rather unrelated scaffolding proteins Atg17 and Atg11 has been lacking up to date.

The fully assembled dimeric pentameric complex is believed to act as a membrane tether of small lipid vesicles (Ragusa et al., 2012; Rao et al., 2016), which are then fused with the help of SNAREs to form the phagophore. Also a regulating GTPase has been suggested: Ypt1 interacts with both Atg17 and Atg1, its homolog Rab1 was found to co-precipitate with Ulk1 (mammalian homolog of Atg1) (Wang et al., 2013).

Upon induction of autophagy 20-40 copies of Atg1 and Atg13 each, and 28 copies of

Atg17 assemble at the PAS. The copy numbers of all subunits remain rather constant in both vegetative and autophagy inducing conditions, however, the number of PAS puncta increases upon induction (Kofinger et al., 2015). Since the copy number remains constant upon induction, the authors conclude that the Atg1 kinase complex nucleates the PAS as a consistent, regular scaffolding structure. Suzuki et al. aimed at localizing GFP-tagged Atg- proteins on the autophagosomal membrane by inducing the formation of large cup-shaped phagophores at giant cargo (Suzuki et al., 2013). Both Atg17 and Atg13 formed single puncta at the tip of the phagophore, adjacent to the vacuole. In contrast, Atg1 localized along the entire cup-shaped membrane. Though this seems to contradict the formation of one initiation complex, it might represent a later step of autophagy, in which Atg1 acts independent of the scaffolding complex. This is supported by functional PAS localization and Atg17 interaction of Atg1 mutants which lack the ability to interact with the autophagosomal membrane (Nakatogawa et al., 2012).
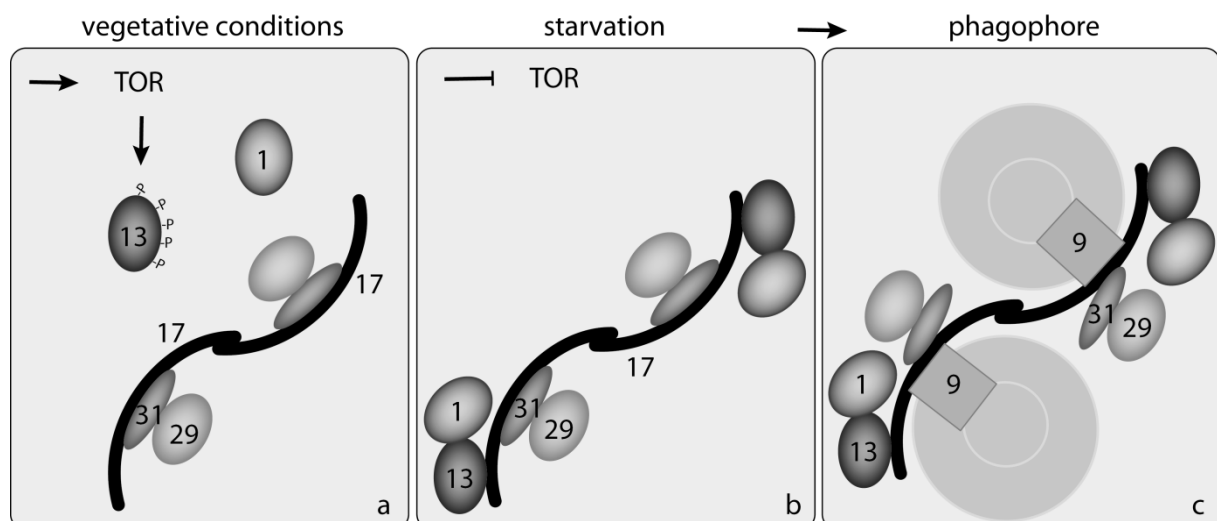
Figure 1 - Initiation of autophagy upon nutrient starvation. In vegetative conditions the active TOR kinase hyperphosphorylates Atg13, thereby blocking its interaction with Atg1 and the dimer of Atg17-29-31 (a). During nutrient starvation TOR is inhibited, allowing dephosphorylation of Atg13 and assembly of the dimeric pentameric complex (b). Atg17 directly recruits Atg9 positive membrane vesicles (c).

1.3.1.2 Atg9: membrane delivery and fusion

Especially at the stage of initiation, when no precursor membrane is existing yet, lipid vesicles destined for the PAS require an intrinsic marker for correct targeting within the cell. The marker is trafficked within membrane donor vesicles from the Golgi to the PAS and has to be recycled by retrograde transport after delivery of the membrane (Yamamoto et al., 2012). This marker has been identified as Atg9, a 115 kD protein possessing six transmembrane domains, which anchor it in 30 - 60 nm diameter lipid vesicles (Mari et al., 2010). Electron microscopy revealed that a single cell

overexpressing Atg9 harbors 2-3 cytoplasmic pools of Atg9 positive vesicles close to mitochondria. Upon induction of autophagy each pool can translocate en bloc to the PAS (Mari et al., 2010). However, in wildtype conditions 3 vesicles are sufficient to initiate the autophagosomal membrane (Yamamoto et al., 2012). The unstructured N- and C-terminal domains are facing the cytoplasm (He et al., 2006). The C-terminus is required for correct sorting of Atg9 through the Golgi to small cytoplasmic vesicles by interaction with Atg23 and another transmembrane protein, Atg27 (Yamamoto et al., 2012). The N-terminus is believed to be involved in regulation and protein-protein interactions. For example, a single point mutation in the N-terminus (histidine 192) has been shown to disrupt the interaction of Atg9 with Atg11 using co-IP and Y2H. This disruption results in dysfunction of selective forms of autophagy (He et al., 2006).

Recruitment of initial Atg9 vesicles depends on the interaction of Atg9 with the above described Atg1 kinase complex, which is scaffolding the PAS. Atg17 has been found to function as autophagy-specific membrane tethering complex, which recruits and tethers Atg9-vesicles at the PAS (see Figure 1 c). This interaction requires Atg1, though not the kinase activity (Sekito et al., 2009). However, Atg9 is phosphorylated by Atg1 in a subsequent step, necessary for further downstream events (Papinski et al., 2014).

After tethering of Atg9 vesicles, they need to fuse to form the initial phagophore. Since the deletion of Q-SNAREs Sso1 and Sso2 results in an accumulation of Atg9-positive vesicles (Nair et al., 2011), it can be assumed that these SNAREs are required for initiation of autopahgy. Also the Q-SNAREs Sec9 and Tlg2 and the R-SNAREs Sec22 and Ykt6 were found to be involved in the trafficking of Atg9, and therefore seem to be play a role in autophagy. However, since the disruption of general cellular trafficking has a strong effect on autophagosomal membrane trafficking as well, the precise function of SNAREs in autophagy remains to be elucidated.

1.3.2 Expansion

Once the first small vesicles are fused at the PAS to form a phagophore, this cup-shaped membrane needs to be extended until a full vesicle is formed. It is rather likely that a large membrane pool like the ER is at least involved in autophagosomal membrane extension. Strong evidence for the membrane source has been presented for the ER-to-Golgi-intermediate-compartment (ERGIC), which was found in an *in vitro* assay with mammalian cells to promote recruitment and processing of autophagic proteins (Ge et al., 2013). A similar membrane source has been suggested in yeast. Vesicles trafficking from the ER to the Golgi bud off the ER at the ER exit sites (ERES) and are covered with coat protein (COP) II. COPII consists of 5 subunits, including Sec23. Recently, Sec23 was found to interact with Trs85 of the Transport-Protein Particle III (TRAPPIII) multi-subunit tethering complex (Tan et al., 2013). TRAPPIII is recruited to the PAS by Atg17.

Additionally, it functions as a GEF of the small GTPase Ypt1, which is in turn recruiting Atg1 to the PAS (Wang et al., 2013).

Trs85 has also been shown to directly interact with Atg9, independent of Atg17 and Atg11 (Kakuta et al., 2012). Continued recruitment of Atg9 allows the regulation of downstream events during extension of the phagophore. Atg9 becomes phosphorylated at the PAS by Atg1. Phosphorylated Atg9 is able to efficiently recruit the downstream factors Atg8 and Atg18 to the phagophore (Papinski et al., 2014) to promote further membrane extension. Phospho-mimicking serine-to-aspartate mutations in Atg9 were not able to constitutively switch autophagy on, indicating the requirement of regulated dephosphorylation. Proper Atg9 function depends on consecutive cycles of Atg1-dependent phosphorylation followed by dephosphorylation (Papinski et al., 2014).

COPII vesicles use the SNAREs Bet1, Bos1, Sed5, and Sec22 for fusion with the Golgi. Knockouts of these proteins resulted in a block of autophagic flux (Tan et al., 2013), though it is unclear at this point if this is due to general disruption of cellular membrane trafficking or if these SNAREs are specifically required for autophagosomal membrane extension.

1.3.2.1 *Phosphatidylinositol-3 kinase complex I*

The Atg1 kinase complex is able to interact with Atg14, the autophagy-specific subunit of phosphatidylinositol (PI) 3-kinase complex I (Obara et al., 2006), whose expression is more than 20 fold induced upon autophagy induction (Chan et al., 2001). This protein coordinates several downstream events. In early stages it is part of the complex that is phosphorylating lipids in the phagophore for signaling. Recently, it has been shown to interact with SNARE Stx17 in the last stages of autophagy (Diao et al., 2015). Atg14 interacts with Vacuolar Protein Sorting (Vps) 30 (also known as Atg6) and Vps34, a PI3-kinase which is regulated by Vps15, another component of the complex. Upon activation, Vps34 phosphorylates the lipid PI to synthesize PI-3-phosphate (PI3P) in the autophagosomal membrane. This signaling lipid is required to recruit the two PROPPIN homologs Atg18 and Atg21 to the membrane. Both contain a seven-bladed β-propeller made up of WD40-repeats and use them for interaction with PI3P and PI3,5P_2 (Dove et al., 2004). Atg21 is believed to be essential in selective forms of autophagy (see chapter 1.4 Selective autophagy), whereas Atg18 belongs to the autophagic core machinery and is required for all types of autophagy (Stromhaug et al., 2004). Atg18 cooperates with Atg2, to ensure proper cycling of Atg9 (Reggiori et al., 2004). The mammalian ortholog of Atg18, WIPI2, has been shown to facilitate conjugation of mammalian protein LC3 to the autophagic membrane (Polson et al., 2010), a crucial step during expansion and maturation of the phagophore.

1.3.2.2 Atg8 and its lipidation pathway

Atg8 is a 13.6 kD ubiquitin-like protein with the unique feature of becoming conjugated to membranes. Increased amounts of lipidated Atg8 are observed in autophagy inducing conditions (Suzuki et al., 2007). The size of autophagosomes correlates with Atg8 expression levels, indicating that Atg8 directly regulates autophagosome expansion (Xie et al., 2008). Atg8 localizes to both the inner and the outer autophagosomal membrane (Kirisako et al., 1999). Atg8 bound to the inner membrane acts as a cargo adaptor in selective forms of autophagy (Shintani et al., 2002). It is transported to the vacuole and degraded with the autophagosomal cargo (Huang et al., 2000).

Atg8 is translated as an inactive 117 amino acid long protein. Its covalent attachment to the membrane is, like ubiquitin attachment to proteins, a step-wise process executed by sequential enzymatic reactions (reviewed in (Nakatogawa et al., 2009). Cleavage of the C-terminal arginine by the cysteine-protease Atg4 makes Atg8 available for membrane conjugation by exposing a C-terminal glycine. This glycine is captured in an ATP-consuming step by a cysteine of the E1-like enzyme Atg7. Next, Atg8 is transferred to the E2-like enzyme Atg3, which then passes the protein on to the headgroup of the lipid phosphatidylethanolamine (PE). This last step is stimulated and directed by an E3-like enzymatic function of the complex Atg12-Atg5-Atg16. The Atg12-Atg5 conjugate is formed in an ubiquitin-like fashion itself. The process starts with Atg12, whose C-terminal glycine is also linked to the active cysteine of Atg7 in an ATP-consuming step. Atg12 is then transferred to another E2-like enzyme, Atg10, and eventually to a lysine of Atg5. Two copies of the Atg12-Atg5 conjugate are further dimerized by a homodimer of Atg16. The covalent bond between the lipid PE and the protein Atg8 is cleaved by Atg4, which releases Atg8 from the outer membrane during late stages of autophagy (Kirisako et al., 2000).

1.3.2.3 Atg8-interacting motifs (AIMs)

The autophagosomal membrane decorated with Atg8 serves as a platform for multiple protein interactions. Taking the small size of Atg8 into account, it is obvious that the interacting proteins can only choose from a limited number of interaction sites. Therefore a conserved Atg8-interacting motif has evolved in a number of proteins. Sequence alignments allowed the identification of the canonical consensus-sequence [W/F/Y]xx[L/I/V], with WxxL being the most common motif in yeast. A similar consensus sequence has been identified for the human ortholog of Atg8, LC3, and termed LC3-interacting region (LIR) (Noda et al., 2010). Nonetheless, also non-canonical interactions with Atg8 have been described, for example when two interactions need to take place at the same time during Atg8 lipidation. The E1-like enzyme Atg7 is binding Atg8 with a non-canonical sequence and passing it on to Atg3 (Noda et al., 2011). Atg3 is

establishing both a thioester bond with Atg8 and occupying the canonical AIM WEDL, an interaction that is essential for the final step of transferring Atg8 to PE (Yamaguchi et al., 2010).

1.3.2.4 Flexible coat structure

Autophagosomes were found to reach variable sizes of up to 900 nm in diameter (Baba et al., 1997). Although Atg8 was identified to play a major role in the determination of autophagosome expansion since its amount is linked to the vesicle size (Xie et al., 2008), the mechanism of this process remained unclear for a very long time. By analyzing the mobility of the Atg8 lipidation machinery it became clear that not only Atg8 but also Atg12-Atg5-Atg16 remain on the outer membrane surface, building a proteinaceous coat around the growing autophagosome (Kaufmann et al., 2014). The coat is an interactive scaffold, which provides stability for the growing autophagosome. It can be disassembled by the interaction of Atg8 with competitively binding proteins, such as Atg32. The releasing action of the cysteine protease Atg4 is able to shed Atg8 and therefore the whole coat from the membrane.

1.3.3 Sealing and fusion with vacuole

In a final step the autophagosome needs to be closed up and fused with the vacuole to deliver the inner membrane sac and the cargo for degradation.

1.3.3.1 Sealing and protein recovery

The mechanism of sealing is largely unknown, but might involve Atg8, which mediates membrane tethering and hemifusion in an *in vitro* system (Nakatogawa et al., 2007). Additional evidence for the importance of Atg8 during maturation was found in mammalian cells. Deletion of Atg3 in mice or sequestration of Atg8 by mutant Atg4 in mammalian cells both result in an accumulation of abnormal, non-sealed autophagosomes. This indicates that elongation progresses instead of sealing the autophagosome if Atg8 is not correctly targeted to the membrane (Sou et al., 2008). At least in higher eukaryotes the last sealing step might also require SNARE activity. Depletion of Syntaxin 13 (Stx13) in mammalian cells increased the levels of LC3-II and multilamellar structures, indicating an accumulation of immature autophagosomes (Lu et al., 2013). Further studies are required to confirm that these structures are unsealed autophagosomes.

Once the sealing is completed, though it is still unknown how the cell is able to sense this completion, remaining Atg proteins are released from the surface of the autophagosome. The signaling lipid PI3P is turned over by its phosphatase Ymr1 and to some degree Sjl3 (Cebollero et al., 2012), a prerequisite for the release of interacting Atg proteins and the fusion with the vacuole. Importantly, Atg4 cleaves Atg8 off the outer

membrane. Only Atg8 anchored to the inner membrane is transported to the vacuole and degraded with the cargo (Kirisako et al., 1999).

1.3.3.2 Autophagosomal transport

Transport of matured autophagosomes was mostly studied in mammalian cells. In yeast, transportation events are limited, since the PAS is generally located in close proximity to the vacuole. In primary neurons sealed autophagosomes are moved during maturation, like endosomes, bidirectionally along microtubules in the axon with dynein and kinesin motors, ending up acidified in the cell soma (Maday et al., 2012).

In contrast to mammalian cells, disruption of yeast microtubules with the chemical nocodazole does not affect bulk autophagy in yeast (Kirisako et al., 1999). However, correct targeting of yeast components of the autophagic machinery, most importantly Atg9 vesicles and cargo, depend on an intact actin network. Interestingly, Atg9 only requires the intact actin network for selective forms of autophagy, but not rapamycin induced bulk autophagy (Reggiori et al., 2005). The actin-binding Arp2/3 protein complex interacts with Atg9 and is essential for selective forms of autophagy (Monastyrska et al., 2008). However, it remains unclear if Arp2/3 is directly involved in autophagy or assists upstream in the generation of Atg9 vesicles. Atg11, an interaction partner of Atg9, might be involved in the interaction of Arp2/3 with Atg9, since this interaction was abrogated by a deletion of Atg11. Also, Atg11 failed to be targeted to the PAS in yeast with non-depolymerizing *act1-159* actin, but localized to mitochondrial puncta instead. Subsequently, it recruited Atg9 to its misdirected location instead of the PAS (He et al., 2006). Reversely, deletion of Atg9 did not affect Atg11 distribution, leading to the conclusion that Atg11 is an upstream Atg9 recruiting factor. Atg11 has even been suggested to act as motor protein due to the structural similarity of Atg11 and yeast myosin class V protein Myo2 (Monastyrska et al., 2006) (see 1.4.4.1 Atg11 structure). However, due to the lack of a motor domain, Atg11 would not be able to move vesicles along actin filaments by itself. Therefore a model is favored in which Atg11 interacts with filament nucleating Arp2/3. After recruitment of cargo and Atg9 vesicles newly polymerizing actin would transport the whole complex into the direction of the PAS (Monastyrska et al., 2009).

1.3.3.3 Fusion with the vacuole

As any membrane fusion event, the fusion of the outer membrane of the completed autophagosome with the vacuolar membrane likely involves SNAREs, regulated by Rab/Ypt GTPases and a tethering complex. A mechanism similar to homotypic vacuole – vacuole fusion is also suggested for autophagosome – vacuole fusion (reviewed in (Noda et al., 2009). So far, the SNARE syntaxin17 (Stx17) has been found on sealed

autophagosomes in mammalian cells at the stage before fusion with the vacuole. Stx17 is recruited to the autophagosome by direct interaction with Atg14 homo-oligomers (Diao et al., 2015). The t-SNARE Stx17, together with SNAP-29 on the autophagosome, is interacting with the v-SNARE VAMP8 on the lysosomal membrane (Itakura et al., 2012). Its activity is regulated by the homotypic fusion and protein sorting (HOPS) tethering complex (Jiang et al., 2014), whose knockdown also affects endocytic pathways. Specificity of the HOPS complex in mammalian cells seems to be provided by one protein, either Stx17 for autophagy or ultraviolet irradiation resistance–associated gene (UVRAG) for endocytosis. Both are dispensable in the alternative pathway.

Only limited data is available at this point about the same process in yeast. Although no v-SNARE has been clearly identified yet in yeast for autophagosome-vacuole fusion, the apparent dependency of autophagy on the yeast HOPS complex (Rieder and Emr, 1997) suggests a rather homologous mechanism. HOPS tethering complex controls fusion through specific interactions with the vacuolar Q-SNARE complex (consisting of Vam3, Vam7, Vti1, and Nyv1) (Kramer and Ungermann, 2011), with at least Vam3 being essential for autophagy (Darsow et al., 1997). Also the SNARE chaperone Sec18 has been identified to be crucial for autophagosome-vacuole fusion (Ishihara et al., 2001).

Ypt7, a GTPase involved in the transport of late autophagosomes, seems to also regulate fusion with the vacuole. Deletion of this protein results in an accumulation of completed autophagosomes, indicating a problem with vacuole fusion (Kirisako et al., 1999). Its mammalian ortholog Rab7 also regulates late steps of the endocytic pathway (Hyttinen et al., 2013), which resembles autophagy in many ways and converges at the point where both vesicles, endocytic and autophagic, fuse with the vacuole. The Ccz1–Mon1 protein complex acts as GEF for Ypt7 in both vacuole-vacuole and autophagosome-vacuole fusion (Wang et al., 2002).

Upon release of the inner autophagic body into the vacuole, resident enzymes digest the cargo for recycling of its subunits.

1.4 Selective autophagy

Autophagy was initially described to transport bulk cytoplasmic material in a non-selective manner, i.e. without regard for the vesicle content. This is especially important during starvation conditions, when the cell needs to quickly turn over cytoplasmic material for survival. However, during normal cellular growth in vegetative conditions it is advantageous for the cell to specifically choose the cargo. Thereby it accelerates degradation of harmful material, ensures targeting of vacuolar enzymes and, at the same time, limits unnecessary disposal of cytoplasmic material. Selective autophagosomes are

the predominant form of autophagosomes in vegetative conditions and are transporting cargo by actively excluding cytoplasm (Sawa-Makarska et al., 2014), whereas non-selective autophagosomes induced by starvation contain large portions of random cytoplasm. This results in morphological differences. Electron microscopy revealed that bulk autophagosomes induced by starvation reach sizes between 300 – 900 nm, whereas selective vesicles in vegetative conditions only reach a size of 140 – 160 nm (Baba et al., 1997). Although both selective and non-selective autophagy share a common set of Atg-proteins, the selection of specific cargo requires additional factors for tethering cargo to the autophagosome.

Depending on the cargo, different selective autophagic pathways have evolved. Important cargos (and their respective selective autophagic pathways) include mitochondria (mitophagy), peroxisomes (pexophagy), ER (ERphagy), nucleus (nucleophagy), aggregated proteins (aggrephagy), Aminopeptidase I (Cvt pathway), lipid droplets (lipophagy), ribosomes (ribophagy) and pathogens (xenophagy) (Reggiori et al., 2012). Two of them are portrayed in the next paragraphs, followed by important characteristics shared by all selective pathways.

1.4.1 Mitophagy

One cargo identified as target of selective autophagy are mitochondria, the process was termed mitophagy (Lemasters, 2005). Mitochondrial homeostasis needs to be tightly controlled. As major source of reactive oxygen species (ROS) within the cell, damaged mitochondria have to be cleared from the cell rapidly. Also a change of environment such as carbon source requires adjustment in the amount of mitochondria. Providing yeast cultures with lactate or glycerol as non-fermentable carbon source results in a strong amplification of mitochondria and mitochondrial proteins, since they solely rely on oxidative phosphorylation at the mitochondrial membrane as energy source. A shift back to standard glucose supplemented media leaves the excessive mitochondria superfluous and they become targeted to the vacuole for degradation. Therefore, mitophagy is important for both mitochondrial quality and quantity control (reviewed in (Wei et al., 2015).

Mitophagy in yeast depends on the receptor protein Atg32 (Okamoto et al., 2009), a 59 kD transmembrane protein anchored in the outer mitochondrial membrane. A short C-terminus is localized in the mitochondrial periplasm and therefore probably not serving any function. The large N-terminal domain is facing the cytosol. Atg32 contains the canonical AIM W_{86}QAI for direct interaction with Atg8. Disruption of this motif by mutation of tryptophane 86 and isoleucine 89 depletes the binding of Atg32 to Atg8 and results in

a partial mitophagy defect (Okamoto et al., 2009). Another consensus sequence found in Atg32 is the $[I_{112}/V]LS$ motif, required for the interaction with Atg11 (Farre et al., 2013). Since Atg32 expression seems rather unregulated and the protein can be found on the surface of mitochondria at all times (Okamoto et al., 2009), another level of regulation is required for induction of mitophagy. Post-translational phosphorylation of serine 114 within the Atg11 binding motif, and to some extent serine 119, seems to be a prerequisite for interaction of Atg32 and Atg11 in vivo (Aoki et al., 2011). The responsible kinase casein kinase 2 (CK2) is specific for mitophagy, since its inhibition specifically blocked mitophagy but not macroautophagy or other forms of selective autophagy, including pexophagy or the Cvt pathway (Kanki et al., 2013). Further regulation by two mitogen-activated protein kinase (MAPK) pathways, Hog1 and Slt2, have been suggested (Mao et al., 2011), but need more detailed investigation.

1.4.2 Cytoplasm-to-vacuole targeting

The cytoplasm-to-vacuole targeting (Cvt) pathway transports hydrolases to the vacuole. The Cvt pathway differs from other selective autophagy pathways in that it is a biosynthetic, and not a degradative, pathway. Initially, it was the hydrolase Aminopeptidase I (ApeI) that was identified as cargo for the Cvt pathway (reviewed in (Umekawa and Klionsky, 2012). ApeI is synthesized and released to the cytoplasm as an inactive 61 kD precursor protein (prApeI), lacking a standard sorting signal. It oligomerizes into large complexes, which are recognized by a receptor, Atg19. Phosphorylation of Atg19 allows recruitment of Atg11 and other components of the autophagic machinery, including Atg8 (Sawa-Makarska et al., 2014), thereby excluding bulk cytoplasm from the approximately 150 nm diameter Cvt vesicle, which is significantly smaller than non-selective autophagosomes (Baba et al., 1997). Upon arrival of the prApeI complex in the vacuole, the N-terminus is processed by proteinase A and proteinase B to yield the fully active 50 kD mature mApeI.

More recently, Cvt vesicles were found to also contain α-mannosidase (Ams1) and the aspartyl aminopeptidase Ape4, rendering the pathway a more general vacuolar targeting mechanism. All three cargos are able to interact with the receptor Atg19 at distinct, non-competitive sites, allowing the formation of super-complexes in vegetative conditions. Moreover, deletion of ApeI results in a decreased transport of Ape4, suggesting that oligomerization of Ape4 depends on ApeI (Yuga et al., 2011). Only Ams1 alone was shown to also utilize another receptor, Atg34, for selective autophagy during starvation conditions (Suzuki et al., 2010).

1.4.3 Homology of cargo receptors

In selective autophagy, cargo needs to be targeted to autophagosomal membranes. For this purpose each cargo possesses a unique cargo receptor protein; however, all receptors need to interact with the autophagosome. Recognition of such diverse receptors is mediated by common interaction motifs. Sequence alignments of different cargo receptors revealed common linear peptide motifs which are recognized by members of the autophagic machinery. Not only the previously characterized AIMs for Atg8 interaction were identified, but also a probable motif for Atg11 interaction (Farre et al., 2013). The consensus sequence [I/V]LS, followed by a high frequency of S, was found in Atg32 and Atg30, the peroxisome receptor in *P. pastoris*. Also the newly discovered nucleophagy receptor, Atg39, is harboring this consensus sequence (Mochida et al., 2015). The interaction of cargo receptors with Atg11 has been suggested to be phospho-regulated. Both the serine 112 of Atg30 and serine 114 of Atg32 become phosphorylated (Aoki et al., 2011) and are located within the Atg11 interaction motif. The receptor molecule of the Cvt pathway, Atg19, is phospho-regulated in a serine-rich region as well (serine 391 being the major phospho-recipient), however, this region differs from the above identified Atg11 interaction motif (Pfaffenwimmer et al., 2014). The responsible kinase for receptor phosphorylation was identified to be Hrr25 in the case of Atg19, Atg36 (pexophagy receptor in *S. cerevisiae*) (Tanaka et al., 2014) and Atg34 (receptor of α-mannosidase Ams1) (Mochida et al., 2014). In contrast, Atg32 is phospho-regulated by the kinase CK2 (Kanki et al., 2013). Whether phosphorylation also regulates recognition of the nucleus or ER by the recently identified receptors Atg39 and Atg40 awaits further analysis (Mochida et al., 2015).

Interestingly, although the AIM and Atg11-interacting motif are spatially separated, binding of one receptor molecule to both Atg8 and Atg11 apparently occurs sequentially rather than simultaneously (Farre et al., 2013). These interactions might serve specific purposes: Whereas Atg11 establishes a transient contact of cargo with selective phagophores, a firm connection between membrane and cargo is mediated through interaction with Atg8, excluding cytoplasm from the thereby not only selective, but also exclusive autophagosome.

1.4.4 Atg11: mediating selective autophagy

Several functions and a large number of interaction partners of Atg11 have been proposed in the past. It is a possible component of the Atg1 kinase complex, a functional homolog of Atg17, an interaction partner of Atg9 and potential motor protein moving Atg9 vesicles and cargo along actin cables, and the common interaction partner of specific cargo receptors. All these findings classify Atg11 as scaffold protein in selective autophagy, which coordinates cargo selection with autophagosome biogenesis.

However, a molecular understanding of the structure and function of this protein remains elusive.

1.4.4.1 Atg11 structure

Atg11 is expressed at a low copy number in yeast, with only 86 copies per cell (Ghaemmaghami et al., 2003). The 135 kDa protein consists of 1178 amino acids, which are predicted to fold into a secondary structure which does not share homology with common protein domains or known protein folds. The only structural characteristic identified by homology domain search are three to four coiled-coil (CC) regions (see Figure 2): CC1 with low confidence, spanning from 272 - 321; CC2 from 536 - 576; CC3 from 689 - 859 with two predicted short breaks in between; CC4 from 991 - 1024 (jpred4 prediction at www.compbio.dundee.ac.uk/jpred4; (Yorimitsu and Klionsky, 2005).
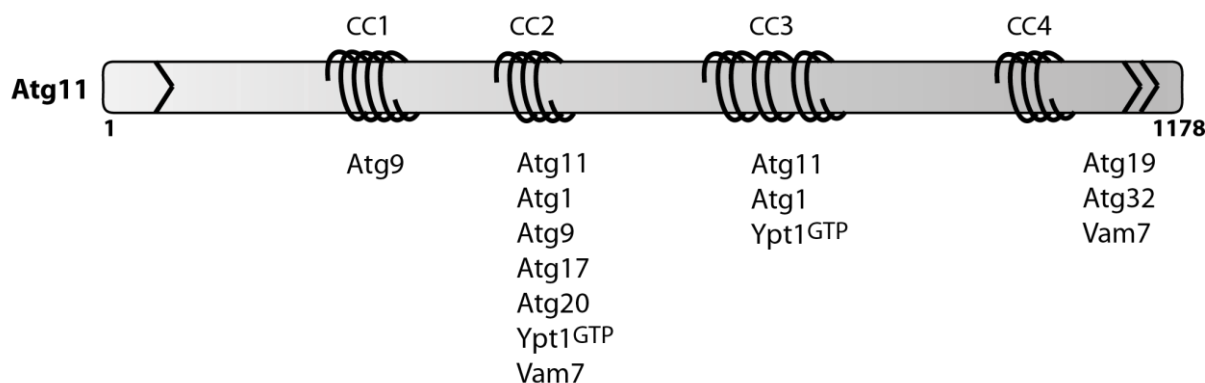
Figure 2 - Scheme of Atg11 structure. Approximate localization of predicted secondary structure is indicated by arrows (β-sheet) and rings (coiled coils). Interaction partners are listed underneath the suggested binding regions.

1.4.4.2 Cellular localization of Atg11

A large yeast protein localization screen in mid-log phase cells in synthetic dextrose medium found Atg11 to be distributed as "punctate composite" (Huh et al., 2003), meaning that it was mostly distributed evenly in the cytoplasm and concentrating to small punctate structures in some cells. As mentioned above, the activity of Atg11 and therefore its localization depends on physiological conditions, including nutrient supply. In vegetative conditions green-fluorescent protein- (GFP-) tagged Atg11 forms one to two perivacuolar puncta (Kim et al., 2001). The peripheral membrane localization can be shifted to mitochondria by inducing mitophagy or disrupting the actin network (Kondo-Okamoto et al., 2012). Some, but not all, Atg11 puncta are colocalizing with Atg8 (Kanki et al., 2009), suggesting that either Atg11 is active at the PAS before Atg8 recruitment, or not all Atg11 puncta represent PAS localization of Atg11. Yeast cells grown in normal vegetative conditions also exhibit Atg11 puncta colocalizing with the Cvt-cargo ApeI and

its receptor protein Atg19 at the PAS. A similar colocalization was found for a C-terminal fragment of Atg11 spanning amino acids 851-1178, indicating that this region is sufficient for cargo interaction (Yorimitsu and Klionsky, 2005).

Deletion of ATG11 results in almost normal levels of bulk autophagy, whereas selective forms of autophagy like the Cvt pathway or pexophagy are essentially knocked out (Kim et al., 2001). Atg19 and its cargo ApeI are still forming a complex without Atg11, but this complex is not localizing to the PAS. Also other components of the autophagic machinery, including Atg1, Atg8 and Atg20, do not localize to the PAS anymore in *atg11Δ* cells growing in vegetative conditions (Yorimitsu and Klionsky, 2005).

1.4.4.3 Atg11 interaction partners

Understanding the position of Atg11 within the intricate network of Atg proteins required for autophagy is important for revealing its molecular function. Most interaction partners of Atg11 have been identified by in vivo methods, including colocalization, Y2H or co-IP (see Figure 2), but have not been verified in vitro.

The earliest study describing the function of Atg11 in selective autophagy suggested homo-oligomerization due to co-immunoprecipitation of myc-tagged Atg11 with HA-tagged Atg11 (Kim et al., 2001). Several regions within Atg11 are required for homo-oligomerization. Y2H assays identified both CC2 and CC3 to be essential. However, these in vivo studies could not rule out the possibility of several Atg11 monomers being involved in one complex bridged by other proteins. Remarkably, CC4, which contains cargo interaction sites, was found to be essential for homo-oligomerization in fluorescence microscopy as well (Yorimitsu and Klionsky, 2005). While an *atg11$^{\Delta CC4}$* strain was not able to form puncta, the complementation with full length Atg11 re-established puncta formation. This implicates the interaction with cargo in the process of homo-oligomerization. The interaction of cargo receptors with Atg11 was investigated by colocalization. Both full length Atg11 and Atg11$^{851-1178}$ were found to colocalize with the cargo ApeI and its receptor Atg19, which suggests that the C-terminal fragment of Atg11 contains a cargo interaction site (Yorimitsu and Klionsky, 2005). A common binding site for cargo receptors in the C-terminus of Atg11 is supported by the finding that also the mitochondrial receptor Atg32 interacts with the same region. Atg32 is localizing to small puncta when degradation of surplus mitochondria is induced. These puncta mostly colocalize with both Atg8 and Atg11 (Kanki et al., 2009). Y2H assays showed that Atg11$^{851-1178}$ is sufficient for interaction with Atg32 (Aoki et al., 2011). This is comparable to the Atg19 binding site, allocating the cargo interaction domain to the C-terminus of Atg11.

The Atg1 kinase complex consists of Atg1, Atg13, Atg17, Atg29 and Atg31 in starvation conditions. Co-immunoprecipitation with Atg1, however, identified Atg11 as component

of the Atg1 kinase complex as well (Kim et al., 2001). The interaction was disrupted in strains missing either Atg11[CC2] or Atg11[CC3] (Yorimitsu and Klionsky, 2005). Further indication that Atg11 is an integral component of the Atg1 kinase complex was provided by the finding that most of the components are interacting with Atg11. Yeast-2-hybrid assays identified close proximity of Atg11 with Atg17 and Atg20, both of which are disrupted when Atg11[CC2] is deleted (Yorimitsu and Klionsky, 2005). However, Atg17 and Atg20 are also interacting with each other independent of Atg11, suggesting that one of them might mediate the interaction of the other one with Atg11. Atg20 has a phox homology (PX) domain for PI3P interaction and is essential for the Cvt pathway (Nice et al., 2002), but its role in autophagy is rather poorly understood. It is noteworthy that there are no data available regarding the colocalization of Atg11 with Atg17. Atg29 was found to interact with Atg11 in a phospho-regulated manner. It forms a constitutive complex with Atg31, which is interacting with and stabilizing its N-terminus. The C-terminus of Atg29 is not or weakly phosphorylated in vegetative conditions and becomes hyper-phosphorylated at up to 23 sites upon autophagy induction. While the wildtype protein co-immunoprecipitated Atg11 in vegetative conditions, the non-phosphorylatable mutant Atg29[23STA] lost this property and was autophagy-deficient (Mao et al., 2013a). Three phosphomimetic mutations (Atg29[3SD]: serine 197, 199, and 201 to aspartate) re-established Atg29 function in bulk autophagy. Direct evidence that Atg11 interacts with Atg29 is still lacking. Atg13, the phospho-regulated interaction partner of Atg1, is recruited to Atg17 in the canonical Atg1 kinase complex via Atg13[424-436] (Fujioka et al., 2014). Colocalization of Atg11 with Atg13 puncta indicated their concurrent presence in the Atg1 kinase complex (Stephan et al., 2009) and Atg13 appears to bridge the interaction between Atg11 and Atg1, since their co-precipitation was severely depleted in *atg13Δ* strains (Kamber et al., 2015). In starvation conditions, the Atg1 kinase complex is closely associated with Atg9. Atg17 becomes activated by Atg13 to tether Atg9 vesicles and thereby initiates non-selective autophagosomes (Rao et al., 2016). However, also early steps in PAS formation of the Cvt pathway depend on the presence of Atg9 (Noda et al., 2000). Atg9 was demonstrated to interact with Atg11 by co-immunoprecipitation and yeast-2-hybrid assays of truncated proteins narrowed down the interaction site to Atg11[CC2] and Atg9[132-255] (He et al., 2006). However, another study found that intact Atg11[CC1] is required as well (Chang and Huang, 2007). The single point mutation Atg9[H192L] disrupted the Cvt pathway by blocking the Atg11 interaction, whereas bulk autophagy could progress normally. Interestingly, overexpression of Atg11 results in increased PAS-localization of Atg9, indicating that besides Atg17, also Atg11 is able to recruit Atg9 for initiation of autophagosomes.

Though the protein interactions described above indicate that Atg11 is a facultative component of the Atg1 kinase complex that becomes essential in selective autophagy, it remains to be investigated for which steps of autophagosome initiation Atg11 is essential. This study focused on revealing the function of Atg11 during initiation of selective autophagy. However, interactions with proteins unrelated to the Atg1 kinase complex indicate further involvement of Atg11 in processes upstream and downstream of PAS initiation. A short summary of these interactions should help to appreciate the manifold functions that allow Atg11 to coordinate earliest steps of selective autophagy like cargo selection, via autophagosome initiation, until fusion with the vacuole.

Atg11 is present at the mitochondrial network prior to mitophagy. Interaction of Atg11 and Dynamin-related1 (Dnm1) coordinates mitochondrial fission with mitophagy (Mao et al., 2013b). Supposedly, Atg11 remains at the mitochondrial fragment after fission and recruits the autophagosomal machinery. Initiation of the phagophore depends on the recruitment and fusion of Atg9-vesicles. Atg11 is involved in the trafficking of Atg9-vesicles, which is regulated by the GTPase Ypt1. Since Ypt1 is also involved in ER-to-Golgi transport, it requires the autophagy-specific GEF TRAPPIII^{Trs85} to mediate autophagy. Incidentally, the subunit Trs85 also interacts with Atg11 (Lipatova et al., 2012). Therefore, GTP-bound Ypt1 might facilitate the interaction between Atg11 and Atg9 for the initial steps in PAS assembly. Upon enclosure of specific cargo by autophagosomal membranes, the cargo receptors are not only in contact with Atg11 anymore, but also bind directly to Atg8. Since Atg8 is coupled to the autophagic membrane from early stages on, it is often fluorescently tagged and then serves as marker of the PAS. In yeast, Atg8 and Atg11 puncta colocalize (Yorimitsu and Klionsky, 2005), suggesting that Atg11 remains as adaptor between cargo and the autophagosomal membrane (Youle and Narendra, 2011). However, the only evidence of Atg11 interacting with Atg8 directly is coming from *A.thaliana* (Li et al., 2014). In late steps of autophagy, the outer membrane of the autophagosome is fusing with the vacuolar membrane in a SNARE-mediated process. Atg11 is involved in the regulation of the fusion by recruiting the vacuolar SNARE Vam7 (Liu et al., 2016). It remains to be investigated how Atg11 is regulated to only fuse sealed autophagosomes to the vacuole and which SNAREs are involved on the autophagosomal side.

1.4.4.4 Atg11 function

Diverse functions have been discussed for Atg11. This might be due to an involvement in different cellular processes, which are all connected to the degradation of specific cargo. Firstly, Atg11 is assisting with fission of organelles and is possibly mediating the transport of cargo and Atg9 vesicles to the PAS via actin. Secondly, it is binding to cargo and is essential for its degradation, suggesting. Thirdly, a possible function as tethering

protein was suggested by (Backues and Klionsky, 2012). On the one hand, Atg11 fulfills the structural requirements of a coiled-coil membrane tether and interacts with the Ypt1-GEF TRAPPIII complex. On the other hand, its connectome strongly associates Atg11 with the Atg1 kinase complex. Interestingly, the Atg1 kinase complex scaffold Atg17 has been suggested to function as membrane tether during non-selective autophagy (Ragusa et al., 2012). Functional homology between Atg17 and Atg11 would assign Atg11 as the membrane tether in selective autophagy.

1.4.5   CUET pathway

In contrast to all other known selective autophagic pathways in yeast, but in good agreement with the diverse pathways in mammalian autophagy, Lu and colleagues recently described Atg11-independent delivery of specific cargo to the autophagosome (Lu et al., 2014). Instead of Atg11, this pathway uses a new class of ubiquitin-binding proteins, so-called CUET proteins, comprising the yeast Cue5 and the mammalian Tollip, to bridge ubiquitin-modified cargo and Atg8. CUET proteins feature an N-terminal Tom1-binding domain (TBD), a phospholipid-binding C2-domain, which also includes two putative AIMs, and they can bind ubiquitin via a non-canonical ubiquitin-binding CUE domain. Aggregated proteins destined for degradation in yeast are marked by the ubiquitin-ligase Rsp5, revealing ubiquitination as new marker for autophagic clearance in yeast. Similar pathways have previously been reported for mammalian cells.

1.5   Autophagy in higher eukaryotes

Higher eukaryotes have evolved a more complex autophagic machinery than *S.cerevisiae* with many isoforms and homologs, required for the adjustment of autophagy to the specific needs of each tissue. Nevertheless, concepts of pathways and regulation are often transferrable from yeast to mammalian cells, rendering yeast a valuable model organism. An understanding of the conservation of autophagy is the basis of a constructive exchange of knowledge from one organism to another. The basic cell biological knowledge eventually leads to the identification of autophagic processes as cause of many human pathologies.

1.5.1   Conservation of autophagy from yeast to plants and mammals

Mammalian cells have evolved homologs of most yeast Atg proteins, in some cases one yeast Atg has several homologs in higher eukaryotes. Homologs identified to date are listed in Table 1.

Table 1 - Homolog yeast and mammalian autophagy proteins.

yeast	mammalian
Atg1	ULK1
Atg13	ATG13
Atg17, Atg29, Atg31	FIP200?
Atg11	?
Vps34, Vps 15	VPS34, VPS15
Atg14	ATG14
Atg6	Beclin1
Atg2	ATG2
Atg18	WIPI2
Atg3	ATG3
Atg7	ATG7
Atg10	ATG10
Atg12, Atg5	ATG12, ATG5
Atg16	ATG16L1
Atg4	ATG4A-D
Atg8	LC3A,B,C;GABARAP,GATE16
Atg9	ATG9

Question marks indicate proteins under discussion (see text). Modified from (Stanley et al., 2014).

Whereas one Atg8 protein appears to exert diverse functions in yeast, mammalian cells harbor 2 subfamilies of Atg8 homologs, each with several members (reviewed in (Shpilka et al., 2011): the first includes members of microtubule-associated protein 1A/1B light chain 3 (LC3A, B, C); the second includes $GABA_A$ receptor-associated proteins, (GABARAP, GABARAPL1) and Golgi-associated ATPase enhancer of 16 kDa (GATE16). Their activation and membrane-conjugation functions similarly to the process described in yeast, however, little is known about the specialized functions of the homologs in autophagy.

FIP200, part of the ULK1 complex (Hosokawa et al., 2009), is generally regarded as the homolog of Atg17, despite rather large structural differences. On the other hand, FIP200 is included in the list of possible homologs that have been proposed for Atg11. The function of FIP200 was suggested to accommodate that of both Atg11 and Atg17 (Mizushima, 2010). A study in *A. thaliana* identified both Atg11- and Atg17-specific domains in the Atg11-ortholog AtATG11, in yeast Atg11 and in mammalian FIP200 (Li et al., 2014). Besides FIP200, also huntingtin shows structural similarities to Atg11 and, like the yeast homolog, is able to interact with ULK1, Atg8 and cargo adaptors (Ochaba et al., 2014). Possibly, mammalian cells employ several Atg11 homologs and adaptors for selective autophagy, depending on the specific cargo.

Diversification of proteins leads to differences in regulation between autophagy in fungi and mammalian cells. Tough components of the autophagic machinery have to be translocated in both yeast and mammalian cells, they employ different strategies to overcome challenges posed by their cellular structure. Whereas the transport of the autophagic machinery and cargo only depends on an intact actin network in yeast, mammalian cells also heavily depend on microtubules for transport over long distances due to their much larger size. Whereas Atg5-positive puncta remain in the periphery of the cell, LC3-positive puncta have been observed using dynein motors to move linearly along microtubule tracks to a perinuclear region where lysosomes are located (Kimura et al., 2008). The interaction of vesicle and motor is mediated by Rab7 and additional factors (reviewed in (Hyttinen et al., 2013).

Mitophagy can be induced in mammalian cells for several reasons. The signal for recruitment of the autophagic machinery is either NIX-mediated in the case of erythrocyte maturation or, in most cases, induced by depolarization. Interestingly, depolarized mitochondria are only degraded by mammalian cells but not yeast. Laser-light irradiated single mitochondria in hepatocytes are permanently depolarized and become decorated with LC3-II in a non-PI3K dependent way (Kim and Lemasters, 2011). Chemical depolarization of mitochondria in yeast was not sufficient to induce mitophagy (Mendl et al., 2011), suggesting that yeast is more tolerable of damaged mitochondria. Requiring a tight regulation of functional mitochondria, mammalian cells seem to have developed several parallel strategies to degrade superfluous or damaged mitochondria. Mitochondrial receptors NIX/BNIP3, FUNDC1 and Bcl2-L13 mediate mitophagy by direct interaction with LC3 (Novak et al., 2010). PINK1/Parkin-mediated mitophagy employs adaptors to recognize surface-displayed ubiquitination signals for the selective removal of mitochondria that have lost their membrane potential (Wei et al., 2015). In yeast, most specific cargos were thought to be subjected to autophagy dependent on specific receptors and Atg11. However, ubiquitination seems to play a role as well. Ribosomes appear to be preferentially taken up into non-selective autophagosomes due to ubiquitination (Kraft et al., 2008). Furthermore, ubiquitinated protein aggregates employ Cue5, but not Atg11, for tethering to Atg8, a pathway termed CUET (Lu et al., 2014). Thus, like mammalian cells, yeast harbors several pathways for recognition of specific cargo, increasing the known degree of conservation of autophagy from yeast to mammalian cells.

Even when protein complex components are conserved from yeast to mammals, they are not always regulated in the same way. The yeast Atg1 kinase complex appears to be separated during vegetative conditions and only associates as the Atg1-Atg13-Atg17-Atg31-Atg29 pentameric complex upon autophagy induction, which also depends on a

massive dephosphorylation of Atg13. The mammalian homolog ULK1 complex, on the other hand, is constitutively assembled and regulated only by shifts of phosphorylation of ULK1 and mAtg13 by mTOR, which associates with the complex during vegetative conditions (Hosokawa et al., 2009).

1.5.2   Medical implications of autophagy

The importance of autophagy for maintaining cellular homeostasis and vitality is emphasized by the number of human diseases which are connected to malfunctions of the autophagic machinery. Cells harboring mutated *ATG* genes, which up- or downregulate autophagy, experience devastating consequences. The resulting pathologies in humans include neurodegenerative diseases, compromised immunity, cancer, and shortened life span. Autophagic dysregulation can be both the primary reason for diseases (mutations in autophagic genes) and, due to autophagy converging with the endocytic pathway at the step of lysosomal fusion, also the secondary (mutations affecting transport to or homeostasis of lysosomes lead to the impairment of autophagy) (Winslow and Rubinsztein, 2008).

Autophagy is involved in the change of cellular homeostasis of the aging organism. Gene expression of several autophagy related proteins declines with age. Concomitantly, ubiquitinated protein aggregates accumulate in the brain of flies. Mutation of the core autophagy protein Atg8a results in strongly decreased life span and accumulation of protein aggregates in *D.melanogaster*. Reversely, overexpression of Atg8a in fly brains decreased ubiquitinated protein aggregates and extended lifespan (Simonsen et al., 2008). Surprisingly, overexpression of Atg1 in the brain of flies activates autophagy in the intestine and results in an increased life span (Ulgherait et al., 2014). This represents the first evidence of non-cell-autonomous regulation of autophagy at a systemic level by induction in a key tissue.

One characteristic of aging is the accumulation of ubiquitinated protein aggregates. These seem to have detrimental effects on neuronal cells, leading to cell death and therefore loss of neuronal matter. This process is enhanced and accelerated if additional mutations decrease autophagic clearance of protein aggregates. An abnormal accumulation of protein is the hallmark of several neurodegenerative diseases, including Alzheimer's (AD), Parkinson's (PD), Huntington's disease and Amyotrophic lateral sclerosis (ALS). Protein aggregates or damaged organelles are normally ubiquitinated as degradation signal, which is then recognized by ubiquitin-receptors, including p62. Mutations in ubiquitin-receptors have been implicated in the development of neurodegeneration, for example mutated p62 is playing a role in ALS (Rea et al., 2014). In AD, autophagic flux was found to be decreased as a secondary effect of reduced

acidification of the lysosome. Mutated presenilin-1 causes abnormal targeting of the proton pump away from the lysosome (Lee et al., 2010). However, not only macroautophagy is affected by protein aggregates, but also CMA. Disease-related CMA substrates, including huntingtin, α-synuclein, LRRK2, and tau, oligomerize into complexes that bind to the CMA translocation complex. They disrupt its stability and inhibit translocation of themselves as well as of other substrates (reviewed in (Schneider and Cuervo, 2014).

PD is a multifactorial disease and, though aggregates of α-synuclein are a histological hallmark, neurodegeneration is not only caused by protein aggregation. Familial forms of PD are caused by a broad range of mutations, but an accumulation was observed in proteins involved in mitophagy (reviewed in (Youle and Narendra, 2011). Mutations in both PTEN-induced putative kinase protein 1 (PINK1) and Parkin have been identified as cause of PD. Normally, PINK1 becomes stabilized on depolarized mitochondria and recruits the E3 ubiquitin ligase Parkin. Parkin ubiquitinates various proteins on the membrane surface, serving as degradation signal. Though p62 can act as adaptor between ubiquitinated mitochondria and autophagosomal membranes, it can be deleted without mitophagy impairment (Okatsu et al., 2010). This is in good agreement with the identification of several adaptors recognizing ubiquitinated cargo and suggests that the early step of cargo selection is the bottleneck of selective autophagy.

The polymorph pathology of cancer is reflected by autophagy being both pro-oncogenic and anti-oncogenic. Active autophagy can be useful in preventing the development of cancer (Takamura et al., 2011), however, once tumor cells have developed they might employ autophagy for their own survival, especially during stress conditions induced by chemotherapy (Mathew and White, 2011). Therefore the most promising strategy of cancer therapy at the moment is chemotherapy combined with autophagy inhibitors. However, taking into account the role autophagy plays in general cellular development and homeostasis, it is not surprising that prolonged systemic ablation of autophagy by *ATG7* deletion in a mouse model entails many side-effects (Karsli-Uzunbas et al., 2014). Therefore systemic ablation of autophagy can only be applied temporarily, raising an interest in selective autophagy regulation, individualized to the respective cancer.

With the importance and molecular mechanism of autophagy becoming increasingly clear, it is considered as a hot potential therapeutic target in the treatment of aging and many diseases. Especially activation or inhibition of selective autophagy would allow a more targeted treatment rather than systemic regulation of autophagy. However, a better molecular understanding is still necessary to maintain the fine balance between cellular renewal and cellular death.

1.6　Aim of study

Selective autophagy emerges as frequently employed pathway by all eukaryotic cells for transportation of various intracellular cargos to the lysosome/vacuole. Mutations of many proteins involved in the pathway are associated with diseases. Moreover, decreasing expression levels of autophagic proteins contribute to aging. The essential function of autophagy for cellular homeostasis limits its systemic regulation for therapeutic purposes. Therefore the importance to identify the common machinery and converging points of selective and non-selective autophagy increases.

The yeast protein Atg11, with several potential functional homologs in higher eukaryotes, is a key factor in selective autophagic pathways, but dispensable in non-selective autophagy. Atg11 interacts with cargo receptors and lipidated Atg8, thereby linking cargo to the autophagosome. The extended coiled-coil structure exhibits similarities to actin motor proteins. In vivo observed protein interactions with the Atg1 kinase complex and structural homology to Atg17 suggest a functional relation to the latter. Together with the observation that Atg11 is an effector of the small GTPase YptI and structurally resembles common membrane tethering factors, Atg11 might function in recruiting and tethering Atg9-vesicles to initiate selective autophagy.

The aim of this thesis was the functional characterization of Atg11 on a molecular level. In addition, the identification of regulatory proteins was supposed to lead towards the regulation of selective autophagy. Therefore, an in vitro approach was applied to unravel the intricate Atg11-interactome. Full length Atg11 was recombinantly expressed and purified for functional studies. In vitro methods included fluorescence microscopy of giant unilamellar vesicles (GUV) decorated with purified proteins to visualize the ordered recruitment of the selective autophagic machinery, biophysical protein characterization of Atg11 and the study of protein – protein interactions. In vivo analysis of mutant yeast strains regarding their autophagic capacity and protein localizations and interactions complemented in vitro findings.

2 Methods and Material

All methods used were standard microbiology, molecular biology or biochemical techniques; changes of standard procedures or manufacturer instructions and non-standard methods are described in more detail below.

2.1 Material

If not stated otherwise, chemicals were purchased from AppliChem, BD, Biomol, Fisher Scientific, J.T.Baker, Merck Millipore, Roth, Serva, Sigma-Aldrich, Thermo Scientific or VWR Chemicals.

Restriction enzymes and Phusion polymerase used in PCR were purchased from New England Biolabs, protein tags were cleaved off with PreScission protease produced in the MPIB core facility and Benzonase used during protein purification was initially purchased from Sigma, later on produced as Sm DNAse from the MPIB core facility.

Primary antibodies produced in-house include α-Atg8, α-ApeI, α-myc, purchased were α-GFP (Roche), α-His (Millipore), α-myc, α-HA (both Santa Cruz Biotechnology) and α-Pgk1 (Invitrogen). α-ApeI was also kindly provided by Prof. Thumm (Göttingen, DE). Secondary HRP-fused antibodies were purchased from Rockland (goat α-rabbit) and Merck (goat α-mouse).

DNA primers were purchased from Metabion, DNA sequencing was performed in the MPIB core facility or by Eurofins.

2.2 Molecular biology methods

E.coli strains employed for cloning and expression of proteins are listed in Table 2.

Table 2 - E.coli strain collection

strain name	genotype	source
XL-1 Blue	*recA1 endA1 gyrA96 thi-1 hsdR17 supE44 relA1 lac [F´ proAB lacIqZΔM15 Tn10 (Tetr)]*	MPIB core facility
Omnimax	*F' {proAB+ lacIq lacZΔM15 Tn10(TetR) Δ(ccdAB)} mcrA Δ(mrr-hsdRMS-mcrBC) φ80(lacZ)ΔM15 Δ(lacZYA-argF) U169 endA1 recA1 supE44 thi-1 gyrA96 relA1 tonA panD*	MPIB core facility
BL21 (DE3)	E. coli B *F– dcm ompT hsdS(rB– mB–) gal λ(DE3)*	MPIB core facility

strain name	genotype	source
Rosetta (DE3) pLysS	F⁻ *ompT hsdS*$_B$(r$_B^-$ m$_B^-$) *gal dcm* (DE3) pRARE (Cam^R)	MPIB core facility

2.2.1 Plasmid preparation

Cloning of pCoofy plasmids (provided by core facility MPIB) was performed according to the published method (Scholz et al., 2013) based on Seamless Ligation Independent Cloning (SLIC). Coding DNA for ATGs or fragments was amplified from BY4741 genomic DNA. Primers added flanking regions (LP1, LP2) for RecA (NEB) homolog recombination with the linearized backbone, followed by transformation into competent Omnimax cells. Cloning of all other plasmids was performed by standard molecular biology techniques or homolog recombination of PCR-amplified sequences and transformation into XL1-Blue cells. Plasmids used in this study are listed in Table 3.

Table 3 - Plasmids used in this study

Expression plasmids

plasmid name	construct	source
pESC-Ura-His6-Atg11	pESC-*His6-Atg11* (URA3 selection)	this study
pCoofy11-Atg11	pIEX-His10-*ccdB::Atg11*	this study
pCoofy29-Atg11	pFastBacM44-His6-MBP-*ccdB::Atg11*	this study
pCoofy37	pBR322-*MBP-PreScission/LP1-ccdB-LP2-His6*	MPIB core facility
pCoofy37-Atg11	pCoofy37-*ccdB::Atg11*	this study
pCoofy37-Atg11N667	pCoofy37-*ccdB::Atg11$^{1-667}$*	this study
pCoofy37-Atg11C211	pCoofy37-*ccdB-His6::Atg11$^{968-1178}$-His10*	this study
pG-KJE8	pACYC-*araB-(dnaK-dnaJ-grpE)-Pzt1-(groES-groEL)*	Takara Bio Inc.
pCoofy1	pETM14-*His6-PreScission/LP1-ccdB-LP2*	MPIB core facility
pCoofy1-Atg32	pCoofy1-*ccdB::Atg32$^{1-376}$*	this study
pCoofy1-Atg32^{SE}	pCoofy1-*ccdB::Atg32$^{1-376,S114E}$*	this study
pCoofy1-Atg32^{WG}	pCoofy1-*ccdB::Atg32$^{1-376,W86G}$*	this study
pCoofy1-Atg8	pCoofy1-*ccdB::C-Atg8$^{1-116}$*	Viola Beier
pCoofy1-Atg3	pCoofy1-*ccdB::Atg3*	Viola Beier
pCoofy1-Atg7	pCoofy1-*ccdB::Atg7*	Viola Beier
pST39-Atg12-Atg5	pST39-*Atg12-His6-C-Atg5-Atg7-Atg10*	Viola Beier

CEN plasmids

plasmid name	construct	source
pTL58pPma1-Atg11-GFP	pTL58pPma1-*Atg11-GFP*	this study
pTL58pAtg11-Atg11-2xGFP	pTL58pAtg11-*Atg11-linker-2xGFP*	this study
pUG36-2xmCherry-Atg8	pUG36pMet25-*2xmCherry-Atg8*	Michael Thumm, Göttingen, DE
pTL58pPma1-Atg9-3HA	pTL58pPma1-*Atg9-3HA*	Yijian Rao
pTL58pAtg9-Atg9-3HA	pTL58pAtg9-*Atg9-3HA*	Yijian Rao
pRS316pPma1-Atg9core-3HA	pRS316pPma1-*Atg9$^{281-779}$-3HA*	Yijian Rao
pTL58pAtg17-Atg17-2xGFP	pTL58-pAtg17-*Atg17-linker-2xGFP*	Yijian Rao
pRS316pAtg29-Atg29	pRS316pAtg29-His6-Atg29	this study
pRS316pAtg29-Atg29^{3SD}	pRS316pAtg29-*His6-Atg29_S197D_S199D_S201D*	this study
pRS316pAtg29-Atg29^{3SA}	pRS316pAtg29-*His6-Atg29_S197A_S199A_S201A*	this study
pRS316pAtg29-Atg29$^{\Delta C}$	pRS316pAtg29-*His6-Atg29$^{\Delta 91-213}$*	this study
pRS316pPma1-Atg32$^{1-376}$	pRS316pPma1-*Atg32$^{\Delta 377-529}$*	this study
pRS316pPma1-Atg32$^{1-376,SE}$	pRS316pPma1-*Atg32$^{\Delta 377-529}$_S114E*	this study
pYX242mtPho8	pYX242-*Su9-Pho8$^{\Delta 1-60}$*	Andreas Reichert, Frankfurt, DE
pCK782	pRS315-pCup1-*Ape1* (LEU2 selection)	Claudine Kraft, Vienna, AT
pCK782URA	pRS315-pCup1-*Ape1* (URA3 selection)	this study

Genomic DNA of Atg32$^{1-376}$ was amplified from BY4741 genomic DNA and SLIC inserted into pCoofy1. Site-directed mutagenesis of serine 114 to glutamic acid (S114E) and tryptophan 86 to glycine (W86G) was performed with two complementary primers containing the respective mutation. BY4741 genomic DNA of Atg11$^{1-1178}$ (full length), Atg11$^{1-667}$ (Atg11^{N}) and Atg11$^{968-1178}$ (Atg11^{C}) was SLIC inserted into pCoofy37, containing a PreScission-cleavable N-terminal maltose-binding protein (MBP) and a C-terminal poly-histidine tag.

For the search of AIMs in Atg11, point mutations were introduced into pCoofy37-Atg11 by PCR amplification of the plasmid with phosphorylated complementary primers containing the respective mutation in the center. Original vector was DpnI-digested for 2 h at 37°C and the

nicked plasmid was ligated prior to transformation.

ATG29 was mutated to 3SD and 3SA (S197, S199, and S201 to D or A, respectively) in previously constructed pST39-Atg29-Atg31 (Perna, 2014) by employing the QuikChange Lightning Site-Directed Mutagenesis Kit (Agilent Technologies). His6-tagged Atg29, Atg29[3SD], Atg29[3SA] and Atg29[1-90] were PCR amplified from original and mutated pST39-Atg29-Atg31 vector. *ATG29* wild type promoter pAtg29 was PCR amplified from BY4741 genomic DNA and fused to *ATG29* variants via homolog recombination. Inserts and backbone pRS316-pAtg9-ATG9-GFP (courtesy Dr. Yijian Rao) were digested with XhoI and NotI-HF and ligated after purification with QIAquick PCR purification or Gel extraction kit, respectively (Qiagen GmbH).

2.2.2   Competent E.coli

E.coli was made competent for plasmid uptake. 100 mL SOB media (2% w/v trypton, 0.5% w/v yeast extract, 8.56 mM NaCl, 2.5 mM KCl, 10 mM $MgSO_4$, 0.5 mM NaOH) were inoculated from glycerol stock, initially grown at 37°C for 1 h and then at 18°C until an OD_{600} of 0.6 was reached. Culture was cooled down on ice for 10 min, then cells were harvested for 10 min at 4000 g. Cells were resuspended in 30 mL ice-cold TB buffer (10 mM Pipes, 15 mM $CaCl_2$, 250 mM KCl, 55 mM $MnCl_2$, filter sterilized) and incubated for 10 min on ice. They were pelleted for 10 min at 2000 g and gently resuspended in 8 ml TB buffer and 560 µL DMSO and incubated for 10 min on ice. Competent cells were aliquoted and frozen in liquid N_2 before storage at -80°C.

2.2.3   Transformation of yeast with CEN plasmids

Centromere-containing (CEN) plasmids propagate with their host yeast cell like an additional chromosome. CEN-plasmids used in this study are pTL58-based (LEU2 selection) or pRS316-based (URA3 selection). Transformation of approximately 1 µg plasmid in 0.5 - 5 µL water was performed in one step by mixing with 85 µL transformation solution (0.24 M LiOAc, 47% PEG 3350 filter sterilized), 10 µL 1 M DTT and 5 µL activated (5 min 95°C) salmon sperm DNA (Invitrogen). Enough *Saccharomyces cerevisiae* grown freshly on a plate was resuspended in the mix to yield a turbid solution after short vortexing. After incubation for 30 min at 45°C, the cells were immediately plated on the required drop-out agar plate (0.67% yeast nitrogen base, 2% glucose, 1x aa drop-out mix, 2% w/v agar) and incubated at 30°C for 2 days.

2.2.4   Chemically competent yeast

S.cerevisiae needs to be made competent to take up DNA into its genome. 50 ml YPD were inoculated to 0.1 OD_{600} and grown to 0.6. Cells were harvested for 10 min at 500 g and washed in 20 mL autoclaved MQ water and then 20 mL sterile filtered SORB buffer (100 mM

LiOAc, 10 mM Tris pH 8.0, 1 mM EDTA, 1 M sorbitol). Competent cells were resuspended in 360 µL SORB buffer, 50 µL aliquots were frozen and stored at -80°C.

2.2.5 Genomic yeast modifications

Genomic modifications were introduced in yeast according to the published protocol (Janke et al., 2004). Briefly, knockout cassettes were PCR amplified from pFA6a-natNT2 or pFA6a-hphNT1 with S1 and S2 primers annealing to the start and end of the cassettes and adding flanking sequences of the target gene. For tagging ATG11 with Myc, the 9xMyc-natNT2-cassette was amplified from pYM21 with S3 and S2 primers. They anneal to the start and end of the cassette, while adding a sequence homolog to the C-terminus of ATG11 and the upstream flanking sequence of ATG11, respectively. Cassettes were purified with QIAquick Gel extraction kit and approximately 1.5 µg were transformed into 50 µL competent yeast together with 5 µL activated salmon sperm DNA in 300 µL PEG buffer (100 mM LiOAc, 10 mM Tris pH 8.0, 1 mM EDTA, 40% PEG 3350). After incubation for 1 h at 30°C, 35 µL DMSO were added and the samples incubated at 42°C for 15 min. For antibiotic selection, cells were pelleted with short centrifugation, resuspended in 300 µL YPD, incubated shaking over night at 30°C, and plated on selection plates the next day. In case of auxotrophic selection, cells could be directly plated on the respective drop-out plate after transformation. Genomic DNA extraction of yeast was carried out with MasterPure Yeast DNA Purification Kit (epicentre, Illumina).

S. cerevisiae Strains generated or used in this study are listed in Table 4.

Table 4 - S.cerevisiae strain collection

strain name	genotype	source
DDY1810	MATa, leu2Δ, ura3-52, trp1Δ, prb1-1122, pep4-3, prc1-407 *gal2*	Thomas Wollert
BY4741	S288C MATa *his3Δ1 leu2Δ0 met15Δ0 ura3Δ0*	Euroscarf
BY4742	S288C MATα *his3Δ1 leu2Δ0 lys2Δ0 ura3Δ0*	Euroscarf
BY4741 Pho8Δ Pgk1-GFP	BY4741 *pho8::natNT2 pgk1-GFP-his3*	Viola Beier
BY4742 Pho8Δ Atg11Δ Pgk1-GFP	BY4742 *pho8::natNT2 atg11::kanMX6 pgk1-GFP-his3*	this study
BY4741 Pho8Δ Atg17Δ Pgk1-GFP	BY4741 *pho8::natNT2 atg17:: hphNT1 pgk1-GFP-his3*	this study
BY4742 Pho8Δ Atg11Δ Atg17Δ Pgk1-GFP	BY4742 *pho8::natNT2 atg11::kanMX6 atg17:: hphNT1 pgk1-GFP-his3*	this study
BY4742 Pho8Δ AIM Pgk1-GFP	BY4742 *pho8::natNT2 atg11Δ::AIM-hphNT1 pgk1-GFP-his3*	this study

strain name	genotype	source
BY4741 Pho8ΔN60	BY4741 *pho8$^{1-60}$::natNT2-pGPD*	Viola Beier
BY4741 Pho8ΔN60 Atg5Δ	BY4741 *pho8$^{1-60}$::natNT2-pGPD atg5::kanMX6*	Viola Beier
BY4742 Pho8ΔN60 Atg11Δ	BY4742 *pho8$^{1-60}$::natNT2-pGPD atg11::kanMX6*	this study
BY4741 Pho8ΔN60 Atg17Δ	BY4741 *pho8$^{1-60}$::natNT2-pGPD atg17:: hphNT1*	this study
BY4741 Pho8ΔN60 Atg11Δ Atg17Δ	BY4742 *pho8$^{1-60}$::natNT2-pGPD atg11::kanMX6 atg17:: hphNT1*	this study
BY4742 Pho8ΔN60 Atg17Δ AIM	BY4742 *pho8$^{1-60}$::natNT2-pGPD atg11Δ::AIM-hphNT1 atg17::kanMX6*	this study
BY4741 Atg13-GFP	BY4741 *Atg13-GFP-his3*	MPIB group WS
BY4741 Atg11-GFP	BY4741 *Atg11-GFP-his3*	MPIB group WS
BY4741 Atg11-GFP Atg17Δ	BY4741 *Atg11-GFP-his3 atg17::hphNT1*	this study
BY4741 GFP	BY4741 *his3Δ1::GFP-his3*	MPIB dept. Mann
BY4742 Atg11Δ	BY4742 *atg11::kanMX6*	MPIB group WS
BY4742 Atg11Δ Atg17Δ	BY4742 *atg11::kanMX6 atg17::hphNT1*	this study
BY4741 Atg11Δ Atg8Δ	BY4741 *atg8::kanMX6 atg11::natNT2*	this study
BY4741 Atg11Δ Atg17Δ Atg8Δ	BY4741 *atg8::kanMX6 atg11::natNT2 atg17:: hphNT1*	this study
BY4741 Om45-GFP AIM	BY4741 *Om45-GFP-his3 atg11Δ::AIM-hphNT1*	this study
BY4741 Om45-GFP Atg5Δ	BY4741 *Om45-GFP-his3 atg5::natNT2*	this study
BY4741 Om45-GFP Atg11Δ Atg17Δ	BY4741 *Om45-GFP-his3 atg11::natNT2 atg17::hphNT1*	this study
BY4741 Om45-GFP Atg11Δ Atg17ΔC	BY4741 *Om45-GFP-his3 atg11::natNT2 atg17$^{321-417}$::hphNT1*	this study
BY4741 Pgk1-GFP	BY4741 *Pgk1-GFP-his3*	MPIB group WS
BY4741 Pgk1-GFP Atg5Δ	BY4741 *Pgk1-GFP-his3 atg5::natNT2*	this study

strain name	genotype	source
BY4741 Pgk1-GFP Atg11Δ	BY4741 *Pgk1-GFP-his3 atg11::natNT2*	this study
BY4741 Pgk1-GFP Atg17Δ	BY4741 *Pgk1-GFP-his3 atg17::hphNT1*	this study
BY4741 Pgk1-GFP Atg11Δ Atg17Δ	BY4741 Pgk1-GFP-his3 atg11::natNT2 atg17::hphNT1	this study
BY4741 Pgk1-GFP AIM	BY4741 Pgk1-GFP-his3 atg11Δ::AIM-hphNT1	this study
BY4741 Atg29Δ Atg11Δ	BY4741 atg29::kanMX6 atg11::natNT2	this study
BY4741 Atg29Δ Atg17Δ	BY4741 atg29::kanMX6 atg17::natNT2	this study
BY4741 Atg9Δ	BY4741 atg9::kanMX6	MPIB group WS
BY4741 Atg9Δ Atg11-9Myc	BY4741 atg9:: kanMX6 atg11-9xmyc-natNT2	this study
BY4741 Atg9Δ Atg11-9Myc Atg13Δ	BY4741 atg9::kanMX6 atg11-9xmyc-natNT2 atg13::hphNT1	this study
BY4741 Atg9Δ Atg11-9Myc Atg17Δ	BY4741 atg9::kanMX6 atg11-9xmyc-natNT2 atg17::hphNT1	this study
BY4741 Atg9Δ Atg11-9Myc Atg29Δ	BY4741 atg9::kanMX6 atg11-9xmyc-natNT2 atg29::hphNT1	this study
BY4741 Atg9Δ Atg11-9Myc Atg31Δ	BY4741 atg9::kanMX6 atg11-9xmyc-natNT2 atg31::hphNT1	this study
yTB0495	S288C MATa his3Δ1 leu2Δ0 ura3Δ0 met15Δ0 APE1-mRuby2-kan	Claudine Kraft, Vienna, AT

MPIB group WS: independent group of Roland Wedlich-Söldner at the MPIB. MPIB dept. Mann: Department of Prof. Matthias Mann at the MPIB.

2.3   Cell biology methods

2.3.1   Yeast strains and culturing

Yeast cells were grown in YPD media (1% yeast extract, 2% peptone autoclaved, supplemented with 2% filtered glucose) or in synthetic dropout media (0.67% yeast nitrogen base autoclaved, supplemented with 2% filtered glucose) with filtered complete (SDcomplete) or dropout (SD−AA) amino acid mix. For growth on plates the respective media was supplemented with 2% agar before autoclaving. Autophagy was induced by changing cultures grown to early log phase into SD-N media (0.17% yeast nitrogen base autoclaved, 2% filtered glucose) for at least 2 hours.

2.3.2 Yeast Pho8 and mtPho8 assay

Autophagic flux was measured quantitatively by measuring the activity of alkaline phosphatase in the vacuole. Non-specific autophagy was reported by genomically engineered Pho8ΔN60, for measurement of mitophagy *Pho8Δ* strains were complemented with 1-60::Su9-Pho8ΔN60 expressed from a plasmid. Cultures were grown to early log phase and autophagy was induced in SD-N media for 2-24 hours as indicated. For Alkaline Phosphatase assays 4 OD units were collected per samples. Samples were resuspended in 200 µl Pho8 assay buffer (250 mM Tris-HCl, pH 9.0, 10 mM MgSO4, 10 µM ZnSO4) and lysed with glass beads. Cellular debris was pelleted for 5 minutes at 13000 rpm after again adding 200 µl assay buffer. Pho8 activity was determined in diluted cleared lysates by addition of α-naphtyl phosphate disodium salt in assay buffer at a final concentration of 0.1 mM. The reaction was stopped after 20 minutes at 30°C by addition of Glycin/NaOH pH 11.0 to 1 M. Color development was measured at 345 nm exc. / 472 nm em. in a BioTek Synergy Neo plate reader. Signal was normalized to protein content of lysates, determined by a bicinchoninic acid protein assay (Pierce BCA Protein Kit, Thermo Scientific).

2.3.3 AminopeptidaseI (ApeI) maturation assay

Maturation of pApeI to mApeI in the vacuole is the endpoint of the Cvt pathway and can be employed for assessment of specific autophagy. One OD samples were collected and cell pellets were resuspended in 100 µl 0.2 M NaOH, 0.1 M DTT and lysed for 15 minutes on ice. Proteins were precipitated with TCA at a final concentration of 10% for 15 min on ice. Protein pellets were washed in acetone and resuspended in sample buffer (0.1 M Tris pH 7.5, 2 % SDS, 10% glycerol, 1 mM DTT, 0.05 % bromophenol blue), separated on SDS-PAGE and blotted on PVDF. Processing of ApeI was analyzed by immuno-detection of pApeI and mApeI and band intensities were quantified with LI-COR Image Studio Lite 5.0 (LI-COR Biosciences).

2.3.4 Yeast subcellular fractionation

Cultures were grown to log phase and autophagy was induced in SD-N media for 2 hours. Five OD units of culture were harvested and resuspended in 100 µl fractionation buffer (50 mM Tris pH 7.6, 0.3 mM MgCl$_2$, freshly supplemented with 1 mM DTT, 0.6 mM PMSF and 3 µl protease inhibitor cocktail [Sigma-Aldrich]). Cells were disrupted with glass beads, lysates centrifuged through a hole in the bottom of the tube and combined with 100 µl fractionation buffer used to wash the beads. Non-disrupted cells were removed in a 1 minute centrifugation step at 300 g. Cleared cell lysate was subjected to 30 minutes of centrifugation at 17000 g, the resulting supernatant was centrifuged for another 30 minutes at 100000 g. Resulting pellets were resuspended in a volume of fractionation buffer corresponding to the respective supernatants. Samples were taken from each supernatant and pellet fraction and TCA precipitated by adding TCA to a final concentration of 10%. After 15 minutes of

precipitation on ice, the protein was pelleted and washed in acetone, aided by an ultrasonic water bath to dissolve pellets. Protein was spinned down after one hour at -20°C, air-dried and then resuspended in 40 µl sample buffer for 10 minutes at 65°C. Samples were separated on SDS-PAGE, blotted on PVDF and immuno-stained with α-GFP, α-HA or α-myc as indicated. Blots were developed with Western Blot Hyper HRP Substrate (Takara) and imaged in a LAS-3000 Reader (Fujifilm). Quantification of Western blots was performed with LI-COR Image Studio Lite 5.0.

2.3.5 Yeast co-immunoprecipitation

Cultures were grown to log phase and autophagy was induced in SD-N media for 2 hours. Fifty OD of each culture was harvested by centrifugation for 3 minutes at 1500 g. Cell pellets were either directly processed or frozen in liquid N_2 until further use. Cells were washed in lysis buffer and lysed by glass beads in 500 µl lysis buffer (25 mM Tris pH 7.2, 150 mM NaCl, 200 mM sorbitol, 1 mM $MgCl_2$, 0.1% Tween20) supplemented with 20 µl protease inhibitor cocktail (Sigma-Aldrich) and 3 mM PMSF. Cellular debris was removed by 2 minutes centrifugation at 6000 rpm, cleared lysates were treated with Tween20 (0.9% end concentration) and gently mixed for 10 minutes at 4°C before centrifugation at 14 000 rpm for 10 minutes at 4°C. For immunoprecipation, 10 µg mouse α-myc antibody (in-house) were added to the rest of each sample supernatant and incubated for 2 hours at 4°C. For each sample 40 µl of Protein A magnetic beads (New England Biolabs) were washed in TBS-T (25 mM Tris pH 7.5, 150 mM NaCl, 0.05% Tween20), added to the lysates and incubated for 30 minutes. Beads were washed twice with lysis buffer, directly resuspended in 2x SDS sample buffer and boiled for 10 minutes. For total lysate analysis 1 OD of cells was subjected to TCA precipitation after lysis in 100 µl 0.2 M NaOH, 0.1 M DTT for 15 minutes on ice. Samples were supplemented with TCA to a final concentration of 10%, protein was precipitated on ice for 15 minutes and pelleted for 5 minutes at 17000 g. Precipitated protein pellet was resuspended in ice-cold acetone in an ultrasonic water bath, spinned down after one hour at -20°C, air-dried and then resuspended in 40 µl sample buffer for 10 minutes at 65°C. Ten µl of each sample were separated on SDS-PAGE, blotted on to PVDF membrane and indicated proteins were immuno-detected.

2.3.6 Yeast confocal microscopy

Cultures were grown to early log phase and autophagy was induced in SD-N media for 2-4 hours. Images were taken in the MPIB Imaging Facility on a LEICA TCS SP8 AOBS confocal laser scanning microscope equipped with a LEICA HCX PL APO 63x/NA1.4 oil immersion objective or on a ZEISS LSM780 confocal laser scanning microscope equipped with a ZEISS Plan-APO 63x/NA1.46 oil immersion objective. Brightness was adjusted with ImageJ when required for facilitation of manual analysis. For quantification of puncta formation Z stacks

encompassing the whole cell were flattened with max. intensity settings in ImageJ (NIH, USA) and cells and puncta were counted manually with the Cell Counter plugin.

2.4 Biochemical methods

2.4.1 Western Blotting

Samples for western blotting were run on home-made SDS-PAGE gels of 8-15% acrylamide or on precast NuPage 4-12% Bis-Tris gradient gels (Novex, Thermo) in SDS running buffer (25 mM Tris, 192.1 mM glycine, 0.1% SDS) or in MES SDS buffer according to manufacturer's instructions, respectively. Finished gels were shortly incubated in transfer buffer (12.5 mM Tris, 38.7 mM glycine, 0.037% SDS, 20% methanol). Blotting paper soaked in transfer buffer, methanol-activated PVDF membrane, gel and more soaked blotting paper were stacked in this order on the anode of an in-house built semi-dry blotting instrument. Proteins were transferred at constant 15 V for 35-50 min, depending on the size of the protein of interest. Membrane was blocked for 1 h at RT in 3-5% milk powder in TBS-T (25 mM Tris pH 7.6, 150 mM NaCl, 0.05% Tween-20), then incubated with primary antibody in the same blocking solution for 1 h at RT or overnight at 4°C. After washing in TBS-T, secondary antibody was applied for 1 h at RT in TBS-T. Blots were developed with Western Blot Hyper HRP Substrate (Takara) and imaged in a LAS-3000 Reader (Fujifilm). In case of subsequent detection of another protein, the blot was stripped for 1 hour in stripping buffer (0.1 M NaOH, 2% SDS, 0.5% DTT) before blocking again.

2.4.2 Production of Atg9^{core} -proteoliposomes

Recombinant protein expression and purification of Atg9^{core} was carried out by Dr. Yijian Rao (Rao et al., 2016). Briefly, Atg9^{core} was expressed in Rosetta (DE3) pLysS in TB media (17 mM KH$_2$PO$_4$, 72 mM K$_2$HPO$_4$, 1.2% tryptone, 2.4% yeast extract, 0.5% glycerol). Cells were lysed with a Microfluidizer cell homogenizer (Microfluidics, Westwood, USA) and precleared for 10 min at 24 000 g, then the membrane fraction containing Atg9 was pelleted at 150 000 g for 1 h. Proteins were solubilized for 1 h at 4 °C in 25 mM Tris pH 8.0, 150 mM NaCl with 40 mM LDAO (Anatrace) and separated from debris by 1 h of 150 000 g centrifugation. Atg9^{core} was purified from the supernatant by Ni^{2+}-NTA batch purification followed by SEC over a Superdex200 10/300 GL column (GE Healthcare) in 25 mM Tris pH 8.0, 150 mM NaCl, 4 mM LDAO. For integration into membrane (20 mol% cholesterol, 10 mol% POPE, 60 mol% POPC and 10 mol% POPS, all Avanti Polar Lipids, total 1 mg lipid /ml), liposomes were supplemented with 6 mM LDAO and then mixed at a protein:lipid ratio of 1:200 with solubilized Atg9^{core}. Rapid 30-fold dilution and incubation for 30 min at RT yields Atg9-

proteoliposomes (Atg9-PL) which can be concentrated by centrifugation at 150 000 g for 30 min.

2.4.3   Protein expression and purification of Atg1, Atg13, Atg29-31 and Atg17

Recombinant protein expression in E. coli of Atg13, Atg29-31 and Atg17 and of Atg1 in insect cells and purification of all of them was carried out by Dr. Marco Perna. Protocols as described previously (Perna, 2014).

2.4.4   Protein expression and purification of Atg8, Atg3, Atg7 and Atg12-Atg5

Ubiquitin-like enzymatic coupling of Atg8 to PE in artificial membranes requires expression and purification of all proteins involved. The machinery was purified as described previously (Kaufmann et al., 2014). Briefly, all proteins were expressed from plasmids as indicated in Table 3 by Rosetta(DE3)pLysS, except Atg7 which was expressed by BL21(DE3), in LB media. Atg7 was co-expressed with chaperones from the plasmid pG-KJE8 (Takara Bio Inc.). Atg8 was constructed with an artificial N-terminal cysteine for labeling and a deleted C-terminal arginine for direct coupling to PE. Cells were lysed by sonication and proteins were extracted in batch with Ni^{2+}-NTA beads and purified on SEC into 25 mM Tris pH 7.2, 275 mM NaCl buffer after cleavage of their tags with PreScission protease.

2.4.5   Protein expression and purification of Atg32$^{1-376}$ and its mutants

Recombinant protein expression of Atg32$^{1-376}$ and its point mutated versions was carried out in batch purification of His-tagged proteins. Expression plasmids were transformed into E.coli Rosetta (DE3). Several colonies from the transformation plate were used for inoculation of an overnight LB (1% tryptone, 0.5% yeast extract, 0.7% NaCl) + antibiotics preculture. Main cultures were inoculated with 15 ml preculture / L LB + antibiotic, grown to an OD600 of 0.5, cooled down to 18°C for 2 h and induced with 0.3 mM Isopropyl β-D-1-thiogalactopyranoside (IPTG). Expression was taking place over night at 18°C. Cultures were harvested by 10 min centrifugation at 4000 rpm. Cell pellets were resuspended in lysis buffer (100 mM Tris pH 8.0, 300 mM NaCl, 5 mM Imidazole, 10% glycerol, 5 mM β-mercaptoethanol, 1:4000 Benzonase Nuclease, 1:80 protease inhibitor cocktail [both Sigma-Aldrich]) and lysed by sonication for 10 min on ice. Cell lysate was cleared by 1 h centrifugation at 19500 rpm and protein was captured from supernatant by Ni^{2+}-NTA agarose in batch for 1 h at 4°C. Beads were washed with 500 ml washing buffer (100 mM Tris pH 7.2, 300 mM NaCl, 5 mM Imidazole, 10% glycerol, 5 mM β-mercaptoethanol) and protein was eluted with 5 ml elution buffer (50 mM Tris pH 7.2, 300 mM NaCl, 250 mM Imidazole, 10% glycerol). Protein was filtered through a 0.2 μm PVDF filter and purified on a Superdex200 16/600 (GE Healthcare) gel filtration column with 25 mM Tris pH 7.2, 275 mM NaCl as running buffer. Protein identity was checked via SDS-PAGE and mass spectrometry and stored at -80°C until use after freezing in liquid N_2.

2.4.6   Protein expression and purification of Atg11 and its fragments

Recombinant protein expression of Atg11 was performed in BL21(DE3) E. coli with additionally expressed chaperones from the plasmid pG-KJE8 (Takara) in TB media (17 mM KH_2PO_4 , 72 mM K_2HPO_4, 1.2% tryptone, 2.4% yeast extract, 0.5% glycerol) supplemented with 0.2% arabinose and 5 µg/L tetracycline. Cultures were grown to around OD_{600} = 1, cooled down to 18°C for 2 h and induced with 0.3 mM IPTG. Expression was carried out at 18°C over night. Bacteria were harvested by 10 minutes centrifugation at 4000 rpm, the periplasma was removed by a wash step in 5 ml sucrose buffer (50 mM Tris pH 8.0, 20% sucrose, 1 mM EDTA) / g wet pellet, centrifugation for 30 minutes at 7000 g, followed by a wash step in 5 mM $MgSO_4$, which was incubated for 10 min and then centrifuged for 20 min at 4500 g. Cells were resuspended in lysis buffer (100 mM Tris pH 8.0, 300 mM KCl, 5 mM Imidazole, 10% glycerol, 0.2% Tween20, 5 mM β-mercaptoethanol, 2 mM PMSF, 1:200 protease inhibitor cocktail, 1:6666 in-house Sm DNAse), lysed by 5 passages through the Microfluidizer cell homogenizer and the cell lysate was cleared by centrifugation for 1 hour at 19500 g. The supernatant was loaded onto a HisTrap FF Crude (GE Healthcare) column, washed with 15 ml washing buffer (0.1 M Tris pH 8.0, 300 mM KCl, 10% glycerol, 20 mM Imidazole) supplemented to 500 mM KCl, 15 ml normal washing buffer and 20 ml washing buffer supplemented to 55 mM Imidazole. Elution was performed with 10 ml washing buffer incl. 500 mM Imidazole and the eluted MBP-fusion protein was cleaved by PreScission protease in the presence of 1 mM DTT and 1 mM EDTA for 15 minutes at room temperature. The protein was gel filtrated on a Superose6 Increase 10/300 (GE Healthcare) into Tris buffer pH 7.2, 5% glycerol, 275 mM KCl. Aliquoted protein was used freshly or frozen in liquid N_2 and stored at -80°C until use.

2.4.7   Protein conjugation to latex beads

Atg32[1-376] was changed into coupling buffer (20mM MES pH 6.0, 100 mM NaCl) by desalting on two consecutive HiTrap desalting columns (GE Healthcare) and concentrated in a Vivaspin4 spin column (Sartorius). The required amount of amino-binding polystyrene beads (chloromethyl latex beads, 1 µm, 4.1 g / 100 mL, Molecular Probes, Thermo Scientific) was washed twice in coupling buffer by dilution and pelleting at 3000 g for 20 minutes. Protein was added to beads and gently mixed at room temperature for 3-4 hours. Beads were pelleted and washed in washing buffer (1x PBS pH 7.2), remaining binding sites were then blocked in blocking buffer (1x PBS pH 7.2, 1% (w/v) glycine) by gently shaking at room temperature for 30 minutes. Beads were washed again in washing buffer and then stored at 4°C until use in storage buffer (1x PBS pH 7.2, 0.1% (w/v) glycine). Two µl of beads were used per 6-10 nmol protein and dissolved in 50 µl storage buffer at the end.

2.4.8   Flotation

Flotation assays were performed by Dr. Yijian Rao as described (Rao et al., 2016). Briefly, a high density fraction was created by mixing 250 µL Atg9-PLs with 250 µL 80% Nycodenz in 25 mM HEPES pH 7.0, 100 mM NaCl containing the proteins of interest. A gradient was achieved by overlaying with 250 µL 30% Nycodenz and 100 µL buffer only. Atg9-PL and interaction partners flotate to the low density – buffer interface during ultracentrifugation for 2 h at 650 000 g at 4 °C. Fractions can be analyzed on SDS-PAGE.

2.5   Biophysical methods

2.5.1   Circular Dichroism (CD)

Protein secondary structure was assessed by Circular Dichroism (CD) spectroscopy with a JASCO 715 spectropolarimeter with peltier-thermostat (JASCO GmbH). Protein was dissolved in 25 mM Tris pH 7.2, 300 mM salt and 10% glycerol at a concentration of 0.15 mg/ml for measurements. The molecular ellipticity was calculated from 4 accumulated CD recordings of each sample from 195 to 250 nm. The change in folding during heating was observed from 4 – 90°C by measuring the CD signal at 222 nm and voltage of the photomultiplier tube (HT). Fitting of the secondary structure was performed by CONTIN algorithm in SPM-2 Spectra Analysis software.

2.5.2   Analytical ultracentrifugation (AUC)

Analytical ultracentrifugation (AUC) for measurement of the sedimentation velocity was performed by the MPIB core facility on an Optima XL-I analytical ultracentrifuge with an An-60 Ti rotor (Beckman-Coulter). Centrifugation was performed at 50,000 rpm, 20°C and sedimentation was scanned by absorbance at 280 nm. Samples varied in concentration between A280 = 0.1 – 6 for detecting a concentration dependent induction of oligomerization. Proteins were dissolved in their respective gel filtration buffer, whose density and viscosity was determined with a DMA 5000 density meter and an AMVn viscometer, respectively (Anton Paar GmbH). Measurements were performed and data was analyzed with SEDFIT software package by Dr. Stephan Uebel, resulting in the display of a concentration distribution c(s) depending on the respective sedimentation coefficient S. Stokes radius and estimated friction ratio and molecular weight were provided for each sample population.

2.5.3   Dynamic Light Scattering (DLS)

Protein sample homogeneity and approximate molecule size (hydrodynamic radius R_H) was measured with Dynamic Light Scattering (DLS). Protein samples were centrifuged 10 min at 17000 g to remove large particles prior to recording 10 acquisitions of 3-15 msec time for each sample. Scattering signal intensity is not linearly correlated to the amount of sample.

Since the signal intensity is proportional to approximately r^6, also small amounts of large particles cause very strong signals. Therefore total intensities were normalized to R_H to estimate the share of differently sized populations. Measurements of lipid vesicles were performed after sonication on ice for about 15 min in single-use cuvettes in a DynaPro Nanostar spectrometer (Wyatt). The average R_H was calculated with the DYNAMICS software package from 5 repeats of the measurement. Samples with a multimodularity of more than 25% (mm = multimodular) were excluded from determining a R_H.

2.5.4   Surface Plasmon Resonance (Biacore)

Surface plasmon resonance (SPR) was performed on a Biacore 2000 (GE Healthcare) instrument. Proteins were diluted in freshly filtered and degassed running buffer (25 mM Tris pH 7.2, 150 mM NaCl, 5% glycerol). NTA chip was charged with 0.5 mM $NiCl_2$ in running buffer. 200 nM Atg11-His6 was loaded at a flow rate of 3 µL/min for around 16 min contact time onto a Ni^{2+}-NTA chip, followed by buffer. One or more consecutive analytes were loaded at a flow rate of 10 µL/min over about 5 min contact time each and resonance units (RU) were recorded. The chip was regenerated after every run with regeneration buffer (25 mM Tris pH 8.0, 150 mM NaCl, 5% glycerol, 350 mM EDTA). RU of every run were corrected for analyte interaction with Ni^{2+}-NTA chip not loaded with Atg11. Data of Atg13 concentration series was also corrected for drift by subtraction of the values measured in the lowest concentration of Atg13 (resonance equivalent to buffer) from all other samples.

2.5.5   Microscale Thermophoresis (MST)

Microscale thermophoresis (MST) creates a microscopic temperature gradient with laser light and measures the thereby induced movement of a fluorescently labeled analyte. The strong hydrogen-shell dependency of the method yields it sensitive to any change in the state of the analyte, for example by substrate binding or conformational changes. 50 nM Atto488-labeled Atg11 was mixed 1:1 with a 16x dilution series of unlabeled Atg13 (final MST buffer: 25 mM Tris pH 7.2, 180 mM NaCl, 10 mM MgCl2, 2.5% glycerol, 0.05% Tween-20, 1 mM DTT), loaded into hydrophilic capillaries and measured in a Monolith NT.115 instrument (NanoTemper Technologies GmbH) at 30% LED power and 40% MST power. A cap scan confirmed initial even fluorescence over the width of all capillaries.

2.5.6   Quantitative MS analysis

BY4741 Atg11-GFP, BY4741 Atg13-GFP and BY4741 GFP were grown in SD-His and starved for two hours in SD-N media. 50 OD of each culture in vegetative and starvation conditions were resuspended in 1.3 mL lysis buffer (50 mM Tris pH 7.5, 150 mM NaCl, 5% glycerol, 1% NP-40, 1 mM MgCl2, 1% benzonase, 1 tablet protease inhibitor [Roche] / 50 mL buffer). Lysis with glass beads, GFP pull down, mass spectrometry and initial analysis of measurements with MaxQuant software was performed by Eva Keilhauer, Mann department,

MPIB. The output data of the measurement in triplicates was further processed with Perseus 1.5.0.9. Both data sets of bait-GFP and GFP pulldown were loaded and the hits for the GFP pulldown were subtracted from the bait-GFP pulldown to extract the specific interactions. After log2(x) transformation of all values, the missing values were filled up from a normal distribution. Hits of both culture conditions were plotted against each other in a volcano plot, showing the degree of enrichment on the x-axis and the significance of interaction (-log p) on the y-axis.

2.6 Artificial membranes

Synthetic lipids were all purchased from all Avanti Polar Lipids: 1-palmitoyl-2-oleoyl-*sn*-glycero-3-phosphocholine (POPC), 1-palmitoyl-2-oleoyl-*sn*-glycero-3-phosphoethanolamine (POPE), 1-palmitoyl-2-oleoyl-*sn*-glycero-3-phospho-L-serine (POPS), cholesterol.

2.6.1 Preparation of LUVs and SUVs

Synthetic lipids of choice (20 mol% cholesterol, 10 mol% POPE, 60 mol% POPC and 10 mol% POPS for Atg9-PL) were dissolved in chloroform, mixed and dried as a thin layer in a manually revolving glass tube by evaporating the chloroform with a constant stream of nitrogen. The film was further dried in vacuum overnight. The lipids were rehydrated in a buffer of choice for about 1 hour at RT with occasional vortexing to form multilamellar vesicles (MLVs) at a lipid concentration of 1 mg/mL. To generate large unilamellar vesicles (LUVs), the vesicle suspension is passed several times through an extruder containing a membrane with defined pore sizes of 100 or 200 nm. Small unilamellar vesicles (SUVs) of 30-50 nm diameter were generated by sonicating the suspension and then passing it through a 30 nm filter.

2.6.2 Preparation of GUVs

Giant Unilamellar Vesicles (GUVs) were prepared by electroformation (Angelova and Dimitrov, 1986) from a lipid mixture consisting of 20 mol% cholesterol, 39.5% POPC, 20% POPE, 20% POPS and 0.5% POPE-Atto633. Four µg of lipid mix were dissolved in 50 µl chloroform and 20 µl were dried in vacuum overnight on indium tin oxide (ITO) covered glass slides. Slides were attached to an AC electric field (1.2 V, 10 Hz) in an in-house built Teflon chamber filled with 5 ml 600 mM sucrose solution. Swelling proceeded for about 6 hours at 30°C and GUVs were harvested by gently wiping them off the slides with a Pasteur pipette.

Alternatively, 7 µl of the lipid mix were dried directly on the electrodes of an in-house built mini-GUV-chamber for one hour in vacuum and then electroformed at 30°C in 350 µl of 600 mM sucrose for 1.5 h at 2 V, 10 Hz followed by 0.5 h at 2 V, 2 Hz.

Fresh GUVs were used within a few hours after preparation.

2.6.3 Enzymatic coupling of Atg8 to membrane in vitro

Three μM Atg8 were enzymatically linked to PE within model membranes as described earlier in (Kaufmann et al., 2014). Briefly, pre-activated Atg8, expressed without its C-terminal arginine, was incubated with Atg7 and Atg3 at a molar ratio of 3:1:1 for 30 min at 30°C in the presence of 0.5 mM ATP and $MgCl_2$ and 0.1 mM DTT in conjugation buffer (10 mM Tris pH 7.2, 137 mM NaCl). In parallel Atg12-Atg5 and Atg16 (provided by Viola Beier) were pre-mixed, continuing the molar ratio with 0.5 each, but kept at 4°C. Both mixes were added to the model membranes and conjugation was allowed to proceed for 30 min at 30°C.

2.7 Fluorophore-based techniques in vitro

2.7.1 Fluorescent labeling of proteins and calculation of DOL

Recombinantly expressed proteins were fluorescently labeled with either thiol- or amine-reactive dyes. For labeling of the thiol group of a cysteine, C5-maleimide-activated dye dissolved in dimethylsulfoxid (DMSO) was added in a 1:1 molar ratio to the protein in 25 mM Tris pH 7.2, 275 - 300 mM NaCl and incubated by gently mixing at room temperature for 30 - 60 min. Unbound dye was removed by gelfiltration over two consecutive HiTrap desalting columns (GE Healthcare) and the labeled protein was concentrated in Vivaspin4 spin columns of appropriate M_w cut off (Sartorius). Only labeled Atg13 was dialyzed against 25mM Tris pH 7.4, 250mM NaCl, 5% glycerol to remove unbound dye. Protein concentration was calculated from 10 mm absorbance of the sample at 280 nm and maximum dye absorbance according to M = [A_{280} − A_{dye}] x dye correction factor CF_{dye} / protein molar extinction coefficient ε_{prot}], the labeling efficiency (degree of labeling, DOL) was determined according to A_{dye}/ dye molar extinction coefficient ε_{dye} x protein concentration M. Constants used for dyes are listed in Table 5, extinction coefficient ε for proteins is given in Table 6.

Prior to labeling with amine-reactive dyes the protein was desalted by gelfiltration on two consecutive HiTrap desalting columns into phosphate buffered saline (PBS) supplemented with 0.2 mM $NaHCO_3$ and 362 mM KCl to a total of 500 mM salt. Protein and *N-hydroxysuccinimide* (NHS) ester coupled dye dissolved in DMSO were incubated at a 1:1 molar ratio for 30 minutes, gently shaking at room temperature. Unbound dye was then removed by another desalting step into Atg11 buffer. Protein concentration and labeling efficiency was determined as described above.

Labeled proteins were either used freshly or frozen in liquid N_2 and stored at -80°C.

Table 5 - Characteristics of small chemical fluorescent dyes employed during this study.

dye	ε_{dye} [$cm^{-1}M^{-1}$]	CF_{280}	A_{dye} [nm]
PacificBlue[1]	30 000	0.20	409
Atto488[2]	90 000	0.10	501
AlexaFluor488[3]	71 000	0.11	494
Atto565[4]	120 000	0.16	563
Atto633[5]	130 000	0.06	629
AlexaFluor633[6]	100 000	0.55	632

Extinction coefficient of the dye (ε_{dye}), correction factor for absorption of the dye at 280 nm (CF_{280}) and wavelength at which the dye reaches maximum absorption (A_{abs}). Sources: [1] PacificBlue Protein Labeling Kit Product Information, 16-August-2005; [3] AlexaFluor 488 Protein Labeling Kit Product Information, 01-December-2006; [6] AlexaFluor 633 Protein Labeling Kit Product Information, 17-October-2004 (all Molecular Probes, Invitrogen, now Thermo Fisher Scientific); [2] Atto488 Product Information, 16-05-2011; [4] Atto565 Product Information, 16-05-2011 (both Atto-Tec GmbH); [5] Atto633 NHS ester Product description (Sigma Life Sciences).

Table 6 – Proteins expressed recombinantly in this study and their characteristics.

protein	sequence	M_w [Da]	ε_{prot} [$cm^{-1}M^{-1}$]	pI
Atg11	GP-Atg11-E-H_6	136 130	92 170	5.95
Atg11[YA]	GP-Atg11_YxA-E-H_6	136 039	90 890	5.90
Atg11[N]	GP-Atg11_1-667-E-H_6	78 165	63 580	5.84
Atg11[C]	GP-Atg11_968-1178-E-H_{10}	25 517	22 190	9.52
Atg32	GP-Atg32_1-376	41 901	15 930	5.75
Atg32[SE]	GP-Atg32_1-376_S114E	41 943	15 930	5.62
Atg32[WG]	GP-Atg32_1-376_W86G	41 772	10 240	5.75
Atg32[SE,WG]	GP-Atg32_1-376_S114E_W86G	41 814	10 240	5.62
Atg8	GP-C-Atg8_1-116	13 728	7 680	8.71

Amino acids linked to the canonical protein sequences or their annotated fragments are indicated in single letter code. Mutations are given by the original amino acid and its location, followed by the inserted mutation. The molecular weight (M_w) of each protein, the extinction coefficient of the protein (ε_{prot}) and the isoelectric point (pI) were calculated by Protein Calculator v3.4 (C. Putnam, The Scripps Research Institute, USA).

2.7.2   Polymerization and fluorescent labeling of actin

Labeling of actin (rabbit skeletal muscle, purchased from Cytoskeleton Inc.) was performed on polymerized actin. Actin was diluted in G buffer (5 mM HEPES pH 8.0, 0.2 mM $CaCl_2$, 0.2 mM ATP) and supplemented with F-solution (10x stock: 500 mM KCl, 20 mM $MgCl_2$, 100 mM Imidazole) and 1 mM EGTA. After incubation at room temperature for 30 minutes, actin polymers were pelleted by centrifugation at 157000 g for 30 minutes at 22°C. The pellet was resuspended in 45 µl G buffer and incubated on ice for 10 minutes. Actin was polymerized

again by addition 5 µl 10x F-solution and 0.2 µl 250mM EGTA and incubation at room temperature for 30 minutes. Atto dye-NHS ester was added at a 1:1 molar ratio and incubated at room temperature for 1 hour. Labeled actin polymers were pelleted by centrifugation at 157000 g for 30 minutes at 22°C. Supernatant was removed and actin resuspended in 50 µl G buffer and incubated on ice for 10 minutes to yield labeled actin monomers.

2.7.3   Fluorescent labeling of lipid

Labeling of the headgroup of the lipid POPE with Atto633 NHS-ester requires deprotonation of the dye. Therefore NaOH was added to 125 mM final concentration to Atto633 dissolved in DMSO. Deprotonated dye was added at a 1:1 molar ratio to POPE dissolved to 1.25 mg/ml in chloroform. Labeling was allowed to proceed at RT for 1 h and was confirmed via mass spectrometry. Aliquots of labeled lipid were stored at -80°C until use.

2.7.4   FRET assay

A constant amount of Alexa488 (Thermo Fisher Scientific)-labeled Atg11 was mixed with a dilution series of Alexa568-labeled Atg9-vesicles in 25 mM HEPES pH 7.0, 100 mM NaCl or a dilution series of Alexa568-labeled Atg13 in 25 mM Tris pH 7.4, 160 mM NaCl in a total of 50 µl. As control, the same dilution series was mixed with constant amounts of free Alexa488 dye. All measurements were performed in triplicates. Samples were incubated at room temperature for 1 hour before fluorescence was assessed by reading 470 nm excitation / 610 nm emission in a BioTek Synergy Neo plate reader. Fluorescence of control samples was subtracted from sample values to correct for bleed-through of donor dye, direct excitation of acceptor dye and non-specific energy transfer.

2.7.5   Confocal fluorescence microscopy of GUVs
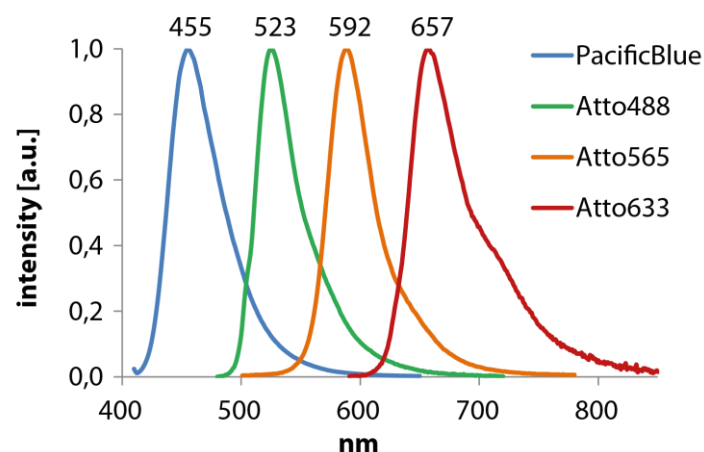
Figure 3 - Emission spectra of dyes employed in multi-color confocal microscopy. Peaks are indicated: 455 nm for PacificBlue, 523 nm for Atto488, 592 nm for Atto565 and 657 nm for Atto633. Imaging was performed in two steps (PacificBlue+Atto565, followed by Atto488+Atto633) to reduce bleed-through. Data for PacificBlue provided on the website of Chroma Technology, all others of Atto-Tec GmbH.

GUVs were observed by fluorescence microscopy in solution on a 8-chambered #1.0 Borosilicate coverglass (Lab-Tek, Thermo), pre-treated with 5 mg/mL BSA to reduce adherence to the coverglass. 100 µL of fresh GUV suspension was mixed in every chamber with 85 µL Atg8-conjugation suspension and up to 15 µL proteins of interest (0.1-1 µM final concentration each) in 25 mM Tris pH 7.2, 137 mM NaCl. In vitro reconstruction of specific autophagy required 4-color imaging; dyes for labeling proteins and membrane were chosen according to their separated emission spectra (see Figure 3). Imaging on a ZEISS LSM780 confocal laser scanning microscope equipped with a ZEISS Plan-APO 63x/NA1.46 oil immersion objective was carried out at RT. Bleed-through of other channels was prevented by two-step recordings (PacificBlue and Atto565, followed by Atto488 and Atto633) and setting conservative filter cut-offs. ImageJ was used for adjustment of brightness and creating sections to better present areas of interest.

3 Results

3.1 Purification and characterization of Atg11

Atg11 is the only known protein essential for most forms of specific autophagy in *S.cerevisiae*. However, its function and regulation is poorly understood. Studying the function of a single protein in a cell biological context is always complicated by the presence of all other cellular components. Insights on protein-protein interactions and their regulation can be obtained by studying protein functions in in vitro systems with controlled conditions. Therefore, a bottom-up approach was chosen for the study of the function of Atg11. Consequently, purified protein was required.

3.1.1 Recombinant expression and purification of full length Atg11

Full length Atg11 had never been successfully recombinantly expressed and purified before the start of this project. Therefore, initial expression tests of Atg11 were performed in *E.coli* for this study, which resulted in insoluble protein, suggesting incorrect folding. Additionally, degradation of Atg11 complicated purification of the full length protein. Expression tests in DDY1810 yeast cells of His-tagged Atg11 resulted in successful expression but fast degradation and insolubility, impeding the efficient purification of soluble full length protein. SF9 insect cells did not express any His-tagged Atg11. However, His-MBP-tagged Atg11 was expressed successfully in Baculovirus-infected H5 and SF9 cells. The beneficial effects of a solubility increasing maltose binding protein (MBP)-tag and the additional folding machinery of higher eukaryotic cells present in insect cells suggested that full length Atg11 requires assistance with folding. Though extensive optimization resulted in insect cells producing full length His-MBP-Atg11 without degradation, the final yield was rather low. Best expression was finally achieved by BL21(DE3) *E.coli* in TB media at 18°C overnight from a pCoofy37 vector (see plasmid list Table 3) with an N-terminal MBP-tag for increased solubility and a C-terminal His_6-tag for purification of only untruncated Atg11 (see construct 1 in Figure 5). Additionally, correct folding was facilitated by co-expressed chaperones dnaK, dnaJ, grpE, groEL and groES. Isolation of Atg11 from periplasma cleared cell lysates was performed via a Ni^{2+}-charged IMAC column (see elution in Figure 4 A). The MBP-tag was cleaved from Atg11 at a PreScission protease site. No sample was lost with a 0.2 μm PVDF filter, indicating that, once folded, recombinant Atg11 is also stable without a solubility tag (see Figure 4 B for samples of every step during the purification process).

Final purification of Atg11 by size exclusion chromatography (SEC) on a Superdex200 column could not separate high molecular weight molecules since Atg11 localized to the void volume. This suggests an elongated, rod-like structure of Atg11, or oligomerization. Best separation from impurities was achieved on a Superose6 Increase 10/300 GL column, resulting in highly pure protein with minimal dnaJ and degradation product contamination

(see Figure 4 C,D). One protein of similar size and reactivity to α-His antibody and therefore probably also Ni^{2+}-NTA could not be separated entirely. Its properties suggest that it is either a large C-terminal degradation product or a conformational variant. Since its amount was always substantially lower than that of full length Atg11, further separation was not required.
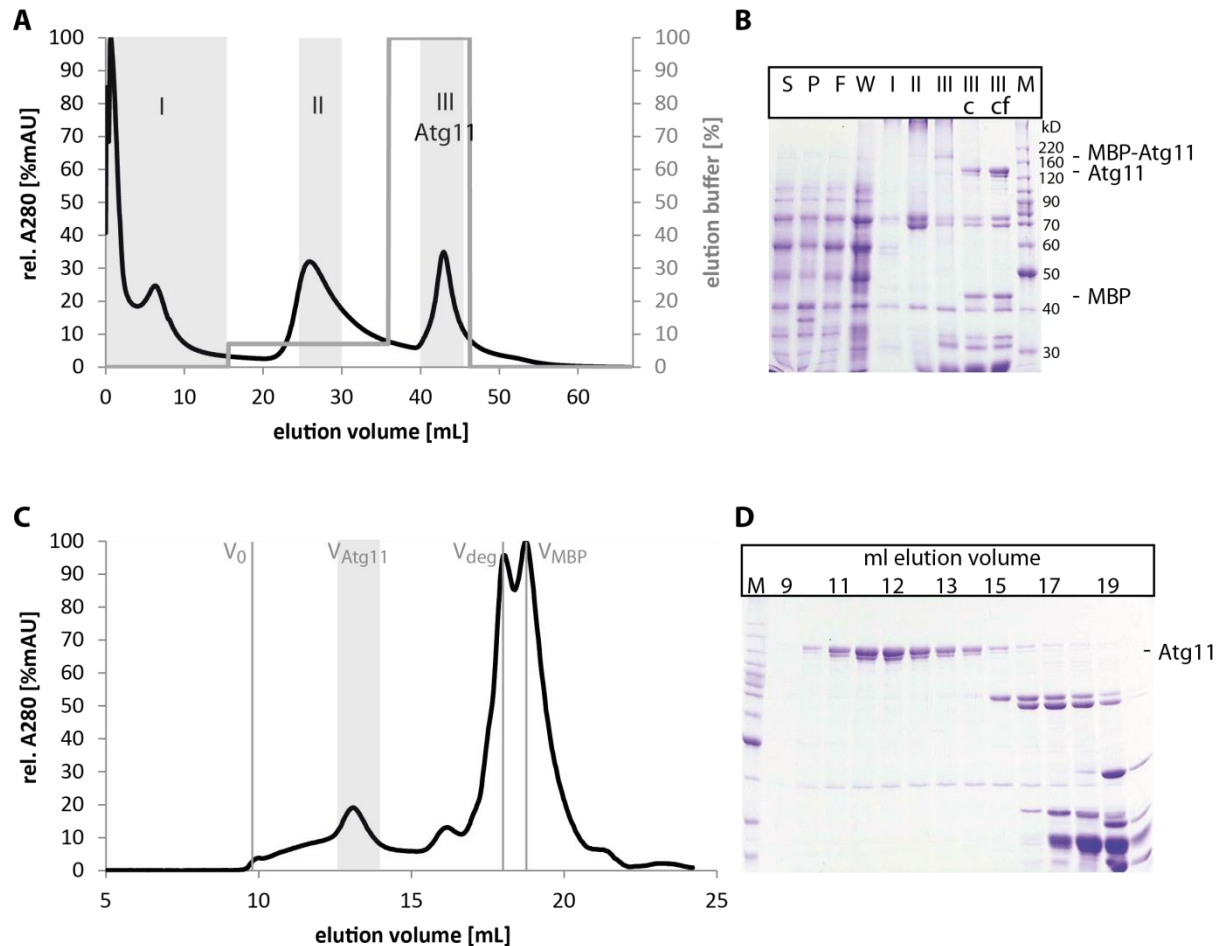
Figure 4 - Elution profiles of Atg11 chromatography and SDS-PAGEs of samples taken. **(A)** Elution profile of IMAC column, pooled fractions indicated. **(B)** Fractions of the step-wise purification of Atg11: soluble (S), pellet (P), flow-through after IMAC loading (F), IMAC washing (W), IMAC elution I (I), IMAC elution II (II), pooled fraction containing Atg11 (III), MBP cleaved off pool III (IIIc), IIIc filtered (IIIcf), marker (M). **(C)** Elution profile of pool IIIcf applied to a Superose 6 Increase 10/300 GL column, void volume (V_0), Atg11 pool (V_{Atg11}), degradation products (V_{deg}) and MBP (V_{MBP}) are indicated. **(D)** 10% SDS-PAGE of samples from 9 to 20 mL elution from (C).

3.1.2 Recombinant expression and purification of Atg11 fragments
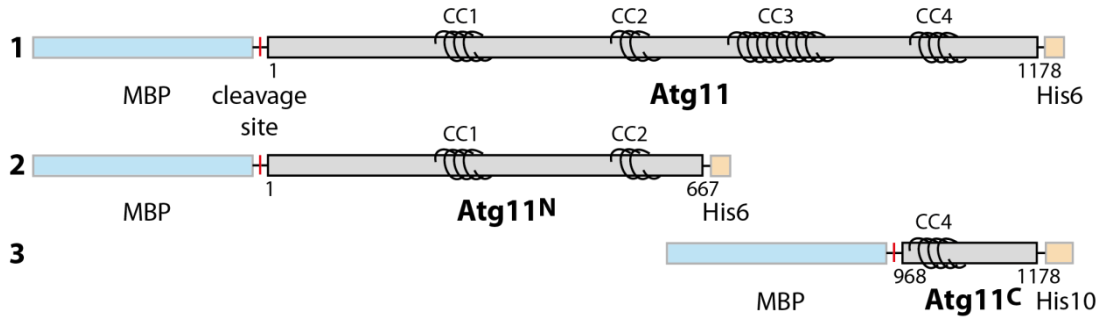
Figure 5 – Constructs used for expression of Atg11 and its fragments. Proteins were fused N-terminally to an MBP-tag, which can be cleaved off with PreScission protease (red line). A His_6- or His_{10}-tag was added C-terminally. **(1)** Full length Atg11 comprises all amino acids from 1 to 1178. **(2)** $Atg11^N$ comprises amino acids 1 to 667 of Atg11. **(3)** $Atg11^C$ comprises amino acids 968 to 1178 of Atg11.

Atg11 is a large protein with no predicted functional domains. In order to assign and investigate the function of individual domains, stable fragments are required. Therefore degradation products of the full length protein were analyzed according to their size and location within Atg11. An N-terminal fragment of 667 amino acid length ($Atg11^N$) was identified as relatively stable degradation product of full length Atg11. For increased solubility it was expressed with a cleavable N-terminal MBP-tag and a C-terminal His_6-tag was added for affinity purification (see construct 2 in Figure 5). $Atg11^N$ was expressed by BL21(DE3) in TB media, but no co-expression of chaperones was required for correct folding. Batch purification with Ni^{2+}-NTA affinity resin followed by SEC on a Superdex200 16/60 (Figure 6 A, B) yielded about 2.5 mg of purified protein from 6 L of TB culture. $Atg11^N$, a protein of 78.2 kD, eluted from SEC at about 61 ml, indicating either a highly elongated conformation or oligomerization.

A stable fragment of 211 C-terminal amino acids of Atg11 (amino acid 968-1178, termed $Atg11^C$) was identified, too. Interestingly, this fragment contains the CC4 domain and cargo interaction sites. Expression was performed as described for full length Atg11 purification (see construct 3 in Figure 5). Batch purification with Ni^{2+}-NTA affinity resin and SEC on a Superdex75 16/60 yielded about 3.5 mg protein from 6 L TB culture. Correct mass of 25.5 kD was confirmed with mass spectrometry.
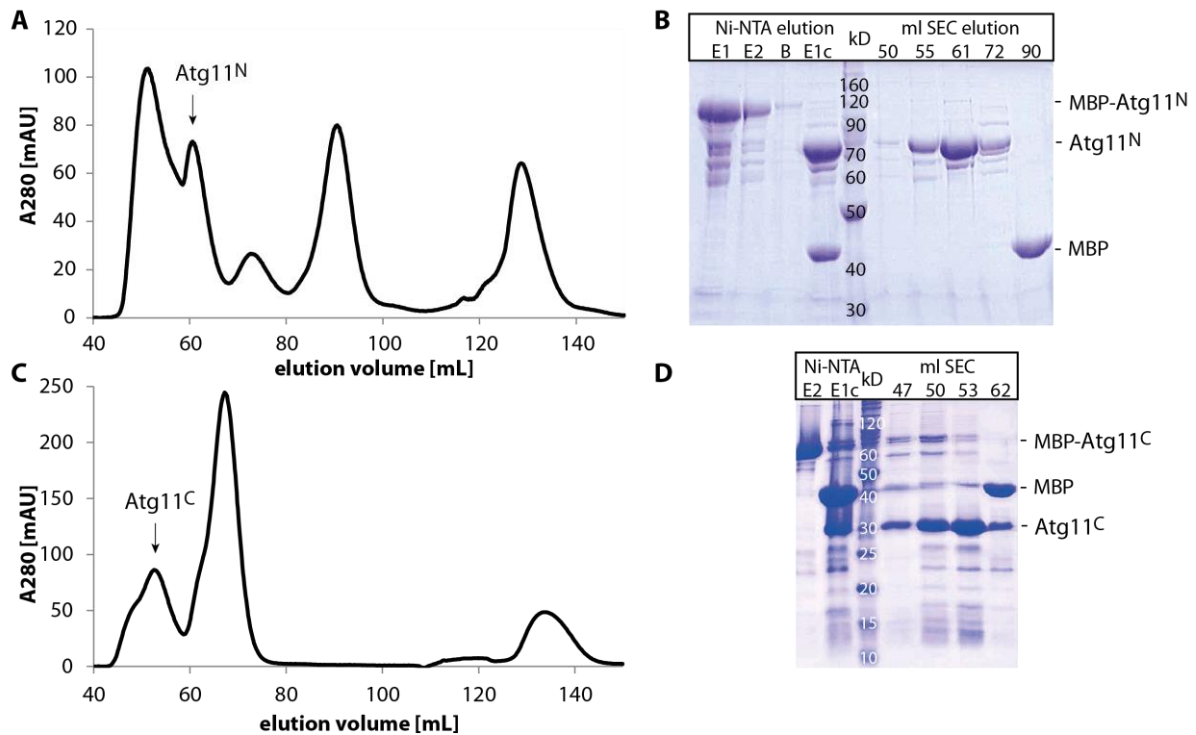
Figure 6 - Purification of recombinant Atg11^N and Atg11^C. **(A)** Elution profile of SEC Superdex200 column; the second peak corresponds to Atg11^N. **(B)** 12% SDS-PAGE with samples from batch Ni-NTA elution: first elution from Ni-NTA beads (E1), second elution (E2), beads after elution (B), MBP cleaved E1 (E1c). Samples taken from SEC shown in (A) at indicated elution volumes. **(C)** Elution profile of SEC Superdex75 column; peak containing Atg11^C is indicated. (D) 15% SDS-PAGE with samples from batch Ni-NTA elution: second elution from Ni-NTA beads (E2), MBP cleaved E1 (E1c). Samples taken from SEC shown in (C) at indicated elution volumes.

3.1.3   Biophysical characterization of Atg11

Recombinant expression and purification of soluble protein does not guarantee a correctly folded, functional protein. Further characterization is necessary to ensure protein integrity prior to using it in functional studies. Mass spectrometric analysis of full length Atg11 confirmed sample purity; only negligible amounts of impurities were present (see Figure 7 A). The measured mass agreed with the calculated mass of 136 130 Da for full length Atg11 with a glycine and proline residue left N-terminally from PreScission protease digestion. The C-terminal His$_6$-tag was retained for protein detection in western blotting later on.

The low retention volume of Atg11 suggested that it might be oligomeric or adapt a strongly elongated fold. To further characterize Atg11, analytical ultracentrifugation (AUC) was performed (see Figure 7 B). More than half of the total protein amount sedimented at 5.39 S (6.87 S normalized to 20°C in water), exhibiting a hydrodynamic radius (R_H) of 6.02 nm. The friction ratio (f/f_0) of 1.63 allowed the calculation of a mass of 173 kD, corresponding to monomers of Atg11. The friction ratio is above the value for a perfect compact sphere (f/f_0 = 1), indicating that Atg11 monomers exhibit a higher friction than a perfect sphere due to a moderately elongated fold of the protein. 16% of the total protein mass sedimented at 7.35 S (20°C,w: 9.36 S) with a R_H of 7.02 nm. The Mw of 275 kD corresponds very well with Atg11 dimers. Since the friction coefficient remained at 1.63 in this calculation, an overall similar

shape of monomers and dimers can be concluded. The remaining 30% of the sample mass forms populations of higher S in regular intervals, suggesting a tendency of Atg11 to form higher oligomers by adding further monomers.
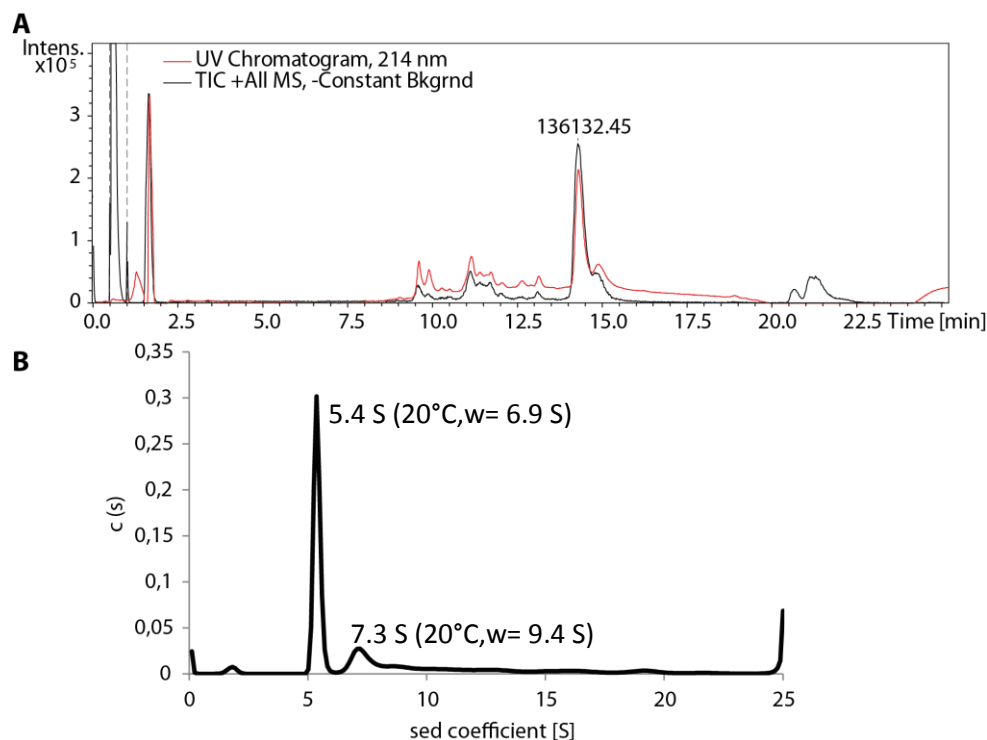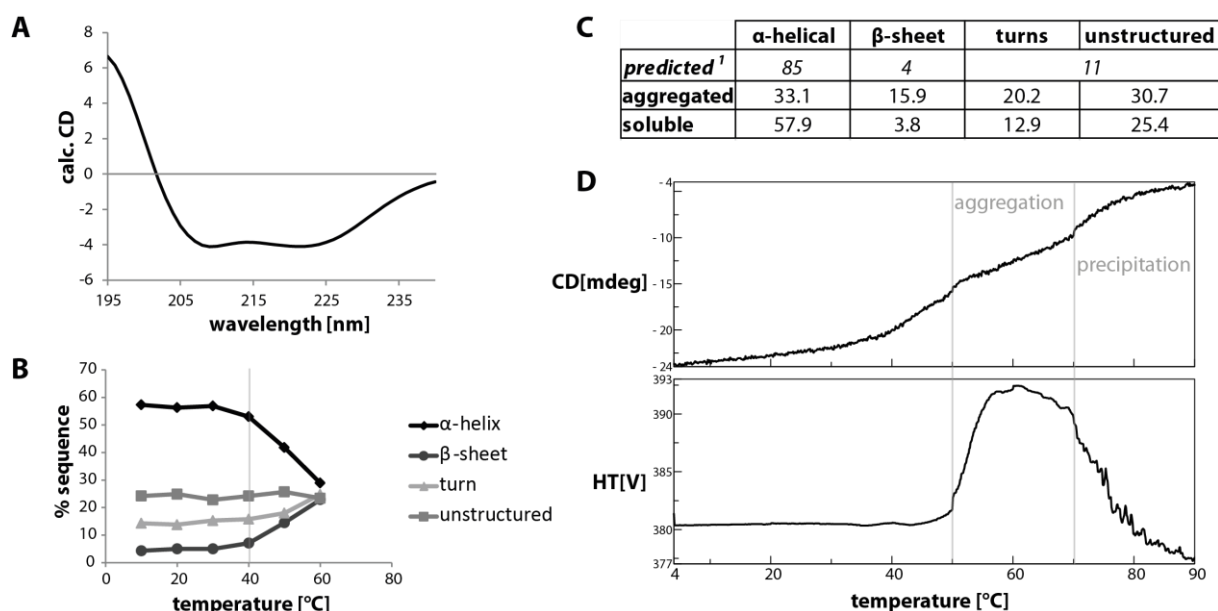

Figure 7 - Mass spectrometry and analytical ultracentrifugation confirm identity and purity of Atg11. **(A)** UV and Total Ion Current (TIC) chromatogram of mass spectrometric analysis of purified Atg11. The mass of the main population agrees with calculated mass for the recombinant protein. **(B)** Sedimentation velocity analysis of recombinantly expressed Atg11 performed at 50000 rpm in an Optima XL-I ultracentrifuge. Besides the major population at about 5.4 S, the sample contains minor amounts of higher molecular weight oligomers.

Secondary structure prediction of Atg11 (ppopen.informatik.tu-muenchen.de) suggests several coiled-coil domains to be present in Atg11. The overall α-helical content was calculated to be 85%, in line with the elongated conformation indicated by AUC. Only 4% are able to form β-sheets and 11% remain unstructured (Figure 8 C, first line). Correct folding of the recombinantly expressed protein was verified with circular dichroism (CD) measurement and analyzed with CONTIN algorithm in SPM-2 Spectra Analysis software (Figure 8 A). Atg11 from concentrated void volume of Superdex200 elution, which contains both soluble and aggregated protein, consisted of only 33.1% α-helix and 15.9% β-sheet. These numbers were significantly changed by ultracentrifugation of the sample for 30 min at 66 000 rpm, clearing the sample of aggregates. Cleared sample consisted of 57.9% α-helix, 3.8% β-sheet, 12.9% turns and 25.4% remained unstructured. Summarized, the fold of the recombinantly expressed soluble protein corresponds very well with the prediction (Figure 8 C). It can therefore be assumed that recombinant Atg11 adopts its native, biologically active,

fold and is suitable for the use in functional studies.

The stability of Atg11 was characterized by recording melting curves. First, CD spectra were recorded as a function of the temperature between 4°C to 90°C at every 10°C increase. Correct folding remained stable between 4 and 30°C, and unfolding of Atg11 was observed at temperatures > 40°C. The spectra were fitted until 60°C, when aggregation prevented any further structure determination (Figure 8 B). Leading up to aggregation, a change in folding could be observed. The predominantly α-helical structure dissolved, concomitantly with an increase of β-sheets. Therefore, aggregated protein featured a higher percentage of β-sheets. In a second step, CD was monitored at 222 nm and the change of high tension voltage (HT) of the detector was recorded. The abrupt change in the CD slope at 50°C indicated that the protein melting point was exceeded (Figure 8 D). At this temperature, more than 50% of the protein assumes a state of aggregation, illustrated by the subsequent rapid increase of HT. Aggregated protein transmits less light than properly folded residues and hence forces the detector to increase its gain (by increasing the voltage) to still record the remaining signal. Aggregation is followed by irreversible precipitation at about 70°C, indicated by a sudden decline of HT. This suggests that irreversible aggregation of Atg11 is preceded by a shift from α-helical to β-sheet conformation. Since aggregated protein in recombinant expression contains a high amount of β-sheets, improper folding seems to cause insoluble Atg11.

	α-helical	β-sheet	turns	unstructured
predicted [1]	*85*	*4*		*11*
aggregated	33.1	15.9	20.2	30.7
soluble	57.9	3.8	12.9	25.4

Figure 8 - Secondary structure analysis of Atg11 by CD. **(A)** CD spectra of Atg11 sample containing aggregates, used for fitting to determine % of secondary structures. **(B)** Change in amount of secondary structure elements upon heating of Atg11. **(C)** Secondary structure of Atg11 in % of the predicted folding, and calculated from CD measurements of a sample containing aggregates and a purified sample consisting mainly of soluble protein. [1] secondary structure of Atg11 predicted at ppopen.informatik.tu-muenchen.de **(D)** Continuously monitored CD at 222 nm and detector voltage as function of temperature reveals step-wise structural changes of Atg11 at 50°C and 70°C: aggregation and precipitation, respectively.

3.1.4 Identification of stable Atg11 fragments

Preparations of Atg11 contained impurities of lower molecular weight, which were thought to be truncation products of Atg11. In order to identify domain boundaries, limited proteolysis was performed. Short-term treatment of Atg11 with the protease trypsin produced two prominent degradation products of around 65 and 75 kD, respectively. Upon prolonged incubation, degradation proceeded until complete digestion of the protein. Truncations of Atg11 were also introduced during long-term incubation at room temperature or at 4°C. Strikingly, degradation consistently resulted in the above mentioned two similar-sized products (see **Figure 9** A). Edman sequencing of the slightly larger fragment produced the sequence GPMADAD, which is equivalent to the N-terminal start of Prescission-cleaved Atg11. The second fragment started with (F)LGASVLLE, corresponding to Atg11_(675)676. Evidently, Atg11 is amenable to proteolytic cleavage after amino acid 674, resulting in a stable N-terminal domain of Atg11$^{1-674}$, and a rather degradation-prone C-terminal fragment. The sequence leading up to the identified cleavage site (KKK) suggests tryptic digestion. Therefore a mutation was introduced (KKK to STS) to prevent recognition and cleavage. However, mass spectrometry of Atg11^{STS} stored for two weeks at 4°C showed that all full length Atg11 had been degraded to the N-terminal fragment and several C-terminal degradation products (see **Figure 9** B). Importantly, the cleavage can be prevented by addition of a reducing agent like Tris(2-carboxyethyl) phosphine (TCEP). Atg11 treated with 5 mM TCEP for two weeks at 4°C remained mostly full length (see **Figure 9** C).
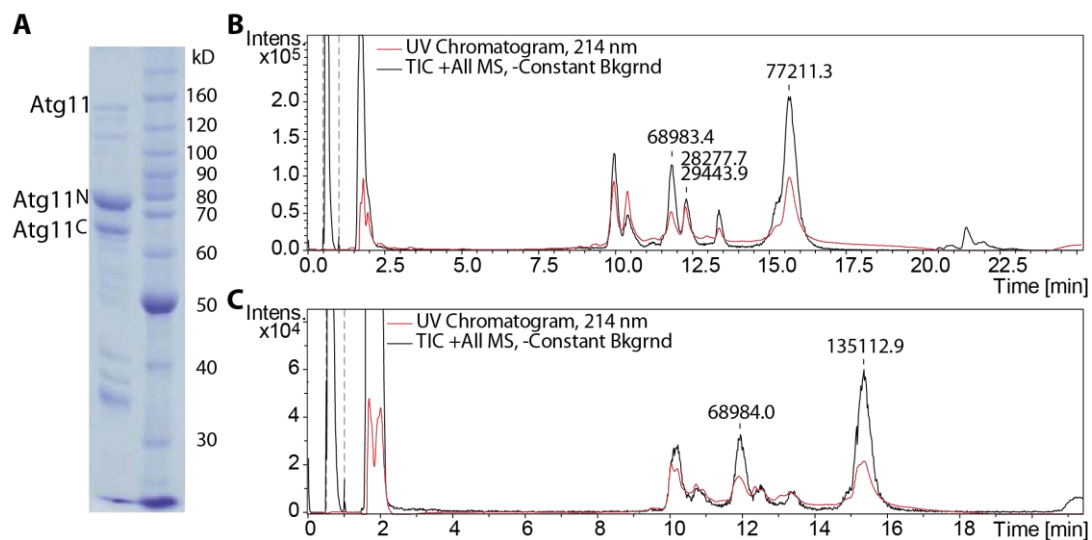
Figure 9 - Atg11 has a cleavage site after amino acid 674. **(A)** 10% SDS-PAGE of degraded Atg11 subjected to Edman-sequencing. Most full length protein has been cleaved into a stable N-terminal and a C-terminal half. Cleavage occurs after amino acid 674. **(B)** UV and Total Ion Current (TIC) chromatogram of mass spectrometric analysis of Atg11^{STS} after two weeks stored at 4°C. All full length protein has been degraded into an N-terminal and two small C-terminal fragments. **(C)** Mass spectrometric UV and TIC chromatogram show that Atg11 stored for two weeks at 4°C in the presence of 5 mM TCEP remained full length. Protein of 68984 Da is the bacterial chaperone dnaK.

3.2   In vitro reconstitution of selective autophagy

Atg11 has been reported to be a scaffold for recruitment of the autophagic machinery in selective autophagy (Kamber et al., 2015). It involves colocalization of Atg11, cargo, and the Atg1 kinase complex at the PAS. To reveal the order of assembly of the components, the process was reconstituted in vitro. The in vivo pathway was mimicked with artificial membranes and recombinantly expressed proteins. Giant unilamellar vesicles (GUVs) served as membrane template to assemble the machinery. Atg8 is an important membrane-bound cargo adaptor and can be conjugated enzymatically to GUVs (Kaufmann et al., 2014). Specific cargo is recognized via cargo receptors and targeted to autophagic membranes in an Atg11-dependent manner. Cargo receptors harbor an Atg8-interacting motif (AIM), which they can use for direct interaction with Atg8. This interaction allows the autophagic membrane to closely wrap around specific cargo like mitochondria and therefore yields selective autophagy to also be exclusive (Sawa-Makarska et al., 2014). The degradation of mitochondria, termed mitophagy, is mediated by the mitochondrial cargo receptor Atg32 (Okamoto et al., 2009). Consequently, cargo was represented by latex beads decorated with the cargo receptor Atg32. The order of recruitment and influence of mutations on the system was analyzed by confocal fluorescence microscopy.

3.2.1   Recombinant expression and purification of soluble Atg32

The transmembrane protein Atg32 mediates degradation of mitochondrial fragments by mitophagy (Okamoto et al., 2009). Anchored in the outer mitochondrial membrane, it becomes activated by phosphorylation to interact with Atg11 (Aoki et al., 2011). The canonical AIM at position 86 mediates interaction of Atg32 with Atg8 (Okamoto et al., 2009). For the purpose of in vitro reconstitution of selective autophagy, the cytoplasmic domain of Atg32 was expressed as a soluble protein. Several constructs with C-terminal deletions of different lengths were designed, based on primary and secondary structure prediction. Expression was tested of all constructs N-terminally tagged with His_6, His_6-GST and His_6-MBP. Best expression was achieved of His_6-Atg32$^{1-376}$ in Rosetta(DE3) in LB media. Batch purification via Ni^{2+}-NTA affinity resin was followed by Prescission protease cleavage of the His_6-tag. The protein was purified using a Superdex200 SEC column, from which it eluted at 71 ml (Figure 10 A). Mass spectrometric analysis confirmed identity and purity of the protein (Figure 10 C). Solubility of Atg32 in different buffer conditions was analyzed by dynamic light scattering (DLS). Atg32 in 300 mM NaCl was a monodisperse sample with R_H = 4.5 nm. Atg32 proved sensitive to changes in salt concentration, since a reduction induced reversible aggregation. More in-depth analysis of protein oligomerization was achieved via AUC, which detected two major populations (Figure 10 B). Since mass spectrometry excluded the presence of large amounts of contaminations (Figure 10 C), Atg32$^{1-376}$ likely exists in a monomer – dimer equilibrium. While 25% of the sample had a Stokes radius of 2.89 nm and

sedimented at 2.68 S (20°C,w), 54% had a Stokes radius of 3.47 nm and sedimented at 3.89 S, likely corresponding to dimeric Atg32.
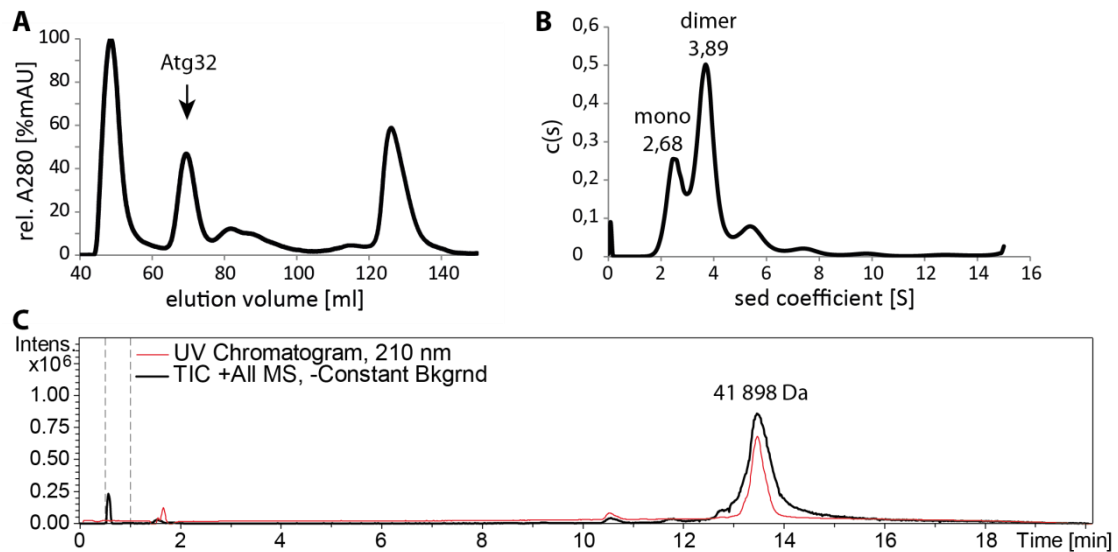
Figure 10 – Purification of Atg32$^{1-376}$. **(A)** Superdex200 elution profile. Atg32$^{1-376}$ elutes at around 71 mL. **(B)** Analytical ultracentrifugation of recombinantly expressed Atg32$^{1-376}$ reveals a monomer – dimer equilibrium. The major population is the dimer with a sedimentation coefficient of 3.89 S. **(C)** Mass spectrometry of the sample analyzed in (B). Only one population can be detected, corresponding to Atg32$^{1-376}$ with a mass of 41 898 Da.

Many cargo receptors have been found to be activated by phosphorylation. Therefore a pre-activated variant of Atg32$^{1-376}$ was cloned and expressed. To ensure interaction with Atg11 (Aoki et al., 2011), serine 114 was mutated to a phosphomimetic glutamate, resulting in Atg32^{SE}. Many proteins interacting with Atg8 have been found to carry a canonical Atg8 interaction motif, termed AIM. The sequence [W/F/Y]xx[L/I/V] is conserved from yeast to mammals (Noda et al., 2010) and is present in Atg32 (Okamoto et al., 2009). To study Atg32 recruitment independent of Atg8, another Atg32 variant was produced that contained a mutation in its AIM. Tryptophane 86 was mutated to glycine, resulting in the variant Atg32^{WG}.

3.2.2 Fluorescent labeling of proteins and membrane

To study the ordered recruitment of components of the machinery coordinating selective autophagy in vitro, the individual analytes were tagged fluorescently for confocal fluorescence microscopy. Proteins are commonly expressed as a fusion protein with green fluorescent protein (GFP) or a derivative thereof. However, GFP is a protein of about 27 kD and might therefore sterically block interaction sites of its fusion protein. To overcome this problem, small fluorescent dyes have been developed, which are available in a broad range of colors and can be fused to proteins via chemical linkers. Brightness, photostability and broadness of excitation and emission spectra are major factors to be considered when choosing a set of fluorescent dyes for multi-color imaging. Here, four-color imaging required

coupling of fluorescent dyes with non-overlapping absorption and emission spectra within the visible range of light to proteins and lipid.

Analytes can be conjugated to dyes either via the thiol group in cysteines or primary amines in lysines and the N-terminus of a polypeptide chain. Since most proteins only have few cysteines, they can be used for controlled, sometimes even site-directed, labeling. However, though it can be advantageous to label proteins at a specific site, consistent labeling can cause sterical hindrance. Since most proteins harbor several lysines, labeling of amines results in different labeling patterns on each protein. The drawback of this method can be massive labeling.

Atg32 has four cysteines. Atg32$^{1-376}$ was mixed with Atto488 C5-maleimide at a 1:1 ratio for 30 min. Non-coupled dye was removed by desalting on two consecutive HiTrap gel filtration columns and the degree of labeling (DOL) was determined of the concentrated protein. Spectroscopically determined DOL was 1.5, which was confirmed by mass spectrometry (Figure 11 A). While a small portion of the sample remained unlabeled, 1, 2 or 3 Atto488 molecules were coupled to most proteins, revealing that the overall DOL of 1.5 reflects stochastic conjugation of dye molecules to cys-residues. Prediction of hydrophobicity (www. vivo.colostate.edu/molkit/hydropathy) suggests that cys 288 is buried and inaccessible for labeling. This is consistent with a maximum of three coupled dye molecules per protein.

Atg8 was labeled with maleimide-activated dyes at an introduced N-terminal cysteine. Site-directed labeling ensured the reactivity of the C-terminus of the small protein for enzymatic lipid coupling.
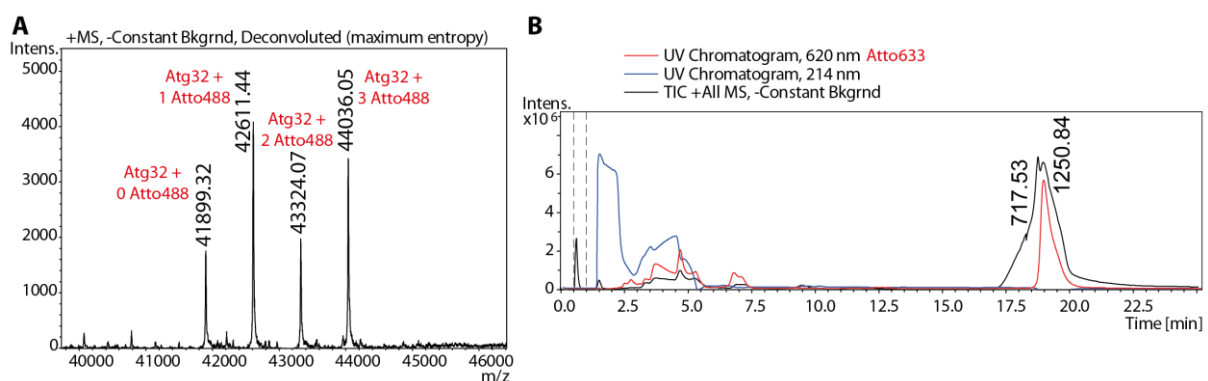
Figure 11 - Mass spectrometry of fluorescently labeled Atg32 and POPE. **(A)** Extracted ion chromatogram of Atto488-labeled Atg32$^{1-376}$. Populations are found for Atg32$^{1-376}$ carrying 0, 1, 2 or 3 labels. **(B)** Total ion current and UV chromatogram of Atto633-labeled POPE. The major peak of 1250.84 Da is deprotonated POPE coupled to Atto633, also marked by the dye's 620 nm UV signal at the same position. It is preceded by a smaller peak of 717.53 Da, corresponding to free deprotonated POPE.

Upon incubation of Atg11 with maleimide-reactive dyes, precipitation of the protein was observed. Atg11 was therefore labeled at its intrinsic lysine-residues with amine-reactive dyes. A benefit of labeling with amine-reactive Atto565-NHS ester was also the sporadic

distribution of labels, avoiding sterical effects in potentially unknown interaction sites. The reaction was performed in high-salt phosphate buffer. Determination of DOL was performed as described above.

Giant unilamellar vesicles (GUVs) are spherical model lipid bilayers of 10-100 μm in diameter. Due to their size they are useful for light microscopic studies of membranes, in this case for modeling of autophagosomal membranes. Artificial membranes were labeled by incorporating approximately 0.5 mol% of lipids coupled to fluorescent dyes. The phosphatidylethanolamine (PE) headgroup of POPE was labeled with deprotonated Atto633 via NHS ester. Labeling efficiency was assessed via mass spectrometry (Figure 11 B), which revealed that almost all Atto633 molecules had been consumed and were coupled to POPE. Some POPE remained unlabeled, which can be incorporated into artificial membranes as normal component.

3.2.3   Mimicking cargo in vitro

Mimicking selective autophagy in vitro requires specific cargo. Since mitophagy is mediated by a mitochondrial surface protein, Atg32 (Okamoto et al., 2009), this protein is thought to be sufficient to link any cargo to the autophagosome. To mimic cargo, functionalized polystyrene beads were coated with the fluorescently labeled mitochondrial cargo receptor Atg32^{SE}. Coupling was confirmed by fluorescence microscopy of the beads, which accumulate at the bottom of the microscopic chamber if they are not bound to GUVs (see Figure 12).

Atg32^{SE,WG}-Atto488
decorated beads
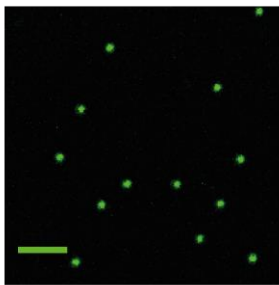
Figure 12 – Mimicking specific cargo in vitro. Polystyrene beads decorated with Atto488-labeled Atg32^{SE,WG} represent mitochondria as specific cargo in in vitro reconstitution of selective autophapy. Scale bar 10 μm.

3.2.4   In vitro reconstitution of selective autophagy including Atg11

The spatial function of Atg11 in cargo recruitment to the autophagosomal membrane was investigated by in vitro reconstitution. Interaction of Atg11 with the autophagosomal membrane is supposedly mediated by Atg8, since *A. thaliana* AtAtg8 was found in close contact with AtAtg11 (Li et al., 2014). Therefore the first step of in vitro reconstitution was enzymatic conjugation of Atg8-Atto488 to PE incorporated in GUVs as performed previously (Kaufmann et al., 2014). Subsequent addition of Atg11^{Atto565} resulted in efficient recruitment of Atg11 to Atg8-decorated membranes, but not to membranes alone (Figure 13). Thus, the

direct interaction of recombinant Atg11 with Atg8 or its conjugation machinery could be shown for the first time in vitro.
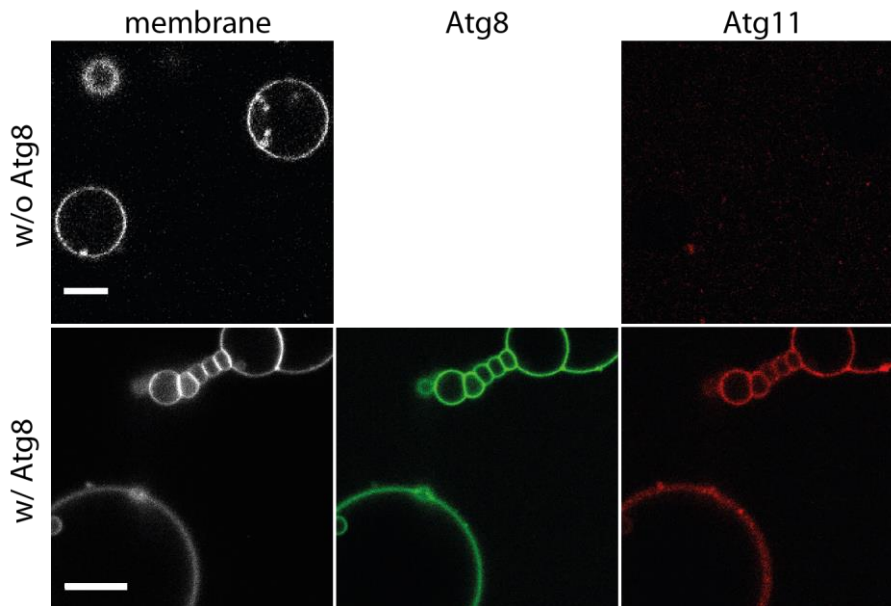
Figure 13 – Atg11 binds GUVs in an Atg8-dependent manner. Atto633-labeled GUVs (grey) were incubated with conjugation machinery and Atto488-labeled Atg8 (green) or left untreated. Atg11[Atto565] (red) was added and colocalized to Atg8-decorated membranes, but not to untreated membranes. Scale bar 10 μm.

In a next step the binding behavior of soluble Atg32 was studied. Atg32 possesses an AIM at position 86, which is essential for its interaction with Atg8 in vivo (Okamoto et al., 2009). To confirm that this is the only binding site for Atg8 within Atg32, Atg8-decorated GUVs were co-incubated with wildtype Atg32 and with a variant, whose AIM had been disrupted (Atg32[WG]). Wildtype Atg32 was recruited to GUVs in an Atg8-dependent manner, but the AIM-mutant Atg32[WG] remained evenly distributed in solution (Figure 14 A). This indicates that the AIM motif of Atg32 is essential for its interaction with Atg8 in vitro. Atg11 has been suggested to crosslink cargo to the autophagosomal membrane by interacting, on the one hand, with cargo receptors, and, on the other hand, with Atg8 on the autophagosomal membrane. The interaction of Atg11 with the cargo receptor Atg32 appears to be phospho-regulated. Phosphorylation of serine 114 is induced and required for functional mitophagy, presumably by mediating the interaction with Atg11 (Aoki et al., 2011). Firstly, an influence of the phosphorylation on the interaction with Atg8 was tested. Addition of a phosphomimetic Atg32 variant, Atg32[SE], to Atg8-decorated GUVs resulted in normal recruitment (Figure 14 A). Therefore, the proposed crosslinking function of Atg11 was tested by adding Atg11 to Atg8-decorated GUVs in the presence of Atg32[WG] or its phosphomimetic variant, Atg32[SE,WG]. While Atg32[WG] is not colocalizing with Atg8 in the absence of Atg11, its addition restores interaction (Figure 14 A,B). Hence, Atg11 can interact simultaneously with the autophagosomal membrane and cargo receptors. Surprisingly, the reported phosphorylation

of Atg32 was not required for interaction with Atg11 in vitro. However, since phosphorylation is required for functional mitophagy due to unknown effects, and phosphomimetic variants did not exhibit any interaction defects, Atg32^{SE} was employed in all further assays to closely mimic the in vivo situation.
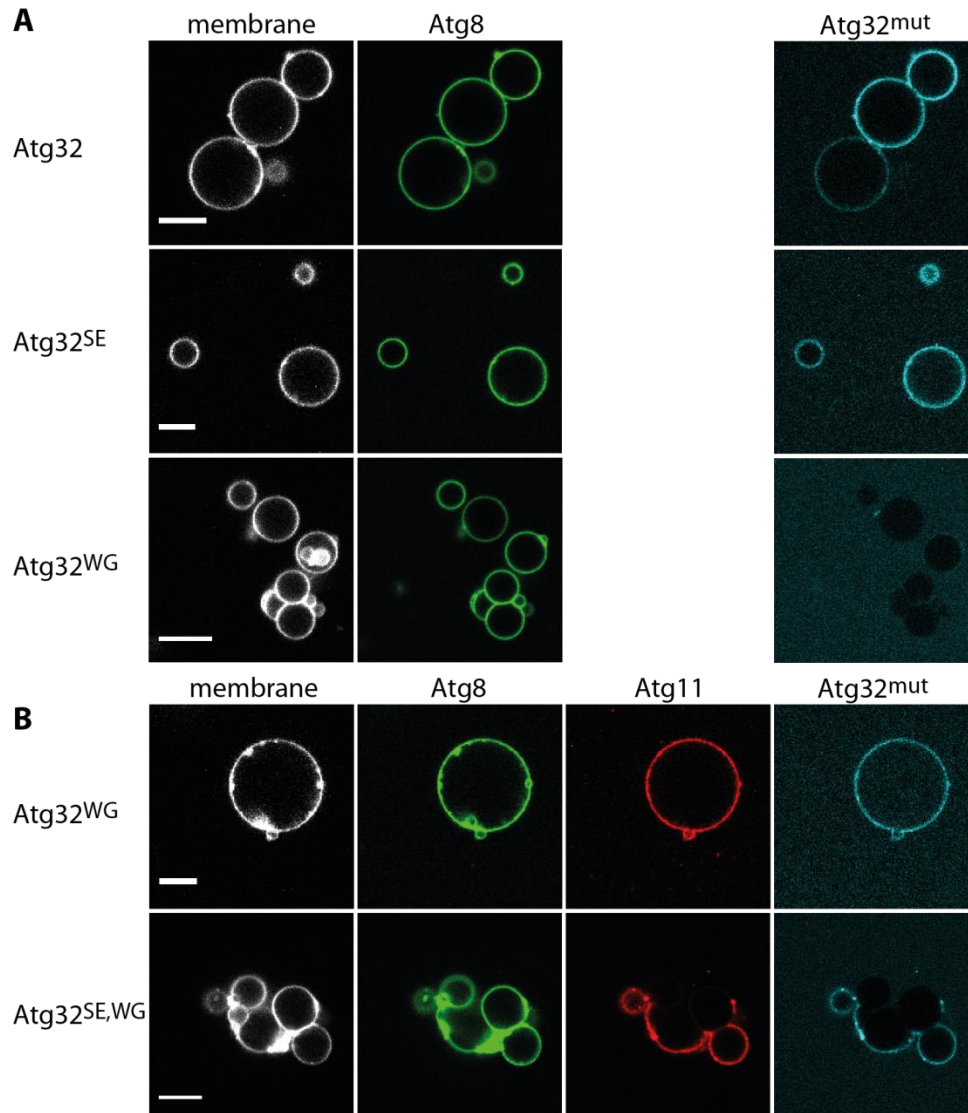
Figure 14 – Interaction of Atg32 variants with Atg8 and Atg11. **(A)** Both wildtype Atg32$^{1-376}$ and Atg32^{SE} are recruited to Atg8 coupled to GUVs. In contrast, Atg32^{WG} remains in solution, proving the disruption of its AIM motif. **(B)** Atg11 added to Atg8 and Atg32^{WG} can interact with both and restores recruitment of Atg32^{WG} to the membrane. Atg32^{WG} and Atg32^{SE,WG} can interact with Atg11 equally well, the phosphorylation is not required. Scale bar 10 µm.

In order to determine the minimal set of proteins sufficient to reconstitute the uptake of model cargo by artificial membranes, soluble Atg32 was replaced in a last step by Atg32^{SE}-decorated latex beads. The beads were expected to be taken up by the GUV in a zipper-like fashion due to numerous contact sites all around the cargo, wrapping the membrane around the bead. The zipper hypothesis was based on the assumption that Atg11 could mediate wrapping of a pre-formed phagophore around specific cargo in vivo. Another

possibility would be that Atg11 recruits the autophagic machinery at the very initial stage and directly mediates elongation of the membrane around the cargo.
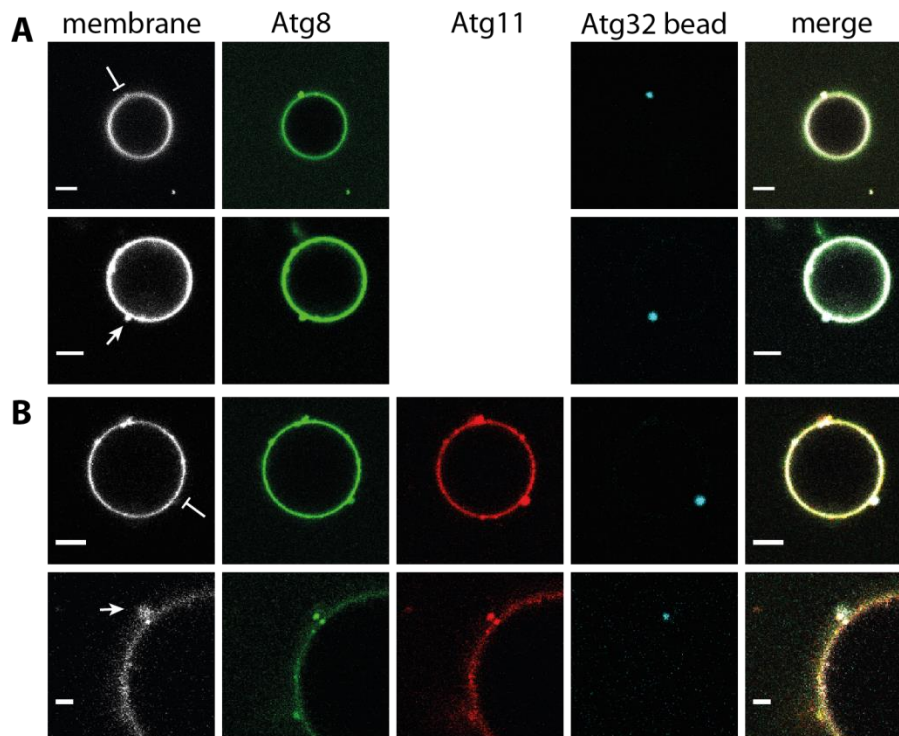
Figure 15 – In vitro reconstitution of selective autophagy. **(A)** PacificBlue-labeled Atg32[SE] coupled to latex beads interacts with Atto488-labeled Atg8 enzymatically lipidated to Atto633-labeled GUV membranes. The interaction can either be a simple surface-to-surface contact without deformation of the membrane (⊥) or the bead is fully enwrapped by the membrane (↑). **(B)** Upon addition of Atto565-labeled Atg11 to the system, it becomes recruited to the membrane; however, membrane deformation is comparable to the situation without (membrane can wrap around the bead (↑), but in many cases does not (⊥). Scale bar 5 µm.

Stepwise addition of all components resulted in interaction of Atg32[SE]-decorated latex beads with lipidated Atg8 (Figure 15 A) and soluble Atg11 (Figure 15 B). While in some cases beads only attached to the GUV via proteins (surface-to-surface), in other cases the membrane seemed to fully enwrap the bead; however, beads were never found inside a GUV. Therefore direct contact of cargo with membrane, mediated by the Atg32-Atg8 interaction, is sufficient to wrap the membrane around the model cargo. Though Atg11 was found to interact with both Atg8 and Atg32 and the presence of Atg11 does not prevent the membrane from wrapping around the cargo, its adaptor function is not required for membrane deformation.

3.3   Analysis of a potential motor protein function of Atg11 in vitro

A minimal system, sufficient to reconstitute the uptake of model cargo by artificial membranes, only requires the interaction of Atg8, coupled to membranes, with the cargo receptor Atg32. Atg11 is able to interact with both the autophagosomal membrane and

Atg32, but it is not required for membrane deformation. Thus, these interactions might be separated in time and space and Atg11 probably has to fulfill a function other than that of a cargo adaptor. Sequence similarities between Atg11 and the actin motor protein Myo2 raised questions about a possible function of Atg11 in the transport of cargo or autophagosomes along actin (Monastyrska et al., 2006). This notion was substantiated by mislocalization of Atg11 following the disruption of actin dynamics (He et al., 2006). In order to characterize direct interaction of Atg11 with actin filaments, purified Atg11 and actin were analyzed in vitro by fluorescence microscopy and differential centrifugation.

3.3.1 Atg11 found to interact with actin in fluorescence microscopy
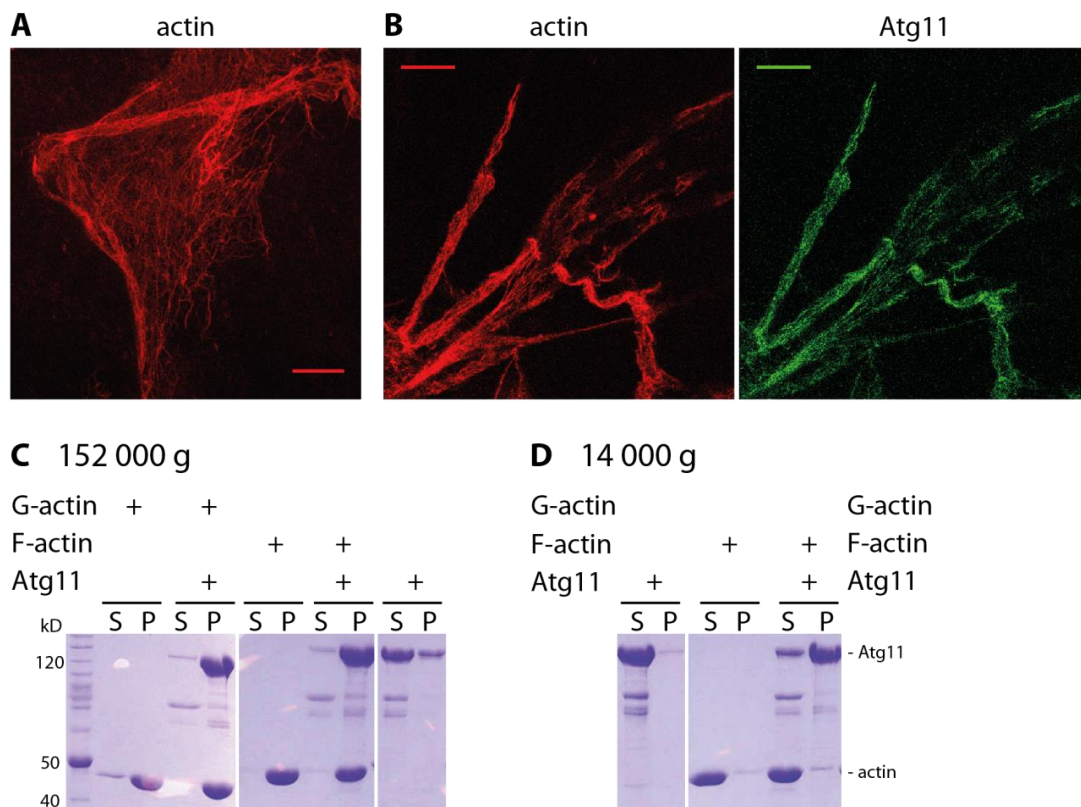
Figure 16 – Atg11 is not an actin motor protein. **(A)** Atto565-labeled actin was polymerized and imaged in confocal fluorescence microscopy (Zeiss LSM780). The image shows a single slice of filamentous and bundled actin. Scale bar 20 µm. **(B)** Atto488-labeled Atg11 colocalizes evenly to actin filaments. Scale bar 20 µm. **(C)** 10% SDS-PAGE of actin polymerization assay. G-actin w/ and w/o Atg11 was treated with F-solution to induce polymerization and centrifuged at 152000 g to pellet F-actin, localizing to the pellet (P). Addition of Atg11 to preformed F-actin results in both proteins localizing to the pellet fraction, too. **(D)** 10% SDS-PAGE of actin bundling assay: large protein aggregates, like bundled actin, are pelleted at 14000 g. Atg11 and F-actin separately both remain soluble (S). Upon addition of Atg11 to F-actin, they become separated by centrifugation, F-actin remaining soluble, Atg11 localizing to the pellet (P).

The hypothesis that Atg11 might fulfill a motor function when moving specific cargo or autophagosomes along actin filaments requires Atg11 to directly interact with actin. Therefore colocalization of Atg11 and actin was investigated by fluorescence microscopy. Actin monomers (G-actin) was polymerized to form filamentous actin (F-actin) and

fluorescently labeled with small chemical dyes (Figure 16 A). Labeled Atg11 was added and binding was analyzed by confocal fluorescence microscopy (Figure 16 B). Interestingly, Atg11 appeared to be recruited to polymerized actin. Strong colocalization was observed at actin bundles. Due to directional movement of motor proteins, an asymmetric colocalization of these proteins with accumulation at the + or − ends has been detected in similar experiments with canonical motors. This is, however, not the case for Atg11. Moreover, fluorescence recovery after photobleaching (FRAP) experiments did not indicate any movement of Atg11 along actin filaments (not shown).

3.3.2 Separation of Atg11 from actin by differential centrifugation

After observing static interaction between actin filaments and Atg11, a more detailed analysis of the mode of action could provide insight on the significance of the interaction. Some actin binding proteins are influencing the polymerization/depolymerization of filaments, which can be analyzed by centrifugation. Polymerized F-actin can be pelleted at high centrifugation speeds, in contrast to G-actin, which remain soluble. Therefore G-actin and F-actin were incubated with Atg11 and subjected to high speed centrifugation. Comparing the supernatant and pellet fractions showed that Atg11 neither inhibits polymerization nor depolymerizes already formed F-actin (Figure 16 C). Another property of actin binding proteins can be bundling of actin filaments. Atg11 exhibited a tendency in fluorescence microscopy to colocalize more strongly with actin bundles than with fine actin filaments. This could be caused by active bundling of F-actin by Atg11. Centrifugation at 14 000 g is able to pellet large protein oligomers like actin bundles, while soluble protein and F-actin remain in solution. Surprisingly, while Atg11 and F-actin separately are both soluble, upon mixing them together Atg11 was found in the pellet fraction, while F-actin remained soluble (Figure 16 D). This indicates that Atg11 is not bundling F-actin. However, Atg11 was found to aggregate upon contact with actin or actin buffer and was pelleted already at low centrifugation speed. The separation of Atg11 and F-actin into separate pellets by low speed centrifugation indicates only weak contact between the two. From this data, substantiated with non-directed localization as seen in microscopy, it can be concluded that Atg11 is rather unlikely to have an actin motor function in autophagy.

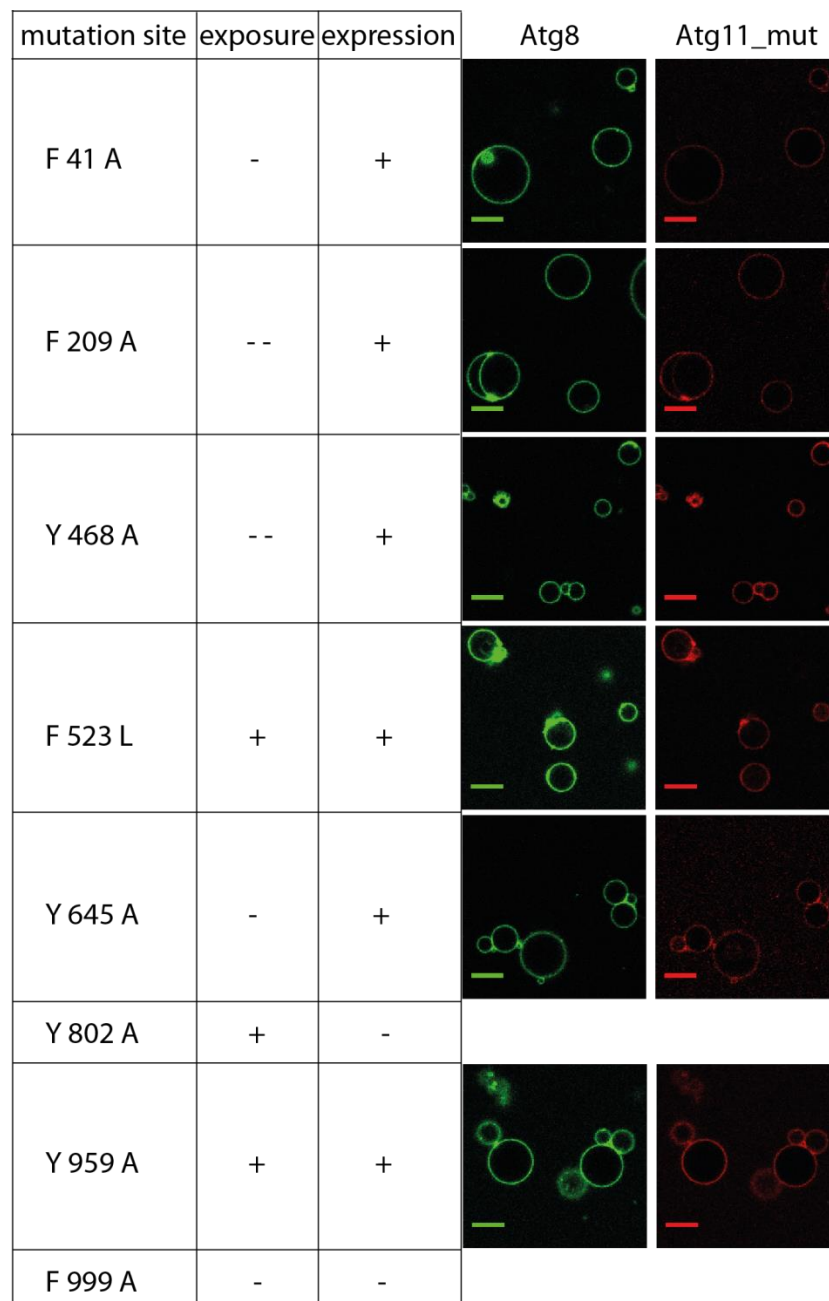## 3.4 Atg11 as linker between autophagosome and cargo

Atg11 is required to deliver receptor-decorated cargo to the PAS (Shintani et al., 2002). To fulfill this linker function Atg11 needs to interact with both a protein at the PAS on one side and the cargo receptor on the other side. Molecular details about these interactions are mostly not known so far.

3.4.1   Search for canonical AIMs within Atg11

Atg11 has been found to colocalize with Atg8 at the PAS (Yorimitsu and Klionsky, 2005) and an interaction of *A. thaliana* AtAtg11 with AtAtg8 was described recently (Li et al., 2014). Direct interaction of Atg11 with Atg8 coupled to membranes was observed in vitro in this thesis (see 3.2). However, the binding sites on both interaction partners are still unknown. Since interaction of Atg8 with many of its binding partners depends on an AIM, this consensus sequence was identified within Atg11 and tested by recruiting Atg11 AIM-mutants to Atg8-decorated GUVs.

The AIM consensus sequence [W/F/Y]xx[L/I/V] (Noda et al., 2010) was compared with the amino acid sequence of Atg11, which allowed the identification of 16 potential AIM sites. To further narrow down the number of possible AIMs, the probability of surface display of the sequence was estimated from an hydrophobicity plot of Atg11 (www.vivo.colostate.edu/molkit/hydropathy). Since amino acid characteristics upstream and downstream of the potential AIM are influencing the interaction (Johansen and Lamark, 2011), these were taken into account as well when selecting the most probable candidates. Finally, 8 potential AIMs were subjected to mutational analysis in vitro (see Figure 17).

The crucial bulky amino acid W/F/Y was mutated to a small A/L, disrupting the potential AIM. Atg11 AIM mutants were expressed as described for the wildtype protein, however, with drastically reduced yield and purity, leading to high 260 nm absorbance which covered up the protein signal at 280 nm. Thus, the protein concentrations could not be determined exactly. Two mutants could not be expressed recombinantly. Purified Atg11 AIM mutants were fluorescently labeled. Since the protein concentration could not be determined, it was also not possible to calculate the degree-of-labeling (DOL) of the respective Atg11 AIM mutant. If protein concentrations and DOL are unknown, signal intensities cannot be compared with each other and do not correlate with the binding intensity. Therefore recruitment of an Atg11 AIM mutant to Atg8 would indicate that the respectively mutated AIM is not essential for Atg8 interaction (yes-or-no assay), but no information on partial contribution to the interaction can be derived. Nonetheless, labeled Atg11 AIM mutants were added to Atg8-decorated GUVs and the interaction with Atg8 was determined by observing the recruitment to the GUVs (Figure 17). No mutant was fully prevented from localizing to the membrane, thus no single AIM appears to be crucial for the interaction of Atg11 with Atg8.

| mutation site	exposure	expression	Atg8	Atg11_mut
F 41 A	-	+		
F 209 A	- -	+		
Y 468 A	- -	+		
F 523 L	+	+		
Y 645 A	-	+		
Y 802 A	+	-		
Y 959 A	+	+		
F 999 A	-	-		

Figure 17 – Testing Atg11 mutants for potential AIM sites. Potential AIMs fulfilling the canonical [W/F/Y]xx[L/I/V] consensus sequence were identified in Atg11. Based on a hydrophobicity plot, the probability of the sites to be exposed at the surface (+) or buried within the folded protein (-) is given. Atg11 AIM mutants were expressed recombinantly if possible (+ yes, - no) and fluorescently labeled with Atto565. Protein concentrations and DOL could not be determined, therefore signal intensity in confocal microscopy images does not correlate with binding intensity. All mutants are still able to interact with enzymatically lipidated Atg8^{Atto488}. Scale bar is 10 µm.

3.4.2 Atg11 localization to giant Ape1 complexes

Atg11 is recruited to the PAS as one of the first factors to coordinate autophagy biogenesis. Its precise location on the expanding phagophore membrane though has not yet been determined. Atg11 can be tracked as a GFP-fusion protein within *S. cerevisiae* cells growing in log phase. Atg11 was observed to colocalize with the specific cargo Ape1-complex (Figure

18 A top panel). However, due to the small size of the endogenous cargo complex, visual analysis by fluorescence microscopy does not allow characterization of the spatial location of Atg11 at the phagophore engulfing the cargo. Overexpression of ApeI has been shown to yield a stable giant ApeI complex (GAC), which recruits the autophagic machinery and membrane.
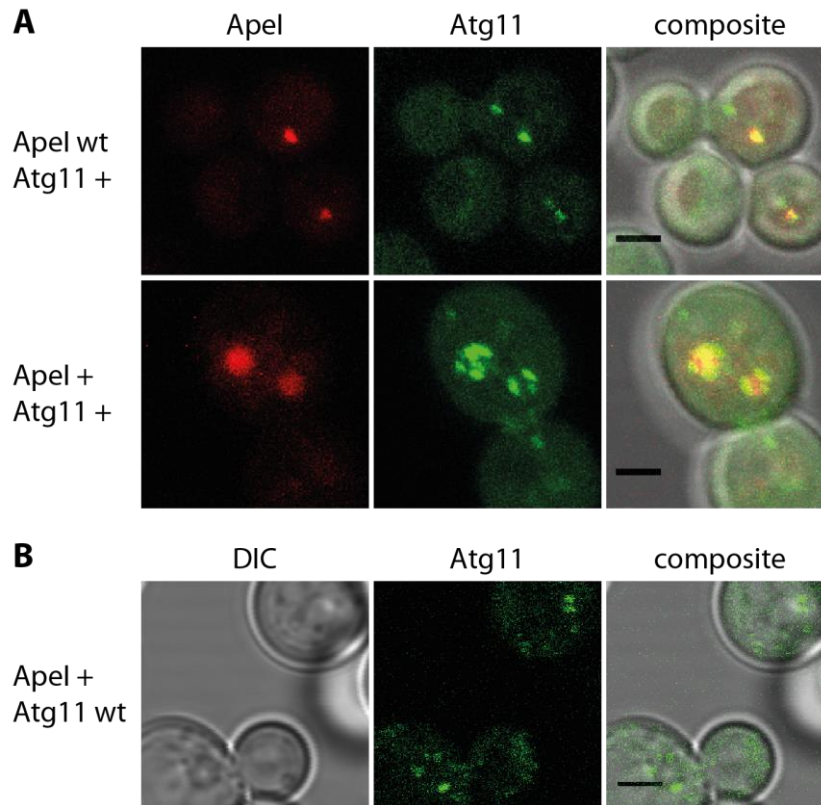
Figure 18 – Colocalization of Atg11 with specific cargo. **(A)** Genomically expressed ApeI-Ruby was complemented with inducible untagged ApeI and analyzed for its colocalization with Atg11-GFP. Shown are flattened z-stacks of log phase growing *S.cerevisiae* without induction of ApeI overexpression (top) and with ApeI overexpression (bottom), resulting in large GAC. Overexpressed Atg11 forms several puncta in the cell; small ApeI complexes recruit one such puncta per complex while GACs are surrounded by about 3-5. **(B)** Though the puncta are much weaker, also endogenously expressed Atg11-GFP localizes in several puncta around GACs (untagged, but visible in DIC). Shown is a single z slice of log phase growing cells. Scale bar is 2 µm.

Due to the large size of this cargo, cup-shaped phagophores are stalled and eventually retract without closing the autophagic vesicle. Therefore the GAC resists full encapsulation and degradation, but allows the visual inspection of proteins involved in promotion of the phagophore (Suzuki et al., 2013). Proteins localizing to the stalled autophagic membrane can be grouped into proteins binding to the tip or middle of the phagophore as punctate structure, and proteins extending along the entire membrane. Proteins localizing to the tip can be involved in expansion, while proteins extending along the membrane might be part of a coat-like structure. Overexpressed Atg11-GFP localized at several punctate structures around the induced GAC (Figure 18 A bottom panel), both in vegetative (shown) and autophagy inducing conditions. Atg11-GFP expressed at its endogenous level localized in the same

pattern, but was weakly visible (Figure 18 B). In conclusion, Atg11 is not distributed along the surface of the GAC or phagophore, but localizes in distinct puncta around the cargo.

3.5 Functional characterization of Atg11 in vivo

Atg11 has been associated with the Atg1 kinase complex in selective autophagy. The Atg1 kinase complex consists of the Atg1 kinase, Atg13, and a dimer of Atg17, regulated by Atg31 and Atg29. Atg17 tethers Atg9-positive membrane donor vesicles to form the PAS (Rao et al., 2016). While PAS formation was found to depend on Atg17 under starvation, Atg11 is required in vegetative conditions; no PAS is formed in the double knockout, suggesting that Atg11 can substitute for Atg17 (Cheong et al., 2008). Further in vivo studies should address the function of Atg11 in vivo and its redundancy to Atg17.

3.5.1 Mass spectrometric analysis of complex components in vivo

To identify the change of components of the Atg1 kinase complex and interactions partners of Atg11 in both vegetative and starvation conditions, mass spectrometric analysis of the complexes was performed. Atg11 and Atg13 were GFP-tagged in separate *S. cerevisiae* strains, a strain expressing GFP alone served as control. IP in both vegetative and starvation conditions and mass spectrometric analysis of co-purified protein complexes was performed by Eva Keilhauer, Dept. Mann, MPIB. Mass spectrometric analysis of the co-IPs identified specific binding partners of Atg11 and Atg13 and their change following induction of non-selective autophagy. Unfortunately many known binding partners were not identified, probably due to stringent washing during sample preparation. Nevertheless, Atg11 significantly (defined as interaction that was at least 1-fold increased in the Atg11-GFP sample in comparison with the GFP only control, with a confidence of -log p > 1) interacted with Atg19 and the cargo ApeI during vegetative growth. Interaction with Atg31 and Atg21 was found, too, though with lower confidence. Starvation disrupted most of these interactions, only Atg31 was still found with a confidence >1. Interestingly, strong interaction of Atg11 with Nde1, an NADH dehydrogenase located to the mitochondrial surface, was found during starvation. These results indicate that Atg11 only interacts with specific cargo during vegetative conditions and possibly locates to mitochondria in starvation conditions.

Direct comparison of Atg11 pull downs of vegetative conditions versus starvation conditions (see Figure 19 A) revealed significantly increased interaction in vegetative conditions not only with specific cargo, but also with Atg13 (approximately 3-fold increase with -log p > 1).
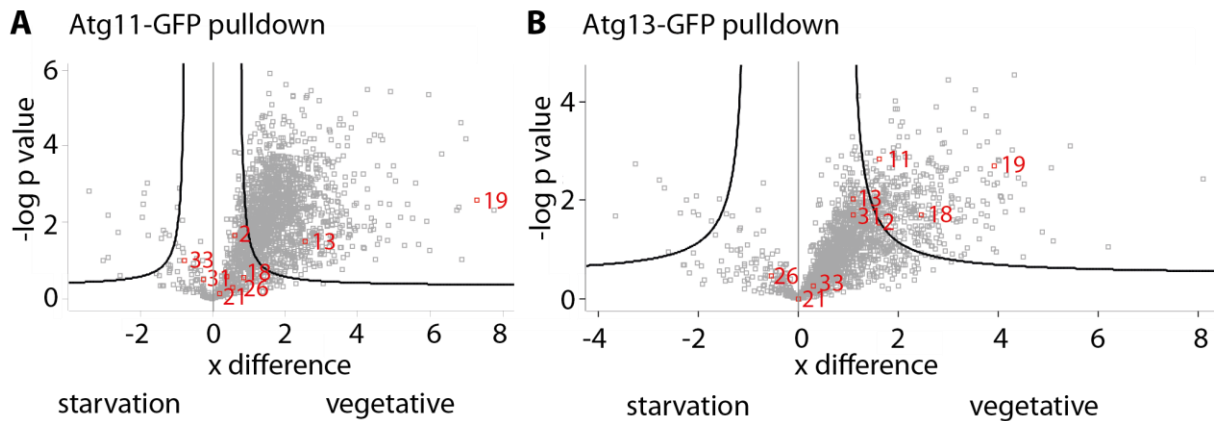
Figure 19 – Volcano plot of mass spectrometric analysis of Atg11 and Atg13 pulldowns. **(A and B)** Samples in triplicates were corrected for GFP-only interactions and enrichment in vegetative conditions (right) was plotted against enrichment in starvation conditions (left). Significant interaction partners (> 1x enrichment and -log p >1) are located above the black cutoff line for both conditions. Atg proteins are highlighted in red. **(A)** Atg11 was used as bait. It significantly interacts with Atg19 and Atg13 in vegetative conditions. **(B)** Atg13 was used as bait. Interaction with Atg19, Atg11 and Atg18 was only found in vegetative conditions.

The reverse pull down of Atg13-GFP detected interaction with Atg19, Atg11 and Atg21 in vegetative conditions, while all these interactions were not identified anymore upon starvation. Difference plotting of starvation versus vegetative conditions confirms the preferred interaction of Atg13 with Atg11 and Atg19 in vegetative conditions (see Figure 19 B). Atg13 seems to play an active role in selective autophagy during vegetative conditions together with Atg11.

3.5.2 Atg11 puncta are upregulated without *ATG17*

Proteins which are involved in formation of the phagophore are recruited to the PAS. Tagging these proteins fluorescently results in bright puncta in fluorescence microscopy when they are recruited to the PAS. Since PAS formation depends on Atg11 in vegetative conditions and Atg17 in starvation conditions, a homolog function was suggested. In that case, Atg11 might be able to substitute for Atg17 in its absence. To investigate this possible redundancy in function, Atg11 puncta were quantified in the presence and absence of Atg17.

While in vegetative conditions Atg11 puncta were observed in 24% of wildtype cells, starvation reduced the number to about 4%. Deleting *ATG17* resulted in a similar phenotype during vegetative conditions, however, the number of Atg11 puncta increased to about 20% in this strain during starvation (Figure 20 A). The increase in Atg11 puncta in starved *atg17Δ* cells was observed independently of Atg11 expression levels, indicating that the regulation of Atg11 is not changed by overexpression (Figure 20 B).
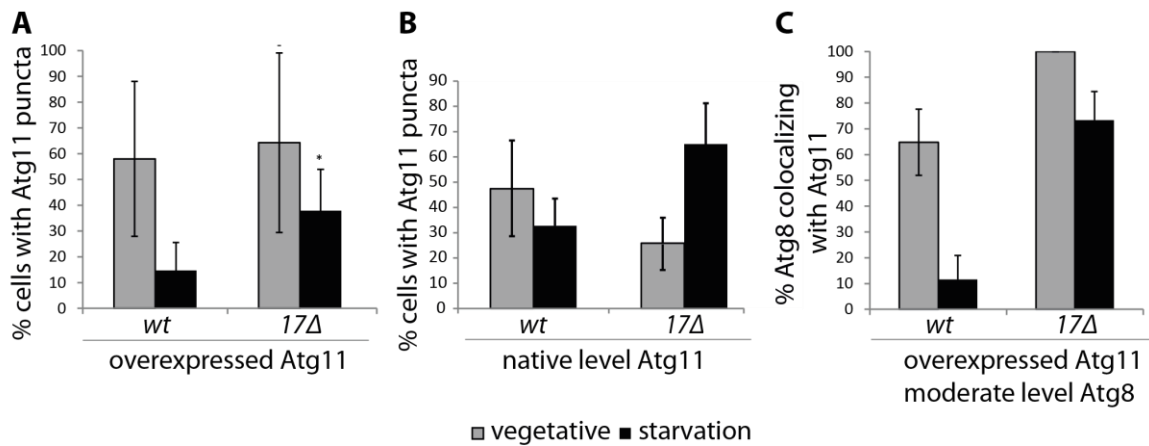
Figure 20 – Atg11 puncta decrease upon starvation, but not in *atg17Δ* cells. **(A+B)** Atg11 was overexpressed **(A)** and expressed at endogenous level **(B)** in *S.cerevisiae* strains with and without *ATG17*. Puncta and cells were quantified in vegetative and starvation conditions. Error bars represent the SD from n=3 independent experiments (A) or from 6 max. intensity projected confocal z-stacks quantified with a total of >100 cells per condition (B). * ($p < 0.05$) was calculated using a paired two-tailed Student's t-test. **(C)** mCherry-Atg8 puncta were quantified in the presence and absence of Atg17 and each puncta was evaluated for the overlapping presence of Atg11-GFP. Error bars represent the SD of 3-6 flattened confocal z-stacks with a total of >130 cells per condition.

3.5.3   Atg11 colocalizes with Atg8

Since a punctum does not necessarily represent a PAS, colocalization of Atg11 with the late PAS marker Atg8 (tagged with mCherry) was analyzed. Most Atg8 puncta (approximately 70%) colocalized with Atg11 during vegetative conditions (Figure 20 C). However, no significant colocalization was observed during starvation. In contrast, 100% of Atg8 puncta in vegetative and more than 70% in starvation conditions colocalized with Atg11 in the absence of Atg17. These numbers closely reflect the total count of Atg11 puncta (Figure 20 A), indicating that strong puncta formation of Atg11 coincides with PAS localization. Most importantly, the strongly induced Atg11 puncta in the absence of Atg17 during starvation conditions are colocalizing with Atg8 and therefore represent PAS. In conclusion, Atg11 is able to take the spot of Atg17 in its absence.

3.5.4   Cellular distribution of Atg11 and Atg9

The significant reduction of Atg11 puncta upon starvation could be the result of its displacement from the PAS or of reduced protein levels in such cells. To exclude that degradation of Atg11 accounts for the reduced number of puncta, vegetative and starved cell lysates were subjected to western blotting. Comparison of band intensities indicated a reduction of Atg11 by about 50% (not shown). The remaining protein must be dispersed in the cytosol to PAS-distant locations. To investigate the intracellular distribution of Atg11, subcellular fractionation assays were employed. Lysed cells were centrifuged at low speed (17 000 g) to produce a pellet fraction containing intact organelles and plasma membrane. The resulting supernatant was centrifuged at high speed (100 000 g), producing a pellet containing small vesicles and large protein complexes like ribosomes. Cytosolic proteins

remain in the supernatant during high speed centrifugation. Abundance of Atg11 was quantified in all fractions from western blots. During vegetative conditions 77% of Atg11 were pelleted by low speed centrifugation (P17), the remaining 23% were mostly cytosolic (S100) (Figure 21 A). The distribution of Atg11 did not change significantly upon starvation. However, only 58% were already pelleted at low speed, leaving 42% which were predominantly pelleted at high speed centrifugation (P100).
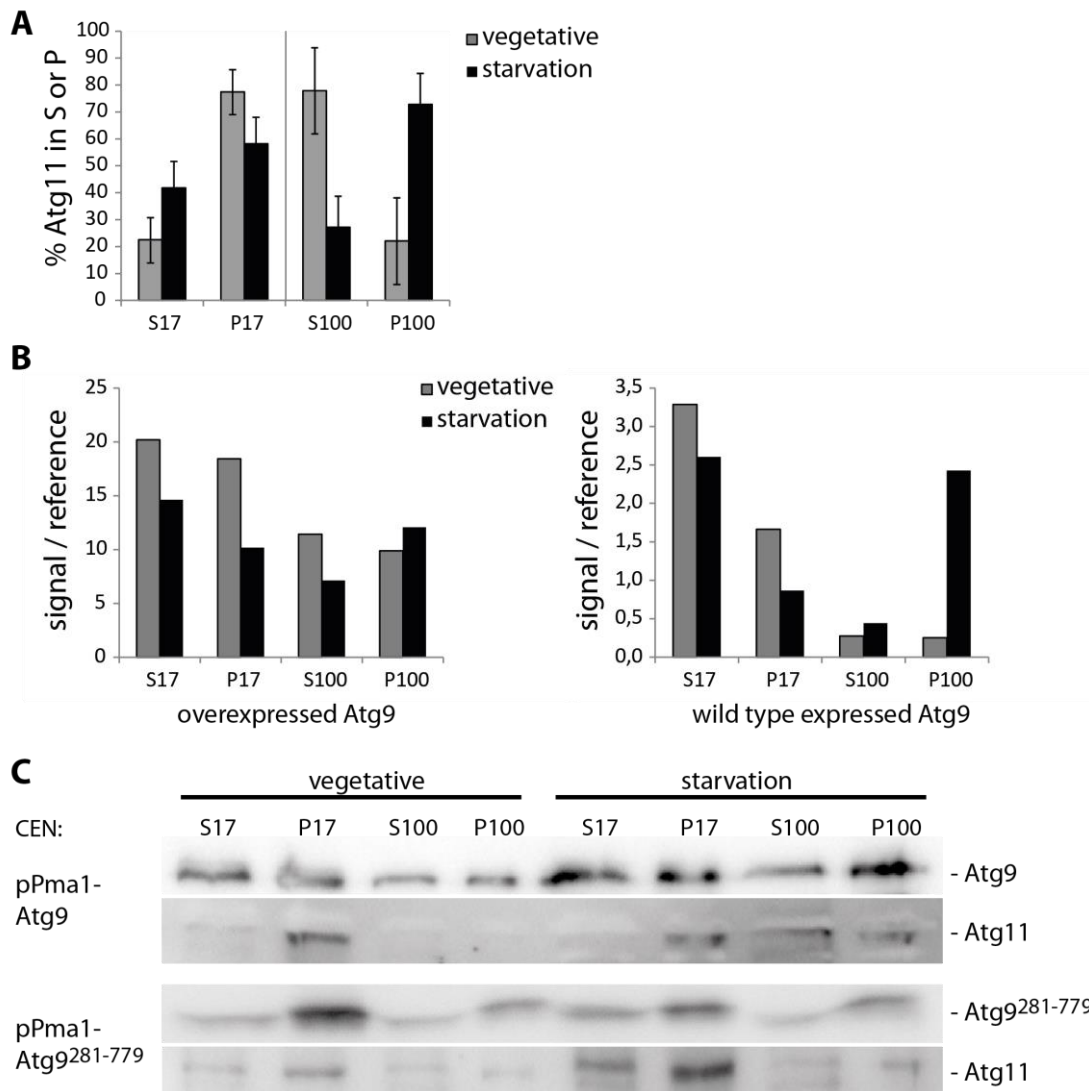
Figure 21 – Subcellular localization of Atg11 and Atg9. **(A)** Atg11-GFP was expressed with Pma1 promoter in vegetative and starvation conditions. Cell lysates were centrifuged at 17 000 g to separate them into supernatant (S17) and pellet fraction (P17). The supernatant was centrifuged at 100 000 g, producing S100 and P100 fractions. Error bars represent the SD of n=3 independent experiments. **(B)** HA-tagged Atg9 was overexpressed and expressed at endogenous levels in *atg9Δ atg11-myc* cells and subcellular distribution was determined as in (A). A standard HA sample was included in western blotting and used for normalization of all samples. **(C)** Western blot of the assay in (B), including a core fragment of Atg9 (Atg9$^{281-779}$) and Atg11. Starvation samples were applied in double amount.

A significant amount of Atg11 localized to fractions containing small vesicles (P100). Small vesicles involved in autophagy are Atg9-positive vesicles of about 30-60 nm diameter which

deliver membrane to the growing phagophore (Mari et al., 2010) and are tethered by Atg17 (Rao et al., 2016). Therefore also the subcellular distribution of Atg9 was analyzed and compared to that of Atg11. Overexpression of Atg9 resulted in almost evenly distributed protein over all fractions, no significant changes of protein distribution were observed upon starvation. In contrast, Atg9 distribution was strongly shifted upon starvation when expressed at an endogenous level, increasing its abundance in P100 more than 5 times in comparison to vegetative conditions (Figure 21 B).

A truncated variant of Atg9 (termed Atg9^{core}) is recombinantly expressable and sufficient for interaction with Atg17 (Rao et al., 2016). It is lacking the cytoplasmic N- (1-280) and C- (780-997) terminal domains, though the C-terminus is required for its correct targeting (Yamamoto et al., 2012). In an additional subcellular distribution assay full length Atg9 was replaced with Atg9^{core}. Atg9^{core} predominantly remained within P17, and starvation did not increase its distribution to P100 significantly (Figure 21 C). Interestingly, Atg11 predominantly localized to P17 in this sample, also starvation did not induce its distribution to P100. This indicates that Atg9^{core} has a strong influence on the localization of Atg11.

3.5.5 Atg11 interacts with Atg9 in vivo

Similarities in protein distribution of Atg11 and Atg9 in the subcellular fractionation assay do not need to correlate with interaction. However, interaction of Atg9 has been reported for both Atg17 (Sekito et al., 2009) and Atg11 (He et al., 2006). Therefore, co-immunoprecipitation of Atg9 with Atg11 was performed. Atg11 was found to interact with Atg9 to a similar extent in both vegetative and starvation conditions (Figure 22).
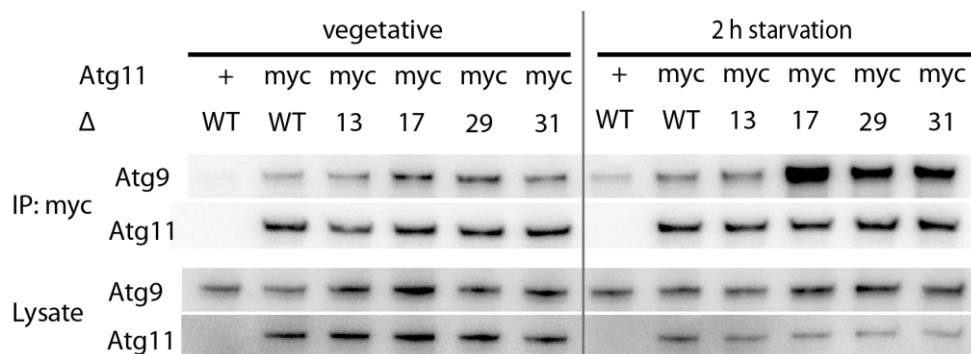
Figure 22 – Atg11 interacts with Atg9, independent of other Atg1 kinase complex components. Immunoprecipitation (IP) of myc-tagged Atg11 and co-IP of HA-tagged Atg9 from lysates of log-phase growing and starved wildtype (WT), *atg13Δ*, *atg17Δ*, *atg29Δ* and *atg31Δ* cells. Lysate of non-tagged *atg11* served as control. Atg11 and Atg9 were detected by α-myc and α-HA immunoblots, respectively.

In order to investigate if the interaction of Atg11 and Atg9 depends on other components of the Atg1 kinase complex, co-immunoprecipitation was also performed in knockout strains. No change in co-IP efficiency was observed in *atg13Δ* cells, indicating that Atg13 has no regulatory function in the interaction of Atg11 with Atg9. Deletion of *ATG17* resulted in a slightly upregulated interaction in vegetative conditions, and was strongly induced upon

starvation. Deletion of the Atg17-regulators *ATG29* and *ATG31* had a similar but less pronounced effect as the *ATG17* deletion, increasing the interaction of Atg11 with Atg9 significantly in starvation conditions (Figure 22). This suggests that Atg11 is occupying free Atg9 in the absence of Atg17 or if Atg17 cannot be recruited to Atg9 by its regulators.

3.6 Atg11 activity in selective and non-selective autophagy

Atg11 is essential in selective forms of autophagy (Kim et al., 2001), but since also non-selective autophagy is impaired in starved *atg11Δ* cells, a possible role in non-selective autophagy cannot be excluded (see Figure 20). In order to characterize possible functions of Atg11 in different types and stages of autophagy, functional autophagy assays were performed.

3.6.1 Early stage: Atg8 lipidation

Atg11 and Atg17 are required for initiating autophagy by recruiting the Atg1 kinase complex (Kamber et al., 2015). Downstream of initiation, Atg8 is covalently attached to the phagophore to coordinate phagophore expansion. Therefore, reduced Atg8-lipidation to PE indicates defects in early steps of phagophore formation. Lipidation in *atg17Δ* cells was found to proceed normally, indicating that the function of Atg17 can be substituted for (Suzuki et al., 2001). No lipidation takes place if *ATG5* is deleted, since Atg5 is part of the enzymatic machinery coupling Atg8 to the membrane. This negative control was compared with *atg11Δ* and *atg11Δ atg17Δ* during induction of autophagy with Rapamycin. Lipidation of Atg8-PE proceeded normally in *atg11Δ* (Figure 23 A). However, the double knockout of *ATG11* and *ATG17* prevented accumulation of Atg8-PE. Initiation of autophagy by Atg17 depends on its ability to form homodimers. Complementation of *atg11Δ atg17Δ* with a monomeric variant of Atg17 (ΔC321-417) (Rao et al., 2016) could not rescue Atg8 lipidation. Therefore the presence of either Atg17 dimers or Atg11 is sufficient for progression in early stages of autophagy.

3.6.2 Final stage: protein processing and enzymatic activity in vacuole

Assays are lacking for examination of intermediate stages of autophagy. Determination of cargo delivery to the vacuole can only indicate reduction of autophagy somewhere en route to the vacuole, but not the exact stage.

3.6.2.1 *GFP accumulation of Pgk1 or Om45 fusion proteins*

When GFP-fusion proteins are degraded in the vacuole, the robust GFP subunit remains stable over long times. Accumulation of GFP, which was fused to proteins targeted by autophagy, is then a readout of autophagic activity. Fusion of GFP to the soluble cytosolic protein Pgk1 results in an assay for determination of non-selective autophagy. After starvation of wildtype (wt) cells for 3 days, free GFP appears as a strong band in α-GFP western blots. Deletion of *ATG5*, part of the core autophagic machinery, blocks any transport

of GFP fusion protein to the vacuole, and thereby serves as negative control. In contrast, deletion of *ATG11* does not block GFP accumulation (Figure 23 B), confirming that Atg11 is not part of the essential core autophagic machinery. Additionally, an Atg11 construct was designed which artificially crosslinks Atg8 and thus the phagophore membrane to cargo receptors such as Atg32 and their cargo. It consists of the confirmed Atg8-interaction motif (AIM) taken from Atg32 (residues 241-282), directly fused to Atg11$^{851-1172}$, and was termed AIM-Atg11C. AIM-Atg11C thus harbors the capacity to interact with Atg8 via the AIM and cargo receptors via interaction sites present in the C-terminus of Atg11 (see mapped interactions in Figure 25), but is lacking the entire N-terminal region of Atg11. Employing AIM-Atg11C instead of full length Atg11 in the Pgk1-GFP processing assay resulted in slightly decreased accumulation of GFP, which is probably related to secondary effects of Atg8 sequestration.
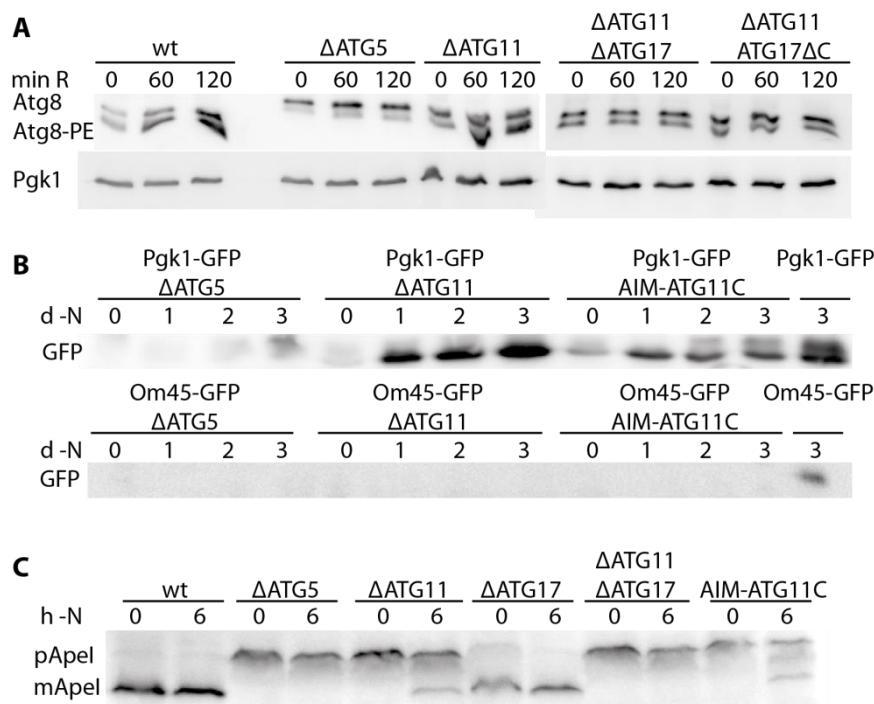
Figure 23 – Functional assays confirm duality of Atg11 and Atg17. **(A)** Lipidation of Atg8 to PE in wildtype (wt) *atg5Δ, atg11Δ, atg11Δ atg17Δ* and *atg11Δ atg17$^{Δ321-417}$* strains after 0, 60 and 120 min of Rapamycin treatment. Detection of cytosolic and lipidated Atg8 with α-Atg8 antibody, α-Pgk1 served as total protein control. **(B)** Accumulation of GFP from Pgk1-GFP and Om45-GFP fusion proteins in *atg5Δ, atg11Δ* and AIM-Atg11C strains after 1-3 days of nitrogen starvation. 3 days starved wt strains serve as positive control. **(C)** Vacuolar processing of pApe to mApe in Pgk1-GFP wt, *atg5Δ, atg11Δ, atg17Δ, atg11Δ atg17Δ* and AIM-Atg11C strains after 1-3 days of nitrogen starvation.

Fusion of GFP to the mitochondrial membrane protein Om45 allows the measurement of mitophagy, which delivers damaged or surplus mitochondria to the vacuole through selective autophagy. After starvation of *Om45-GFP* cells for 3 days, free GFP appears as a band in α-GFP western blots. However, starvation also induces non-selective autophagy, which might

contribute to the delivery of mitochondria to the vacuole. The signal detected might therefore be caused by both selective and non-selective autophagy. Since both forms of autophagy depend on Atg5, no free GFP is accumulated in *atg5Δ* (Figure 23 B). Similarly, no Om45-GFP seemed to be transported to the vacuole in *atg11Δ*. AIM-Atg11C was not able to rescue the Atg11 knockout, suggesting a more elaborate function of Atg11 than crosslinking cargo to autophagosomes. However, western blotting for GFP is a rather insensitive method and levels of regulation of autophagy might therefore be missed.

3.6.2.2   Cvt pathway: Ape1 processing

The final stage of the Cvt pathway, a form of selective autophagy, is the processing of pre-Ape1 (pApe1) to mature Ape1 (mApe1) in the vacuole. In wildtype yeast this is a constitutive process going on in both vegetative and starvation conditions, which is completely blocked in *atg5Δ* (Figure 23 C). Deletion of *ATG11* fully inhibits maturation in vegetative conditions as well, but it can be rescued to some degree by induction of autophagy. Deletion of *ATG17* appears to have no significant influence on the Cvt pathway; therefore Atg11 alone seems to be sufficient for mediating the Cvt pathway. However, a double knockout of *ATG11* and *ATG17* prevents the rescue seen under starvation conditions in *atg11Δ*, indicating that non-selective autophagy mediated by Atg17 contributes to the transport of pApe1 to the vacuole in starvation conditions. The artificial crosslinker AIM-Atg11C was not able to rescue the Cvt pathway in *atg11Δ*.

3.6.2.3   Quantification of autophagy

Since western blotting is a semi-quantitative and not very sensitive method, a quantitative enzymatic assay is advantageous for comparing levels of autophagic reduction. The vacuolar alkaline phosphatase Pho8 is normally recognized by its N-terminal signal sequence and trafficked through the ER and Golgi to the vacuole. Its enzymatic domain then faces the vacuolar lumen, where it becomes active. Removal of 60 N-terminal amino acids produces a cytoplasmic protein (cytPho8) which is transported to the vacuole only by non-selective autophagy. The enzymatic activity of *atg5Δ* cells remained at background level after 4 h of starvation, indicating that non-selective autophagy was inactivated (Figure 24 A). While *atg11Δ* exhibited impaired cytPho8 activity, it retained significant residual activity (57% of wildtype). This indicates that Atg11 facilitates non-selective autophagy, but is not essential. A*tg17Δ* and a*tg11Δ* a*tg17Δ* double knockout cells, in contrast, were not able to activate cytPho8, confirming the requirement of Atg17 for non-selective autophagy. As expected, AIM-Atg11C was not able to rescue a*tg11Δ* a*tg17Δ*.

To compare the requirements of Atg11 and Atg17 for non-selective autophagy with selective forms of autophagy, a similar enzymatic assay was used. Addition of an N-terminal mitochondrial signal sequence (Su9) targets Pho8$^{\Delta N60}$ to mitochondria. When mitochondria were targeted to the vacuole by mitophagy in wildtype cells, mtPho8 became progressively

activated during starvation. Cells lacking Atg11 did not show any mtPho8 activity after 4 h of starvation and only a very low level of activity after 24 h of starvation (Figure 24 B). Therefore Atg11 is essential for mitophagy. By contrast, mitophagy was reduced in *atg17Δ*cells, but not disabled (67% of wildtype), indicating that Atg17 facilitates, but is not sufficient to mediate selective autophagy by itself. Both the double knockout *atg11Δ atg17Δ* strain and its variant complemented with AIM-Atg11C are defective in mitophagy.
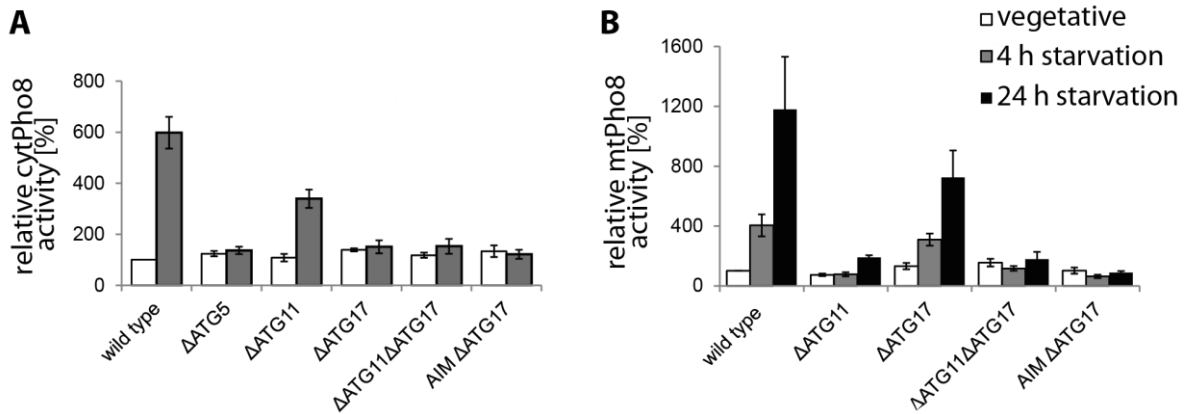
Figure 24 – Quantification of non-selective and selective autophagy by Pho8 activity. **(A+B)** Cytoplasmic Pho8^{ΔN60} (cytPho8, **A**) and mitochondrial Pho8^{ΔN60} (mtPho8, **B**) assay of log-phase growing, 4 h and 24 h starved wildtype, *atg5Δ* (negative control), *atg11Δ*, *atg17Δ*, *atg11Δ atg17Δ* and *atg11Δ atg17Δ + AIM-atg11C* (AIM ΔATG17) cells as indicated. Pho8-activity was corrected with total protein amount of each sample and normalized to the signal of the respective wildtype cells growing in vegetative conditions (set to 100%). Shown are mean values ± SD of n = 3 independent experiments.

3.7   In vitro analysis of protein – protein interactions

Though the autophagic activity was reduced to baseline levels in *atg17Δ* cells, increased numbers of Atg11 puncta, colocalizing with Atg8 and therefore representing the PAS, during starvation indicate that Atg11 and Atg17 share structural similarities. Homology of Atg11 and Atg17 has been proposed before (Suzuki et al., 2007) but has not been investigated in detail. In vitro protein interaction analysis can be employed for studying the interaction of Atg11 with interactors inferred from confirmed binding partners of Atg17.

3.7.1   Sequence similarity of Atg11 and Atg17

In order to investigate structural similarity between Atg11 and Atg17, protein sequence alignments were performed. Due to their very different lengths, alignment of full length Atg11 and Atg17 does not reveal consistent homology regions. However, a protein was identified in *A. thaliana* (At4g30790) that shows homology to yeast Atg11 as well as Atg17 and mammalian FIP200 (Li et al., 2014). The protein was assigned a homolog of Atg11 based on a conserved sequence in the C-terminus and the presence of coiled-coil motifs. Additionally, the study identified the Atg17-family consensus sequence Y-X-X-X-L/V/I-X-E-V/I-X-R-R-R/K

in the N-terminal region. Based on their sequence alignment, the full Atg17 sequence was aligned to Atg11[122-536] with 15% sequence identity and 45% homology in amino acid properties (Figure 25). The Atg17-like domain in Atg11 encompasses the homodimerization region as well as interacting sites of Atg17 with Atg9, Atg13 and Atg31. An interaction site for Atg9 has also been mapped to the equivalent region in Atg11 (Chang and Huang, 2007), indicating conservation of protein interaction sites.
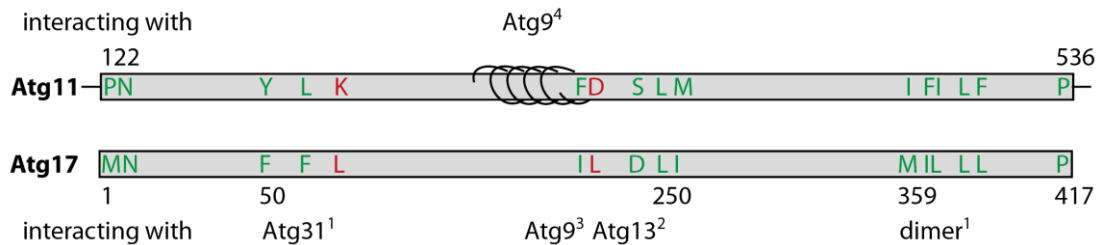
Figure 25 - Atg17-like domain of Atg11. Protein sequence alignment of Atg11[122-536] and Atg17. Interacting partners suggested for Atg17 ([1](Ragusa et al., 2012), [2](Fujioka et al., 2014), [3](Rao et al., 2016)) are indicated below the sequences, for Atg11 ([4](Chang and Huang, 2007)) above. Similarities (green) and differences (red) of interaction motifs are indicated. The spiral indicates CC2 of Atg11 (amino acids 272-325). Alignment was performed with Clustal 2.1 Multiple Sequence Alignment (EMBL-EBI Web Tool 2014).

3.7.2 Surface Plasmon Resonance analysis of Atg11 interaction with Atg13

Sequence alignment and colocalization as well as immunoprecipitation studies in yeast suggest Atg11 to interact with Atg1, Atg13, and Atg9, amongst others. In order to investigate whether these are direct interactions, the recombinant proteins were analyzed by in vitro protein interaction assays. Atg13 connects the Atg1 kinase to Atg17 in the Atg1 kinase complex (Fujioka et al., 2014). Atg11 has been suggested to interact with Atg1 (Yorimitsu and Klionsky, 2005), however, it appears to be an indirect interaction via Atg13 as well (Kamber et al., 2015). This was investigated by surface plasmon resonance (SPR; Biacore). Atg11 was immobilized via a C-terminal His$_6$-tag on Ni-NTA chips and its interaction with different concentrations of Atg13 was recorded. A clear concentration dependent response was visible in the drift corrected intensity plots (Figure 26 A), confirming the direct interaction between Atg11 and Atg13.

Though Atg11 was found to interact with Atg13 and thereby indirectly with Atg1, also an Atg13-independent interaction with Atg1 is possible. Therefore Atg11 was immobilized on Ni-NTA chips and loaded with Atg13 or buffer. The recruitment of Atg1 by Atg11, in the presence or absence of Atg13, was recorded (Figure 26 B). A significant response was induced by Atg1 when loaded to Atg13-activated Atg11, while it only showed weak interaction with Atg11 directly.
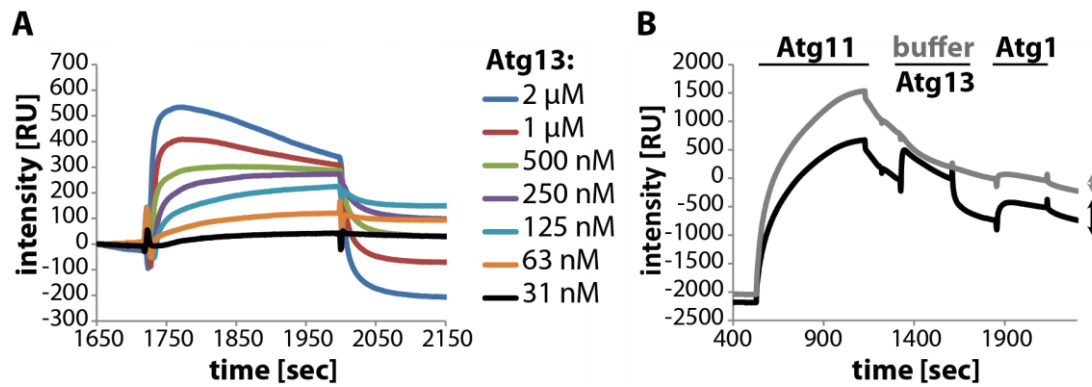
Figure 26 – SPR measurement (Biacore) of Atg11 with Atg13 and Atg1. **(A)** Resonance intensity of decreasing amounts of Atg13 with Ni-NTA-immobilized Atg11-His$_6$. Samples are corrected for non-specific interaction with the chip and for drift. **(B)** The chip was loaded with Atg11 as in (A), followed by 1 µM Atg13 (black line) or buffer (grey line) and 1 µM Atg1. Samples are corrected for non-specific interaction with the chip.

3.7.3 Förster Resonance Energy Transfer (FRET) analysis

Atg11 was found to interact with Atg9 in vivo and recruits Atg9 to the PAS. In vitro studies allow the characterization of this interaction. Transmembrane proteins like Atg9 pose several challenges for in vitro studies. First, the interaction with its binding partners should preferentially be measured in its natural lipid environment, integrated into lipid vesicles. Second, physical separation of Atg9-vesicles from its aqueous solution might disrupt transient interactions. Therefore, an in vitro FRET assay was developed, which allows the measurement of protein interactions with Atg9, incorporated in vesicles, in solution. One binding partner was labeled with a donor dye (Alexa488), the second partner with an acceptor dye (Alexa568). Excitation of the donor dye results in excitation of the acceptor dye by non-radiative energy transfer, if the distance between donor and acceptor is close to the dye's Förster radius R_0. Highest transfer rates for the chosen dyes are at about 6.3 nm. Since this is in the range of protein-protein interactions, the measurement of acceptor emission provides information on physical contact of proteins. Background corrected cFRET values were determined by correcting the measured FRET values for bleed-through of donor emission, direct excitation of acceptor and non-specific donor-acceptor energy transfer.

3.7.4 Atg11 interacts with Atg13

Since Atg11 was found via SPR to interact with Atg13 (Figure 26), this interaction was used to validate the cFRET setup. Alexa488-labeled Atg11, Atg11^N (1-667) and Atg11^C (968-1178) were tested for their interaction with Alexa568-labeled Atg13. Figure 27 A illustrates the increase of cFRET intensity proportional to the increase of Atg13 concentration. Besides full length Atg11, both the N- and C-terminal fragment exhibited interaction as well. This suggests that Atg11 potentially harbors two independent Atg13 binding sites. The highest Atg13 concentration tested (1 µM) was not high enough to reach saturation of the cFRET

signal, preventing the calculation of a dissociation constant K_D. However, the calculation of K_D depends on known amounts of freely interacting molecules. Aggregation of protein would therefore prevent correct calculations. Propensity of Atg13 towards aggregation at different concentrations was revealed by microscale thermophoresis (MST). The method records the movements of fluorescently labeled molecules in a microscale temperature gradient. This movement is strongly dependent on the conformation of the measured molecule, which changes upon interaction with other molecules. It is therefore sensitive to both protein interactions and aggregation. Tracing of Atto488-labeled Atg11 mixed with Atg13 reveals concentration-dependent interaction below 5 µM Atg13 (Figure 27 C). At 11.1 µM Atg13, on the other hand, the tracing became erratic, indicating protein aggregation. Therefore, it was not possible to reach the concentrations required for K_D determination in the FRET assay. Nevertheless, in vitro FRET can be used for qualitative determination of protein interaction.

3.7.5 Atg11 interacts with Atg9-PL

Next, the in vitro FRET assay was employed to test the interaction of Atg11 with Atg9 incorporated into small vesicles. The Atg9 concentration available for interaction partners in a preparation of proteoliposomes (PL) depends on both the rate of incorporation into the lipid bilayer and the orientation within the membrane. Protein concentration of detergent-solubilized Atg9 was determined by a BCA assay and 50% of the total protein was assumed to take a native topology with the cytoplasmic domain facing the exterior. An increase in cFRET intensity depending on the Atg9-PL concentration used indicates direct interaction of Atg11 with Atg9 (Figure 27 B). However, Atg9 is able to self-interact and thereby leads to vesicle aggregation (Rao et al., 2016), preventing the calculation of a K_D.

3.7.6 Flotation of Atg9-PLs with Atg11

While FRET has the advantage to also capture transient interactions, flotation in a density gradient is the method of choice to investigate tight interaction of transmembrane proteins with binding partners. The low density of proteoliposomes allows them to flotate in density gradient centrifugation. Interaction partners co-flotate and can be detected semi-quantitatively alongside the transmembrane protein via SDS-PAGE gels or immunoblots of the flotated fractions. When doing so, the band intensity of the transmembrane protein serves as internal standard for quantification of binding intensities of interaction partners. The transmembrane protein Atg9 was found to interact with Atg11 in vivo, and FRET experiments could already confirm direct interaction in vitro. The interaction was further characterized via flotation experiments employing Atg9-PLs. Flotations were carried out by Dr. Yijian Rao. Atg11 was flotated with Atg9-PLs and liposomes without protein (LUVs) as control for membrane binding of Atg11. While Atg11 was not able to co-flotate with LUVs, it was recovered from Atg9-PL fractions (Figure 28). Therefore Atg11 is tightly binding to Atg9^{core} in

vitro, but does not interact with lipids. This resembles Atg17 interacting with Atg9-PLs. (Rao et al., 2016).
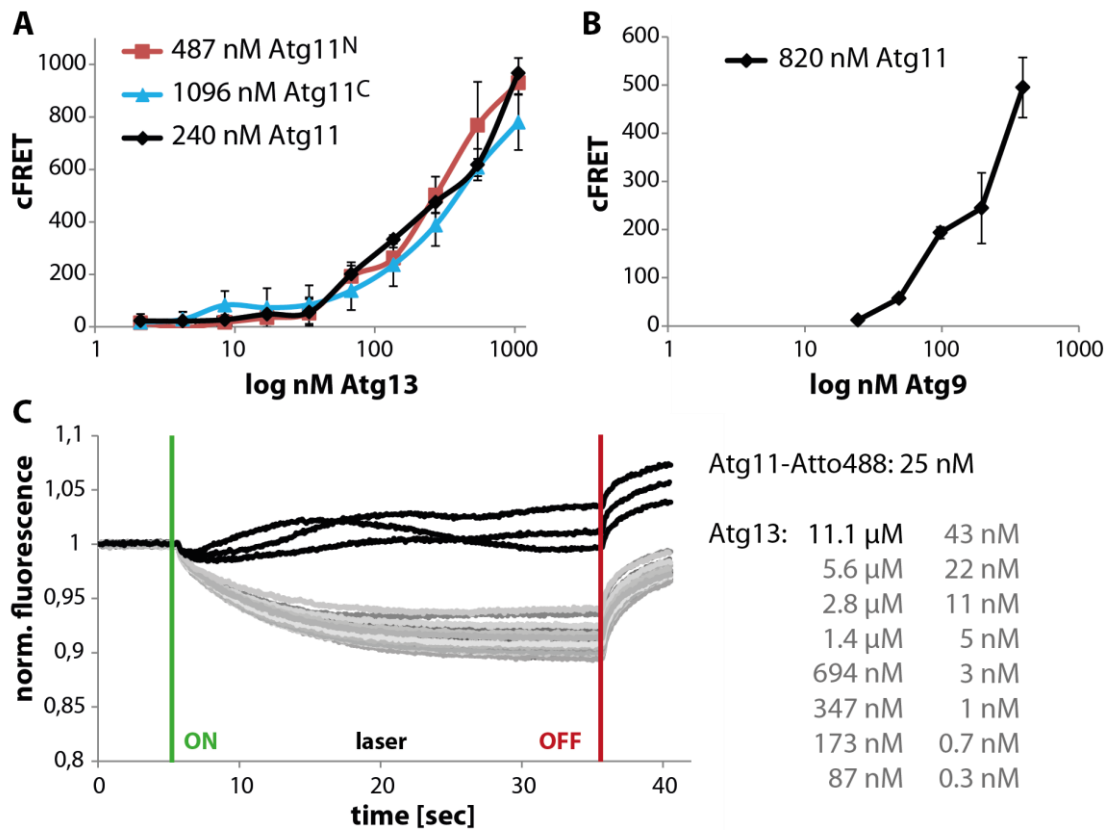
Figure 27 – Förster resonance energy transfer (FRET) indicates direct interaction of Atg11 with Atg13 and Atg9. **(A)** Concentration dependent increase of FRET signal of Alexa488-labeled Atg11 or its N- and C-terminal fragments with Alexa568-labeled Atg13. **(B)** FRET assay of Atg11[Alexa488] and increasing amounts of Atg9[Alexa568]-proteoliposomes. Atg9-concentrations correspond to estimated amount of protein with native topology. **(A+B)** Values are corrected (cFRET) for unspecific signal. Error bars are SD of 3 individual assays performed with same protein preparations. **(C)** Microscale thermophoresis of Atto488-labeled Atg11 with a concentration series of Atg13, measured in triplicates. Highest Atg13 concentration (11.1 µM) indicated in black.

Atg17 recruits Atg9 to the PAS in non-selective autophagy, similar to the function of Atg11 in selective autophagy. Hence, a switch between Atg11 and Atg17 seems to be a prerequisite for changing from selective to non-selective autophagy. Due to the higher copy number of Atg17 than Atg11, it is conceivable that competition for Atg9 would drive the switch. Therefore, the influence of Atg17 on the interaction was investigated by co-flotation. However, Atg17 alone is not able to reduce the interaction of Atg11 with Atg9 (Figure 28, far right). In vivo, Atg17 is forming a constitutive trimeric complex (TC) with Atg29-Atg31, which block the Atg9 binding site when Atg17[TC] is inactive. Upon activation, Atg17 can tether Atg9-vesicles to initiate non-selective autophagy (Rao et al., 2016). Induction of non-selective autophagy also requires hyperphosphorylation of Atg29. Therefore Atg29 is a likely candidate for regulating the interaction of Atg17 and Atg11 with Atg9. The influence of Atg29

on the interaction of Atg11 with Atg9 was tested by co-flotation as wildtype and phosphomimetic (3SD: S197, S199 and S201 to D) variant in combination with Atg17 or alone. Neither wildtype nor phosphomimetic Atg29-Atg31 or Atg17^{TC} reduced the interaction of Atg11 with Atg9, however, the 3SD-variants were found to co-flotate more strongly. Therefore phosphomimetic Atg29 seems to recruit Atg17^{TC} to Atg9, supported by Atg11.
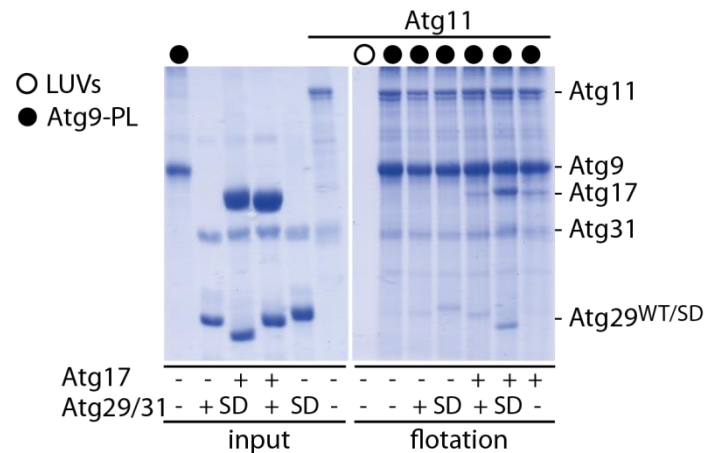
Figure 28 – Flotation of Atg9-PLs with Atg11. SDS-PAGE of input and flotated fractions of Atg11 mixed with Atg9-PL (●) or LUVs without integrated protein (○). Atg17 and Atg29-Atg31 were added where indicated, Atg9 was used as wildtype (+) or phosphomimetic variant (SD). Input corresponds to 20% of total protein of Atg9-PL and Atg11 and 100% of Atg29$^{WT/SD}$-Atg31 and Atg17 used for co-flotation. Flotation was performed by Dr. Yijian Rao.

## 3.8 Function and regulation of Atg11

Atg11 is essential for selective forms of autophagy and recruits Atg9 to the PAS in vegetative conditions; Atg17 promotes initiation of non-selective autophagosomes in starvation conditions by tethering Atg9-vesicles (Rao et al., 2016). Therefore Atg11 and Atg17 might fulfill redundant functions in the respective forms of autophagy. Recruitment and release of both proteins have to be tightly regulated to allow spatio-temporal coordination of their activity.

3.8.1 Atg29^{3SD} recruits Atg17 to the PAS and reduces Atg11 activity in vivo

Atg29, part of a constitutive trimeric complex with Atg17 and Atg31, becomes hyper-phosphorylated by starvation conditions. Phosphorylation of S197, S199 and S201 allows for the interaction with Atg11 and is sufficient to promote autophagy (Mao et al., 2013a). However, in vitro experiments by Dr. Yijian Rao showed that both wildtype Atg29 and phosphomimetic Atg29^{3SD} are interacting with Atg11. On the other hand, only the phosphomimetic Atg29 was found to directly interact with Atg9-PLs. Thereby Atg29^{3SD} promotes the formation of a stable complex consisting of Atg9-PLs, Atg11, and the phosphomimetic TC (Figure 28). Co-immunoprecipitation was employed to investigate the

effect of phosphomimetic Atg29 on the interaction of Atg11 and Atg9 in vivo. Surprisingly, a reduction in the interaction of Atg11 and Atg9 was observed in the presence of phosphomimetic Atg29^{3SD} compared to wildtype Atg29. During vegetative conditions the amount of Atg9 co-precipitated with Atg11 was reduced to about 50% in the presence of Atg29^{3SD} (Figure 29 A). Both the non-phosphorylateable 3SA mutation and the deletion of the phospho-sites containing C-terminus of Atg29 (Δ91-213) only had a minor inhibiting effect. A similar trend was observed in starvation conditions, which lead to stronger interaction of Atg11 and Atg9 compared to vegetative conditions, but also here the interaction between Atg11 and Atg9 was decreased in *atg29^{3SD}* cells. This indicates that the complex formed in vitro by phosphomimetic Atg17^{TC,SD} with Atg9 and Atg11 is highly transient, leading to the sequestration of Atg9 from Atg11 by Atg17^{TC,SD}.

Phosphorylated Atg29 interacts with Atg11 (Mao et al., 2013a), and phosphorylation was found to regulate the interaction of Atg17^{TC} with Atg9 (Figure 28). PAS localization of Atg11 and Atg17 is a prerequisite for nucleation of autophagosomes and therefore serves as indicator of their activity. To investigate the effect of Atg29-phosphorylation on the recruitment of Atg11 and Atg17 to the PAS, puncta formation was quantified in wildtype and phosphorylation-site mutant strains. Consistent with previous observations, Atg11-puncta decreased upon starvation in wildtype cells. In contrast, they increased upon starvation of *atg29Δ* cells, but no change was observed in *atg29^{3SD}* cells (Figure 29 B, left). Mutation of the phosphorylation sites to alanine or deletion of the C-terminus of Atg29 slightly decreased puncta formation of Atg11 in vegetative conditions, however, not significantly. Overall, mutations of Atg29 only had a minor effect on Atg11-puncta formation. Atg17, on the other hand, formed very few puncta in *atg29Δ* cells, whereas the number was substantially increased in *atg29^{3SD}* cells compared to wildtype, especially in vegetative conditions (Figure 29 B, right). Both *atg29^{3SA}* and *atg29ΔC* were strongly impaired in Atg17-puncta formation. This suggests that Atg17 requires phosphorylated Atg29 for recruitment to the PAS, and deletion of Atg29 has a similar enhancing effect on Atg11-puncta formation as deletion of Atg17 (Figure 20). Interestingly, Atg29^{3SD} appears to be sufficient for inducing the nucleation of autophagosomes by recruiting Atg17 to the PAS in vegetative conditions, bypassing the activation of Atg17 by inactivation of TORC1.
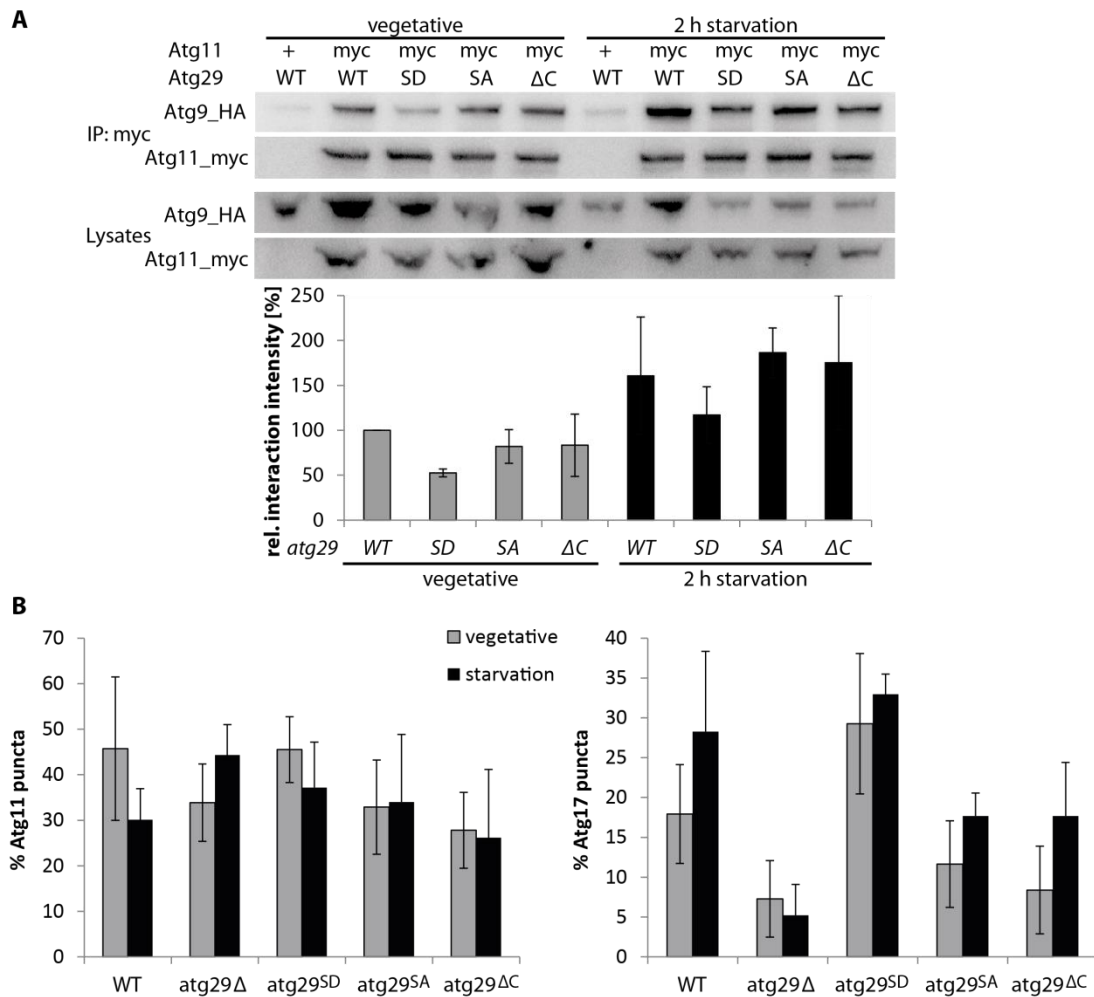
Figure 29 – Phosphorylated Atg29 recruits Atg17 and sequesters Atg9 from Atg11. **(A)** Co-immunoprecipitation of HA-tagged Atg9 with myc-tagged Atg11 in wildtype *atg29* (WT), *atg29*[3SD] (SD), *atg29*[3SA] (SA)and *atg29*[ΔC](ΔC) cells. A strain without myc-tag serves as control for unspecific binding. Shown are the western blots of one exemplary co-IP; below is the mean quantification of 3 independent repeats +- SD. **(B)** Quantification of Atg11- (left) and Atg17- (right) puncta in wildtype *atg29* (WT), *atg29Δ*, *atg29*[3SD], *atg29*[3SA] and *atg29*[ΔC] cells in vegetative and 2-3 h starved conditions. *Atg11Δatg29Δ* and *atg17Δatg29Δ* strains were complemented with CEN plasmids encoding Atg11-2xGFP and Atg17-2xGFP, respectively, and Atg29 variants. All proteins were expressed with their respective wt promoter. Error bars represent the SD from n=3 independent experiments with >50 cells /condition/n.

3.8.2　Atg11 dimerization is auto-inhibited

Homodimerization of Atg11 had been suggested previously by in vivo studies (Kim et al., 2001). Recombinantly expressed Atg11 eluted at 12.5 mL during SEC on a Superos6 10/300 column, which corresponds to the range of the standard Thyroglobulin (669 kD) with a hydrodynamic radius (R_H) of 8.5 nm (Fasman, 1989). The large R_H of Atg11 can be explained by either extended conformation of the monomeric protein or oligomerization. High protein concentration shifts the equilibrium between monomer and dimer towards dimer formation, resulting in a molecule of larger R_H and sedimentation coefficient. This shift can be monitored in solution by analytical ultracentrifugation (AUC), which is measuring the sedimentation coefficient of individual components of a heterogeneous sample. Depending on the

dissociation constant, the peak corresponding to monomers either decreases in favor of an emerging second peak corresponding to the dimers (slow dimerization) or shifts as a whole to a higher sedimentation coefficient (fast dimerization) at higher protein concentrations (Brown et al., 2008).Therefore, to test for dimer formation of Atg11, two different concentrations were subjected to AUC. Figure 30 A shows that the sedimentation coefficient of full length Atg11 does not change from 5.4 S with a ten-fold increase of concentration, indicating that full length Atg11 is monomeric. Interestingly, a shift in the sedimentation coefficient of a small degradation product, which might correspond to an often appearing N-terminal fragment of Atg11, was observed. The N-terminus of Atg11 features an Atg17-like domain (see 3.7.1). Atg17 forms constitutive dimers in vivo and in vitro (Ragusa et al., 2012). Therefore Atg11^{N}, which contains the Atg17-like domain, was subjected to AUC at two different concentrations as well. Figure 30 B shows that the sedimentation coefficient shifted from 4.4 S to 4.7 S upon increasing the protein concentration, indicating fast dimer formation. In addition, peaks of higher sedimentation coefficient appeared, corresponding to oligomers. In conclusion, while the N-terminus of Atg11 is able to dimerize, full length Atg11 seems to be kept in a monomeric state by its C-terminus.
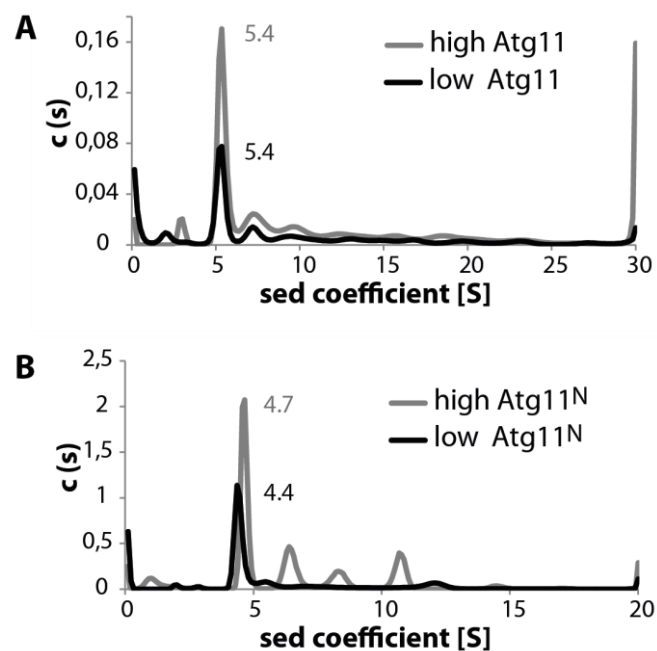
Figure 30 – Analytical ultracentrifugation reveals dimer formation of Atg11^{N}, but not full length Atg11. **(A)** Purified full length Atg11 was subjected to AUC analysis at high (1.63 mg/ml, grey line) and low (0.15 mg/ml, black line) concentration. Sedimentation coefficients are indicated. **(B)** Purified Atg11^{N} was subjected to AUC analysis at high (6.47 mg/ml, grey line) and low (0.19 mg/ml, black line) concentration. Sedimentation coefficients are indicated.

3.8.3 Atg11^N, but not Atg11, can tether Atg9-PLs

Due to the homology of Atg11 and Atg17, but contrasting regulation in selective and non-selective autophagy, redundancy of function can be presumed. Dimeric Atg17 functions as a tether for Atg9-PLs (Ragusa et al., 2012). Single vesicles have a substantially different R_H in comparison to that of two tethered vesicles. Determining size and polydispersity of molecules in solution by dynamic light scattering (DLS) therefore allows the identification of tethered vesicles. Dr. Yijian Rao had found previously that Atg9-PLs tend to self-associate and aggregate and therefore need to be sonicated prior to DLS experiments. Without the addition of stabilizing interactors they quickly form aggregates again. However, if Atg17 dimers are added, Atg9-PLs become stabilized and tethered, as indicated by the increase of R_H by a factor of two in comparison to small unilamellar vesicles (SUVs) lacking Atg9, which cannot be tethered and thus serve as control (Rao et al., 2016); * Figure 31 A). In order to investigate a possible tethering function of Atg11, the R_H of Atg9-PLs was determined by DLS in the presence of Atg11, Atg11^N and Atg11^C and compared to the R_H obtained in the presence of Atg17. Like Atg17, dimerizing Atg11^N was able to tether Atg9-PLs as indicated by the increase of R_H by a factor of two (Figure 31 A). In contrast to previous FRET experiments, Atg11^C, whose addition resulted in a multi-modular sample, failed to interact with Atg9-PLs. This indicates that the middle domain of Atg9 directly interacts with the N-terminus of Atg11, which is sufficient to tether vesicles. Full length monomeric Atg11 bound Atg9 as well, but was not able to tether vesicles. This suggests that dimerization is a prerequisite of Atg9-PL tethering and that dimerization of full length Atg11 is self-inhibited by its C-terminus. Homodimerization of Atg11 needs to be induced to activate its tethering activity.
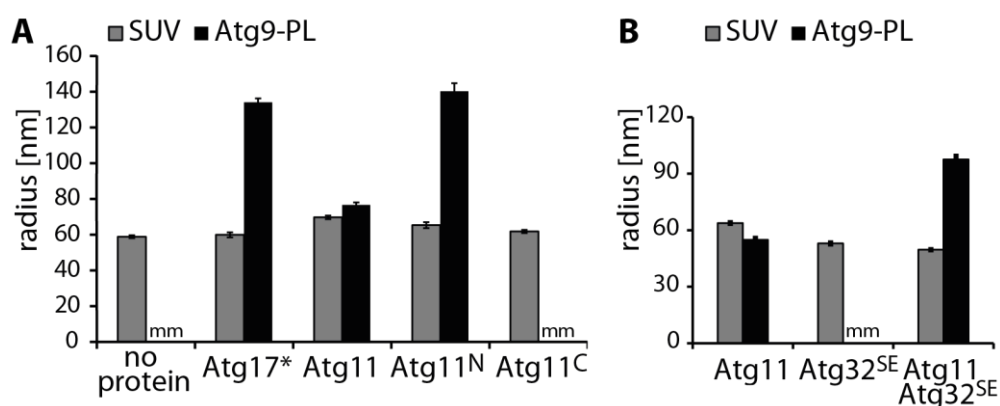
Figure 31 – Dynamic Light Scattering reveals tethering function of Atg11^N and Atg32^{SE}-activated Atg11. **(A+B)** Mean R_H of SUVs and Atg9-PLs mixed with indicated proteins as determined by Dr. Yijian Rao via DLS. Error bars are the SD obtained from n=5 consecutive measurements. mm = multi-modular **(A)** *Values for Atg17 are taken from (Rao et al., 2016) for comparison with a confirmed Atg9-PL tether.

### 3.8.4   Atg11 tethering function is activated by cargo interaction

Full length Atg11 is able to bind Atg9, but since it cannot dimerize, it is lacking the tethering function in vitro. This raises the hypothesis that Atg11 needs to be activated by a natural interaction partner. Although Atg17 and Atg11 share many properties in vitro and in vivo, they fundamentally differ in that Atg11 features cargo binding sites. Therefore a cargo receptor would be a reasonable activator for Atg11. Indeed, the addition of soluble Atg32[SE] to Atg9-PLs and Atg11 resulted in a R_H of about two vesicles (Figure 31 B).

The activation of Atg11 by Atg32 was also confirmed in vivo. The same soluble fragment of Atg32 used in vitro (Atg32[1-376] and its phosphomimetic variant Atg32[1-376,SE]) was overexpressed in the presence of GFP-tagged Atg11 and Atg11-puncta were quantified. Consistent with previous experiments, Atg11-puncta decreased in wildtype cells upon starvation. In contrast to that, the numbers of Atg11-puncta remained constant or were even slightly increased when cells overexpressed Atg32[1-376] and Atg32[SE] (Figure 32 A). The reversal of the normal trend could be counteracted by the concurrent overexpression of also Atg11. Though that resulted in a higher overall number of puncta, they decreased upon starvation, indicating correct regulation.

3.8.1   Cargo receptors regulate Atg11 activity in vivo

Atg32 is the cargo receptor for mitochondria destined to be targeted to the vacuole via mitophagy. The interaction of Atg32 with the C-terminus of Atg11 is essential for functional mitophagy (Aoki et al., 2011). In vitro experiments showed that this interaction stimulates Atg11 to tether Atg9-PLs and the overexpression of Atg32 and Atg32[SE] induces a slight increase in Atg11-puncta. In order to investigate whether these puncta correspond to an enhanced formation of mitophagosomes, the activity of mitochondria-targeted mtPho8 was assessed in cells with endogenous levels of Atg32 and with overexpressed soluble Atg32[1-376] and Atg32[1-376,SE]. Interestingly, while the overexpression of Atg32[1-376] had no effect on mtPho8 activity, it was doubled in vegetative conditions when Atg32[1-376,SE] was overexpressed (Figure 32 C). This indicates that, although wildtype Atg32 is able to interact with Atg11 in vitro, only phosphorylated Atg32 is able to stimulate mitophagy.

While Atg11 promotes selective autophagy by recruiting Atg9, Atg17 has the same function in non-selective autophagy. Therefore an increase in Atg9-sequestration by hyper-activated Atg11 might reduce the Atg9-vesicles available for Atg17. This was tested by measuring non-selective autophagy as expressed by cytPho8 activity in cells with endogenous levels of Atg32 and with overexpressed Atg32[1-376] and Atg32[1-376,SE]. In agreement with the prediction, cytPho8 levels were significantly reduced by both Atg32[1-376] and Atg32[1-376,SE] (Figure 32 D). This suggests competition between Atg11 and Atg17 for a limited amount of Atg9.
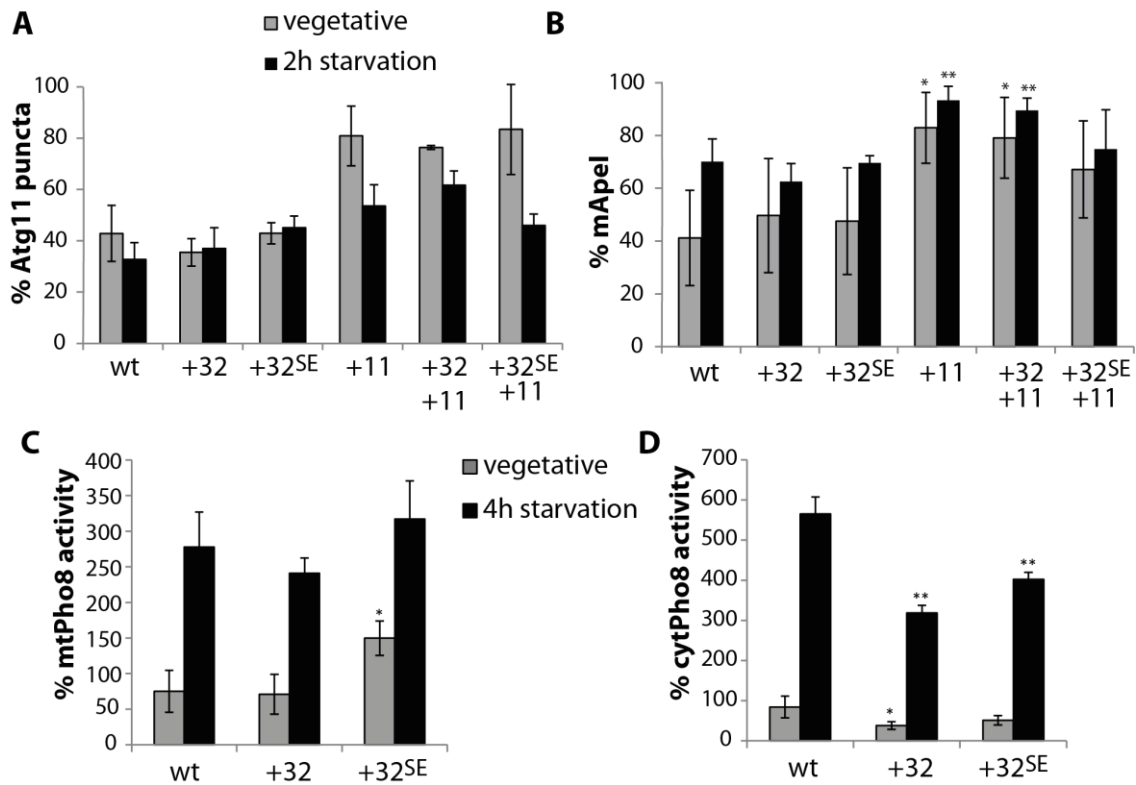
Figure 32 – Activation of Atg11 by soluble Atg32 in vivo. **(A)** Quantification of Atg11-puncta in vegetative and starvation conditions in wildtype (wt) cells and with overexpressed Atg32$^{1-376}$ (+32), its phosphomimetic variant Atg32^{SE} (+32^{SE}) and Atg11 (+11) where indicated. Error bars are the SD of n=3 independent experiments (except +11, which is of n=2) with >110 cells/condition/n. **(B)** Apel was detected in all samples from (A) by western blotting and band intensities of preApe and mApe were quantified. Shown are the % mApe of total ApeI (preApe+mApe). **(C+D)** Quantification of mtPho8 **(C)** and cytPho8 **(D)** activity in vegetative and starvation conditions in wildtype (wt) cells and with overexpressed Atg32$^{1-376}$ (+32) and its phosphomimetic variant Atg32^{SE} (+32^{SE}). Error bars are the SD of n=3 independent experiments. **(B-D)** P-values (*$p<0.05$, **$p<0.01$) were calculated versus the respective wt using a homoscedastic two-tailed Student's t-test.

Since Atg32 is binding to the C-terminus of Atg11, which also contains binding sites for other cargo receptors, overexpressed soluble Atg32 might block other forms of selective autophagy also depending on Atg11. The cargo receptor Atg19 marks ApeI for the Cvt pathway and shares a similar binding site on Atg11 with Atg32 (Yorimitsu and Klionsky, 2005). Competition between Atg19 and Atg32 for Atg11 would result in a decrease of ApeI processing when Atg32 is overexpressed. This was analyzed by quantifying the processing of preApeI to mApeI in the vacuole. About 40% of the total ApeI was mApeI in wildtype cells growing in vegetative conditions, starvation increased the processing to 70% (Figure 32 B). Interestingly, neither overexpressed Atg32$^{1-376}$ nor Atg32$^{1-376,SE}$ inhibited the Cvt pathway, indicating that the cargo receptors are not competing for Atg11. Overexpression of Atg11 increased the share of mApeI to around 90% in both vegetative and starvation conditions, concomitant overexpression of Atg32$^{1-376}$ or its phosphomimetic mutant again had no negative effect. This illustrates how Atg11 is the limiting factor in the degradation of specific cargo.

In conclusion, the mitophagy receptor Atg32 activates the tethering function of Atg11 at the expense of non-selective autophagy, but without compromising other forms of selective autophagy.

4 Discussion

In this study the function of Atg11 in autophagy as well as its regulation was investigated. The combination of in vitro and in vivo methods is a powerful approach to gain and validate insights at a molecular level. Atg11, a protein essential to selective autophagy in *S.cerevisiae*, was found to be a cargo-activated tether of Atg9-positive vesicles. Regulation of Atg11 allows the cell to switch from selective autophagy in vegetative conditions to non-selective autophagy in stress conditions.

4.1   Interaction analysis of recombinant full length Atg11

Since the discovery that Atg11 is linked indispensably to selective forms of autophagy, like the Cvt-pathway or pexophagy (Kim et al., 2001), its molecular function remained enigmatic. The literature proposed the involvement of Atg11 in various steps of autophagy. However, no function could be correlated conclusively with structure, localization and activity of Atg11. The purification of the functional full length protein in this study allowed all these functions to be addressed in vitro in addition to in vivo.

Previous in vivo interaction analysis found Atg11 to colocalize with cargo receptors like Atg32, the receptor of mitochondria destined for mitophagy, as well as with Atg8 coupled to autophagosomal membranes at the phagophore assembly site (PAS) (Yorimitsu and Klionsky, 2005). However, since many Atg proteins reside within large protein complexes at the PAS, these interactions might be indirect. In vitro studies were essential to validate direct interactions. Previously, only fragments of Atg11 were stable after recombinant expression. A weak interaction was found for a recombinant C-terminal fragment (685–1178) of Atg11 with phosphomimetic Atg19[3SD] (Pfaffenwimmer et al., 2014). In contrast, the present study used full length Atg11. GST-tagged full length Atg11 purified in a previous study was prone to degradation (Tanaka et al., 2014). Due to its four coiled-coil domains Atg11 is prone to self-aggregation and proves difficult to be expressed as soluble protein. The strategy developed here included fusion of the complete *ATG11* open reading frame to that of cleavable maltose binding protein to increase the protein solubility during bacterial expression. Additionally, folding of the protein was enhanced by concomitant overexpression of chaperones. This was key to produce pure and stable full length Atg11 (shown by MS and AUC in Figure 7).

A minimal system of selective autophagy was reconstituted from purified components previously. Sawa-Makarska et al. (Sawa-Makarska et al., 2014) found that ApeI-coated latex beads with a diameter of 2 μm, representing the cargo of the Cvt pathway, are recruited in an Atg19-dependent manner to GUV membranes decorated with Atg8[His] via the interaction with DGS-Ni-NTA. The cargo-mimicking beads were able to deform the membrane and induce their uptake by lipids. This represents a minimal system of selective uptake of cargo by Atg8-

decorated model membranes. Sawa-Makarska et al. observed a direct dependency of the frequency of membrane deformation on the amount of DGS-Ni-NTA in the membrane and achieved strongest deformation with 15 mol%. In contrast to that, in the present study Atg8 was conjugated enzymatically to 20 mol% PE in the GUV lipid mix to model autophagic membranes. Supposedly, the density of Atg8-PE on the membrane is similar by either chemical or enzymatic coupling. Due to the enzymatic coupling, Atg8 remains together with Atg12-Atg5-Atg16 as scaffold on the membrane (Kaufmann et al., 2014).

Here, a minimal system of mitophagy was developed. This includes the cargo receptor for mitochondria, Atg32 (Okamoto et al., 2009), which was chemically coupled to 1 µm beads for mimicking mitochondria destined for degradation. The interaction of the Atg32-decorated beads with Atg8 enzymatically coupled on GUV membranes was found to be sufficient for the uptake of model cargo by the phagophore surrogate. Comparably with the previous study, the cargo-mimicking bead became enclosed by lipid (see Figure 15 A).

Though Atg11 has been proposed to act as linker between cargo and the autophagosomal membrane (Youle and Narendra, 2011), it is not required in the minimal system of cargo uptake. Including Atg11 for the first time in in vitro reconstitutions, it was found to concurrently interact with the Atg8-decorated membrane as well as with Atg32 (Figure 13 and Figure 14 A top panel, respectively). Colocalization of Atg11 and Atg8 (Yorimitsu and Klionsky, 2005) and several possible AIM motives within the ATG11 sequence suggested direct interaction between them. Though possible AIMs were also proposed in *A.thaliana* ATG11 (Li et al., 2014), no single AIM responsible for Atg8 interaction could be identified in the present study (Figure 17). Possibly, Atg11 interacts with Atg8 via several AIMs or a non-canonical AIM as described for Atg7 (Noda et al., 2011). Since not only Atg8 alone but also its enzymatic Atg8-coupling machinery remains on the GUV membrane, potential candidates for the interaction of Atg11 with the membrane also include Atg12, Atg5 or Atg16. Atg12 was detected in a complex with Atg11 once in affinity-capture MS (Ho et al., 2002), suggesting either direct for indirect complex formation. On the other hand, mammalian ATG16L1 has been demonstrated to directly interact with FIP200 (Gammoh et al., 2013), a potential homolog of Atg11 in higher eukaryotes (Li et al., 2014). Further testing of Atg8 or other Atgs chemically coupled to the GUV membrane would be required to differentiate between Atg8 or other components of the coupling machinery as interaction partner of Atg11 on the autophagosomal membrane.

In conclusion, though Atg11 binds both cargo receptors and the autophagosomal membrane, it is not required for the interaction of cargo with the autophagosomal membrane in vitro.

4.2   Phospho-regulation of cargo receptors

Several cargo receptors have been found to mediate the degradation of their respective cargo in a phospho-regulated manner. Atg32 has a phosphorylation site at serine 114, which was reported to be essential for the interaction of Atg32 with Atg11 (Aoki et al., 2011). The in vitro reconstitution system can also be employed for studying the effect of mutations on direct protein interactions. As shown in Figure 14 B, both Atg32 with and without a phosphomimetic mutation at serine 114 can interact with Atg11. Interestingly, though both variants of Atg32 interact with Atg11, only Atg32^{SE} can induce mitophagy. Overexpression of wildtype and phosphomimetic Atg32 in vivo showed that the phosphorylation increases mtPho8 activity, but is not promoting other forms of selective autophagy, like the Cvt pathway (shown in Figure 32, C and B, respectively). The phosphorylation of cargo receptors therefore does not seem to be necessary for their interaction with Atg11, but for inducing the respective form of selective autophagy.

4.3   Atg11 is more than a cargo adaptor

Atg11 is essential for many forms of selective autophagy. Due to the interaction of Atg11 with both cargo receptors and autophagosomal membrane, it was suggested to act as cargo adaptor. However, in vitro reconstitution showed that the direct interaction of the cargo receptor with Atg8 is sufficient to induce cargo uptake in vitro. Therefore spatial analysis of Atg11 on the phagophore membrane was employed to investigate the adaptor function in vivo. Imaging of GFP-tagged Atg11 in cells harboring stable giant cargo revealed a defined punctate structure rather than an isolation membrane staining (Figure 18). This suggests a spatially constricted function at a certain point of the autophagosomal membrane and therefore conflicts with an adaptor function, which has to cover the entire phagophore. Previously, punctate localization was categorized into binding the tips or at the center of the expanding autophagosomal membrane, in contrast to extending along the whole membrane (Suzuki et al., 2013). Only Atg1 and Atg8 with its scaffold-forming lipidation machinery (Atg12-Atg5-Atg16) were found to extend along the whole expanding isolation membrane. In contrast, Atg11 exhibits a punctate distribution pattern similar to that of Atg13 and Atg17 at the vacuole-isolation membrane contact site. This indicates that Atg11 does not remain at the interface of cargo and autophagosomal membrane and does therefore not become degraded in the vacuole. This is confirmed by the lack of GFP accumulation in the vacuole of *GFP-atg11* strains. The release of cargo by Atg11 prior to degradation in the vacuole is consistent with the in vitro observation that interaction of the cargo receptor with membranes is sufficient for the uptake of cargo by the membrane. The unclear adaptor function of Atg11 was further tested in vivo by an artificial construct consisting of an Atg32-derived AIM in replacement of the N-terminal Atg17-like domain of Atg11, and fusing it to the cargo-interacting C-terminus of Atg11. Since this minimal construct is able to crosslink cargo and

Atg8, it would have fulfilled a simple linker function of Atg11. However, it was found incompetent of functionally rescuing selective autophagy in *atg11Δ* cells (Figure 23 B and C; Figure 24 B). In the light of cargo being able to interact with autophagosomal membranes independently of Atg11, the function of Atg11 cannot be limited to that of an adaptor. Instead, the double sided interaction of Atg11 with cargo and membrane suggests that these are transient interactions required in an early step of delivering cargo to the phagophore.

4.4 Atg11 is not an actin motor protein

Atg11 interacts with both cargo receptors and Atg8-decorated membranes; however, it is not required for tethering cargo to the autophagosomal membrane during expansion of the phagophore. Therefore possible functions in earlier steps of cargo delivery were investigated. Protein sequence comparison of Atg11 with other sequences found homology to the structure of actin motor proteins like Myo2 (Monastyrska et al., 2006). In support, Atg11 recruitment to the PAS is disrupted when actin mobility is perturbed in *act1-159* mutated strains (Reggiori et al., 2005). However, disruption of this important cellular network obviously has many deleterious effects on the cell, not only on Atg11. Mislocalization may therefore also be caused by indirect effects, not perturbed interaction of Atg11 with actin. Motor proteins like Myo2 strongly adhere to polymerized actin. Centrifugation experiments of polymerized actin mixed with Atg11 resulted in a separation of both (shown in Figure 16 C), indicating that no stable interaction occurs. Movement of actin-interacting proteins through the cell can also occur by inducing or inhibiting polymerization of filaments. However, Atg11 is also not interfering with the polymerization of actin. Furthermore, though Atg11 was found to colocalize with actin filaments in vitro (see Figure 16 A), the distribution pattern appeared rather random and not localized to the tips of the filaments like most actin-binding proteins do. In conclusion, no evidence could be identified for Atg11 to act as actin motor protein. Nevertheless, a possible indirect function of Atg11 in actin-dependent transport of autophagosomal components by interacting with actin-binding factors like the Arp2/3 complex (Monastyrska et al., 2008) remains to be explored.

4.5 Atg11 fills in for Atg17 at the PAS

Function of Atg11 was further investigated by localization studies. During vegetative growth, GFP-tagged Atg11 forms visible puncta, many of which colocalize with the PAS marker Atg8 (Yorimitsu and Klionsky, 2005). PAS forming in vegetative conditions are thought to be mostly derived from the Atg11-mediated Cvt pathway, which forms smaller autophagosomes than non-selective autophagy in starvation conditions (Baba et al., 1997). This fits well with the reduction of fluorescent Atg11-puncta in starvation conditions to 26% compared to vegetative conditions. Also only few Atg8 puncta are still positive for Atg11 upon induction of autophagy (Figure 20 A,C). However, though the overall protein level of Atg11 decreases in

starvation conditions (compare Atg11 levels in lysates in Figure 22), it mostly becomes redistributed within the cell. Upon starvation, concurrent with a decrease in PAS localization, a significant amount of Atg11 associates with small vesicular structures in the cell (Figure 21A). In striking contrast, Atg17 only localizes to few puncta in vegetative conditions, but the number of puncta is clearly induced by starvation (Figure 29 B). Interestingly, a deletion of Atg17 increases the Atg11 puncta during starvation conditions to 60% compared to vegetative growth (Figure 20 A and C). The data indicates that in wildtype cells Atg17 replaces Atg11 upon induction of autophagy, but both proteins are similar enough, so that Atg11 is able to compensate for Atg17. Interestingly, the deletion of ATG17 indeed leads to the formation of smaller autophagosomes in starvation conditions, reminiscent of autophagosomes formed in the Atg11-mediated Cvt pathway (Kabeya et al., 2005). However, at this point it could not be excluded that retention of Atg11 at the PAS in the absence of Atg17 is a secondary effect. Therefore spatial regulation of both proteins needed to be investigated at a molecular level.

4.6   Competition of Atg11 and Atg17 for interaction partners

Both Atg11 and Atg17 have been proposed to be components of the Atg1 kinase complex (Kim et al., 2001). However, Atg17 displaces Atg11 from the PAS and both have non-redundant functions in vivo, suggesting that they are not active simultaneously. Correspondingly, cargo activates Atg11 to recruit Atg1 (Kamber et al., 2015), while Atg17 is activated by Atg1-Atg13 to tether of Atg9-vesicles (Rao et al., 2016). Atg17 physically interacts with Atg13, Atg31 and Atg9 (Kabeya et al., 2005). Atg31 and Atg29 form a regulatory subcomplex tightly associated with Atg17. The resulting heterotrimer is dispensable in the Atg11-dependent Cvt pathway (Cheong et al., 2005), while most other proteins of the canonical autophagic machinery are still required for selective autophagic pathways. This suggests Atg13 and Atg9 to act as common interactors, and both have indeed been found to interact with Atg11 by in vivo studies previously (Kamber et al., 2015). Interestingly, Atg9 binding sites have been mapped in both Atg11 and Atg17 to homolog regions (see Figure 25). Atg13 interacts with Asp247 of Atg17 via Ser428 and Ser429 during starvation, but becomes phosphorylated at these sites in vegetative conditions, preventing its interaction with Atg17 (Fujioka et al., 2014). Intriguingly, the Atg13-interacting region differs in Atg17 from the homolog Atg11 sequence. The negatively charged Asp247 and Asp248 of Atg17 are Ser and Gln in Atg11. Since Atg1 needs to be recruited by Atg13 to both proteins, the differently charged Atg13 interaction sites in Atg11 and Atg17 might therefore allow the regulated recruitment of either Atg11 or Atg17, mediated by the phosphorylation state of Atg13. Here, substantial evidence was gathered to confirm the direct interaction of Atg13 and Atg9 with Atg11 in vitro.

The physical interaction of Atg11 with its supposed interactor Atg13 could be shown by in vitro FRET (Figure 27 A) and by SPR (Figure 26 A) measurements. Microscale thermophoresis (MST) was tested as well, but it only revealed that Atg13 is prone to aggregation at higher concentrations, which prevented concentration-dependent correlation of the sensitive fluorescence signal. In vivo, Atg13 is hyper-phosphorylated in vegetative conditions, and starvation induces dephosphorylation. Supposedly, the phosphorylation regulates the interaction with Atg11, since Atg13 was enriched in affinity-capture MS of Atg11 in vegetative compared to starvation conditions (Figure 19). However, Atg13 interacted with Atg11 in vitro without modifications. It is conceivable that phosphorylation might increase the interaction efficiency, or the binding site differs from the phospho-regulated Atg17-binding site. In the light of Atg17 interacting with Atg13, and thereby recruiting Atg1, a similar bridging function of Atg13 was assumed in the case of Atg11. This is in contrast to a purported interaction of Atg1 with Atg11^{CC2} and Atg11^{CC3} (Yorimitsu and Klionsky, 2005). A strong indication that Atg11 recruits Atg1 via Atg13 was found in Atg1 interacting with Atg13, but not Atg11 directly, in SPR (Figure 26 B). This clearly demonstrates the weak point of in vivo protein interaction analysis, which cannot exclude indirect interactions. The direct interaction with Atg13 confirms that Atg11, like Atg17, is able to take part in a selective Atg1 kinase complex.

Atg9^{core}, a fragment of Atg9 from amino acid 281 to 779, was embedded in liposomes and subjected to protein-protein interaction analysis in solution. Both in vitro FRET analysis (Figure 27 B) and co-flotation (Figure 28) detected Atg9-interaction with Atg11, confirming previous in vivo studies (Chang and Huang, 2007). However, a reported binding site in the N-terminus of Atg9 (He et al., 2006), which is not included in Atg9^{core}, was dispensable, suggesting that the core region of Atg9 is sufficient for Atg11 interaction. Furthermore, interaction of full length Atg9 with Atg11 is not mediated by either Atg13, Atg17, Atg29 or Atg31 in vivo, since their deletions are not reducing the co-immunoprecipitation of Atg9 with Atg11 (see Figure 22). To the contrary, deletion of Atg17 or its regulatory subunits Atg29 and Atg31 even significantly increase the interaction between Atg11 and Atg9. This suggests that the trimeric complex is competing with Atg11 for Atg9 binding sites.

Atg11 is the scaffolding protein of the Atg1 kinase complex, which recruits Atg9 in selective autophagy. Analysis of subcellular location of Atg9 and Atg11 in vegetative and autophagy induced conditions contributes to the understanding of the order of recruitment of the autophagic machinery. Substantial amounts of the transmembrane protein Atg9 reside in large membrane structures in vegetative conditions, but become increasingly sorted to small vesicles upon starvation. In contrast, Atg9^{core} is retained within large membrane structures during starvation as well, in agreement with the deleted C-terminal sorting signal (Figure 21C). Interestingly, in the presence of Atg9, Atg11 is localizing mainly to fractions containing

large membranes in vegetative conditions, and becomes enriched in fractions with small vesicles upon starvation. However, if Atg9 [core] is used instead, Atg11 colocalizes with large membranes. This constitutes a surprising match in localization between Atg9 and Atg11, indicating that not only Atg11 contributes to the recruitment of Atg9 (He et al., 2006), but also Atg9 is able to define the location of Atg11. Since their interaction is independent of other components of the autophagic machinery, like Atg1 and Atg13, Atg11 and Atg9 seem to interact upstream of Atg1 kinase complex formation.

4.7 Atg11 and Atg17 are not interchangeable, but cooperate

Both Atg11 and Atg17 co-flotate with components of the Atg1 kinase complex and Atg9, and co-precipitation suggested that they collaborate at the PAS (Mao et al., 2013a). However, Atg17 displaces Atg11 from the PAS and both have non-redundant functions in vivo, raising the question whether Atg11 and Atg17 are active at one PAS simultaneously, colocalize at the PAS transiently, or initiate distinct PASs? Components of the PAS have been quantified and about 28 copies of Atg17 and Atg1 kinase complexes were found per PAS in both vegetative and starvation condition (Kofinger et al., 2015), indicating that the recruitment of Atg11 to the PAS in vegetative conditions is not changing the composition of Atg17-positive PAS. Though the number of Atg11 puncta significantly drops during starvation, still there are always a few Atg8 puncta Atg11-positive. With Atg11 being able to interact with several proteins present within the Atg1 kinase complex, it is not surprising to detect both Atg17 and Atg11 within one PAS by either yeast-two-hybrid (Yorimitsu and Klionsky, 2005) or co-precipitation (Mao et al., 2013a). Atg8-lipidation is an early event of PAS formation, and is therefore commonly employed for the study of autophagy defects. Atg8 lipidation and the transport of Atg8 to the vacuole depend on Atg11 and Atg17, since both is inhibited in double deletion strains. However, deletion of either Atg11 or Atg17 neither reduces Atg8 lipidation nor the transport of Atg8 to the vacuole (Suzuki et al., 2007); Figure 23 A). If PAS formation is possible in the absence of either Atg11 or Atg17, cooperation is not essential and PAS formation could proceed independently for selective and non-selective autophagy. However, the question arises if in deletion strains the remaining protein is able to substitute for one another functionally, i.e. Atg11 mediating non-selective autophagy and Atg17 mediating selective autophagy, or if the processing of Atg8 is only observed due to the remaining form of autophagy. Selective and non-selective autophagy can be quantified separately by observing the processing of mitochondrial or cytoplasmic cargo, respectively. Both GFP-processing assays and Pho8 activity (Figure 23 B,C; Figure 24 A,B) confirm that *atg11Δ* cells are dysfunctional in selective autophagy, indicating that Atg17 is not able to replace Atg11 in the transport of selective cargo. Conversely, *atg17Δ* strains are defective in non-selective autophagy, ruling out that Atg11 functionally replaces Atg17. These functional studies therefore suggest that detection of both proteins within one complex does not indicate that

both are required or active. Instead, Atg11 is required non-substitutably for selective and Atg17 for non-selective autophagy.

Nonetheless, Atg11 and Atg17 seem to have a supportive function in the respectively alternate pathway. An *atg17Δ* strain is 25% reduced in its selective autophagy after 4 hours of starvation, and an *atg11Δ* strain is 43% reduced in its non-selective autophagy (Figure 24 A,B). This indicates that, though Atg11 and Atg17 are required non-substitutably for initiation of selective and non-selective autophagy, respectively, both support the alternate pathway at later stages. The complex formation required for cooperation has been observed both by co-precipitation in vivo and co-flotation in vitro. However, due to reduced PAS localization of Atg11 in starvation conditions, cooperation of Atg11 and Atg17 is thought to be a transient event. Thus a model is possible, in which Atg11 initiates a selective PAS and is later on replaced by Atg17, leading to elevated levels of selective autophagy. Interestingly, the specificity of selective autophagosomes can be maintained upon activation of Atg17 by starvation. Selective autophagosomes do not require Atg11 for the exclusion of cytoplasm from their lumen, since the cargo receptor can interact with Atg8 directly in the absence of Atg11. The exclusion of bulk cytoplasm from selective autophagosomes has been shown before (Sawa-Makarska et al., 2014) and was confirmed here in *atg17Δ* cells, which show mtPho8 activity but at the same time no cytPho8 activity.

The role of Atg11 in non-selective autophagy is rather elusive. It might involve facilitated initiation due to augmented recruitment of Atg17[TC] to Atg9 by Atg11, as was observed in this study in vitro. However, Atg17 is sufficient to initiate non-selective autophagosomes. Therefore Atg11 seems to play an important unidentified role at later stages of non-selective autophagy. This renders the question of how Atg11 and Atg17 amplify the autophagic response in the alternate pathway at a molecular level an interesting open question. Additional studies are required to understand if one PAS features both Atg11 and Atg17, or if they form separate PAS.

4.8   Atg11 acts as vesicle tether

Atg11 was found to act as membrane tether in this study, however, it is not the first protein reported to act as tether in autophagy. On the one hand, regulation between selective and non-selective autophagy seems to involve the switch from Atg11 to Atg17, which is tethering Atg9-vesicles for initiation of non-selective autophagosomes (Rao et al., 2016). On the other hand, deletion of many proteins involved in cellular membrane trafficking results in autophagy inhibition. However, this is not always due to direct involvement of these proteins in autophagy, but their role in the generation of the Atg9-vesicle pool. Therefore, reduction of autophagy can be a secondary effect of disrupted cellular membrane trafficking, which is

complicated to functionally separate from autophagy in vivo. This increases the relevance of the in vitro approached used here to reveal the tethering capacity of Atg11.

The small Rab GTPase Ypt1 is activated by its GEF TRAPPI complex to interact with its downstream effector Uso1, a coiled-coil tether in ER-to-Golgi transport (Cao et al., 1998). Lynch-Day et al. (Lynch-Day et al., 2010) showed that in the context of autophagy also another GEF, TRAPPIII, can interact with Ypt1. The TRAPPIII-subunit Trs85 colocalizes with both Atg11 and Atg9 in vivo (Kakuta et al., 2012)Kakuta et al., 2012) , and Ypt1 also interacts with Atg11[CC2,CC3] directly (Lipatova et al., 2012). This indicates that Atg11 functions as an effector of Ypt1 in autophagy, similar to Uso1 in the ER-to-Golgi trafficking. The largely α-helical secondary structure of Atg11 is comparable to coiled-coil tethers as well. 58% of soluble Atg11 fold into α-helices; 25% remain unstructured in solution but might become structured upon contact with interaction partners. These numbers correspond well to the prediction of 85% being able to fold into α-helices (see comparison of prediction with actual structure determined by CD in Figure 8). It is unclear at this point if both Atg11 and Atg9 interact with Trs85 directly, or if Atg11 acts as bridge to promote close contact between Atg9 and Trs85. Priming of SNAREs is a typical function of membrane tethering complexes downstream of GTPases to regulate membrane fusion events; direct interaction of the vacuolar SNARE Vam7 with Atg11 (Liu et al., 2016) therefore supports the hypothesis that Atg11 acts as a membrane tether.

When testing tethering activity of Atg11 in vitro, it was found that Atg11 needs to be activated through concurrent interaction with cargo receptors and Atg9. While Atg11 alone is able to interact with Atg9 in vitro, it does not yet tether vesicles (see Figure 31 A). This agrees with published data for monomeric mutants of Atg17, which are only able to interact with Atg9, but do not display any tethering function (Rao et al., 2016). However, wildtype Atg17 is forming dimers and thereby tethers two Atg9-vesicles. Also Atg11 is able to form dimers in vivo (Kim et al., 2001). In vitro, the dimerization is self-inhibited by the C-terminus of Atg11, as only the N-terminus alone is showing dimer formation (see shift in AUC shown in Figure 30). The C-terminus of Atg11 harbors the cargo interaction site. Addition of soluble Atg32[SE], the mitochondrial receptor protein, induces the formation of a population equivalent in R_H of two tethered vesicles (see Figure 31 B). Arguably, this suggests that interaction with a cargo receptor activates Atg11 dimerization. The dimer then acts, similarly like Atg17 (Ragusa et al., 2012), as a tether of two Atg9-vesicles. However, activation might also translate to structural changes of Atg11, exposing a second Atg9 binding site within one Atg11 molecule. Further studies are required to confirm regulated dimerization of Atg11.

4.9 Regulation of the switch from selective to non-selective autophagy

S.cerevisiae was found to employ separate membrane tethers for selective and non-selective autophagy. While Atg11 is able to tether Atg9-vesicles to initiate selective autophagy, the cell switches to Atg17 for non-selective autophagy. It appears to be puzzling as to why two different Atg9-vesicle tethers are required, however, the alternating activity of Atg11 and Atg17 in different conditions provides some insights. While Atg11 is mostly active at the PAS in vegetative growth conditions, it is handing over its function to Atg17 in starvation conditions (see quantification of fluorescent puncta in wildtype strains in Figure 29 B). Atg17 is abundantly present in the cell with a copy number of about 360 proteins per cell (Ghaemmaghami et al., 2003). On the other hand, Atg11 only has about 85 copies per cell (Ghaemmaghami et al., 2003). Therefore the more abundant Atg17 could easily outcompete Atg11 and massively induce autophagy in all conditions. This is prevented in vegetative conditions by keeping Atg17 in an inactive state by the Atg31-Atg29 subcomplex (Rao et al., 2016). In addition, Atg11 is activated in vegetative conditions by simultaneous regulation by at least Ypt1, Atg9 and a cargo receptor (see Figure 33 a,b). The latter are phospho-regulated themselves (Pfaffenwimmer et al., 2014) and thereby also ensure that Atg11 only mediates autophagosome biogenesis when the transport of a specific cargo to the vacuole is required. The multivalent regulation is probably the reason for Atg11 to remain at the PAS in the absence of Atg17 (Figure 20) and continue the interaction with Atg9 during starvation conditions (Figure 21 and Figure 22), without becoming fully activated for mediating non-selective autophagy (Figure 24). To effectively switch from selective to non-selective autophagy in response to stresses like nutrient deprivation the cell seems to deactivate Atg11 concurrently to activating Atg17 (see Figure 33b). Impeding the deactivation of Atg11 by overexpression of phosphomimetic Atg32 increases selective mitophagy and at the same time reduces non-selective autophagy in starvation conditions (Figure 32 C,D).
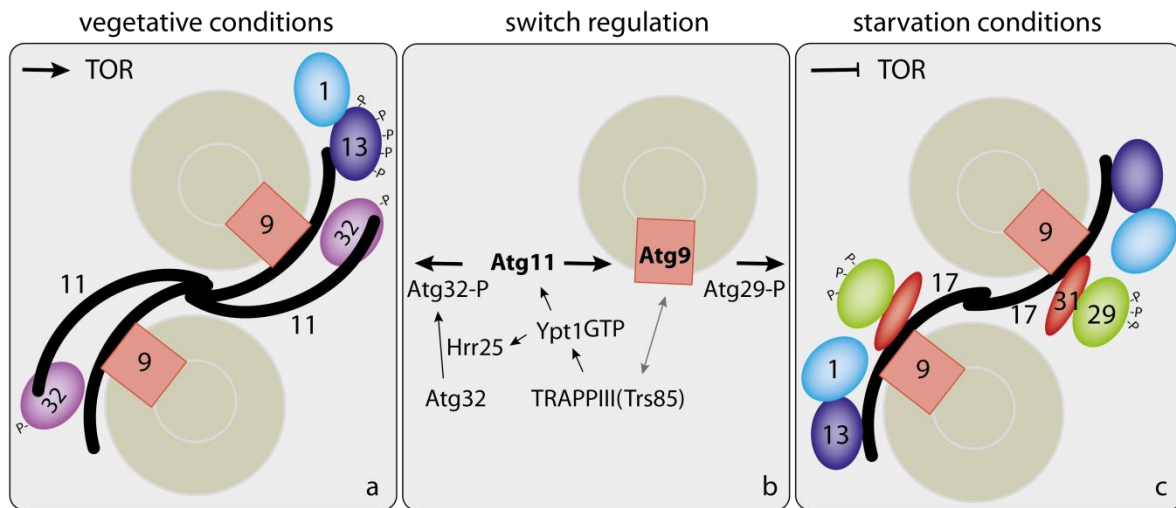
Figure 33 – Scheme of the regulated switch of Atg9-vesicle tethers. **(a)** Atg11 is tethering Atg9-vesicles for selective autophagy in vegetative conditions. Minimum activation of Atg11 involves interaction with Atg9 and the cargo receptor Atg32. Interaction with Atg1 via Atg13 further promotes autophagy. P indicates phosphorylation. **(b)** Mitophagy is mediated by interaction of Atg11 with phosphorylated Atg32. Hrr25, which is recruited by Ypt1^{GTP}, phosphorylates cargo receptors. Ypt1^{GTP} also interacts with Atg11 and via its GEF TRAPPIII^{Trs85} with Atg9. Upon induction of non-selective autophagy, the switch to Atg17 requires recruitment of the trimeric complex Atg17-Atg31-Atg29 via interaction of phosphorylated Atg29 with Atg9. **(c)** Dimeric Atg17 tethers Atg9-vesicles in non-selective autophagy, induced by starvation. It replaces Atg11 at the binding sites of Atg9 and Atg13.

Activation of Atg17 involves, on the one hand, interaction with dephosphorylated Atg13 (Rao et al., 2016). Dephosphorylation of Atg13 is prompted by canonical induction of autophagy (Kabeya et al., 2005). On the other hand, recruitment of Atg17 to Atg9 was found to be mediated by phosphomimetic Atg29 in vitro. The trimeric complex strongly associated with Atg9 in a phospho-dependent manner and Atg11 was found to increase the interaction. These results are in line with Atg29 becoming phosphorylated in starvation conditions in vivo. The finding that only phosphorylated Atg29 co-precipitates Atg11 (Mao et al., 2013a), can be attributed to the phospho-regulated interaction of Atg29 with Atg9, augmented by the interaction of Atg9 with Atg11. Confirming the in vitro results, Atg11 puncta formation was only little affected by phosphomimetic Atg29 (Figure 29 B). However, Atg29^{3SD} reduced the interaction of Atg11 with Atg9 (Figure 29 A) concurrently to increasing the number of Atg17 puncta, suggesting that activation of non-selective autophagy via increased recruitment of Atg17 reduces selective autophagy. Therefore a model is plausible, where induction of autophagy leads to phosphorylation of Atg29, which then recruits the trimeric complex Atg17-Atg31-Atg29 to Atg9 at the PAS (see Figure 33 b,c). There the complex exists probably transiently in a state with both Atg11 and Atg17 bound, as seen in the in vitro experiments. Thus, by employing two independently regulable tethers for different needs, the cell limits unnecessary break-down of still useful components while ensuring quality control.

4.10 Modulation of autophagy is becoming tangible

In humans, several pathologies, including cancer and neurodegenerative diseases, have been shown to be closely linked to autophagy. The tumor suppression factor p53 directly interacts with mammalian FIP200 and inhibits autophagy (Morselli et al., 2011). Therefore deletion of various autophagy core machinery proteins, including FIP200, prevents tumor initiation and progression in mammary tumorigenesis in mouse models (Wei et al., 2011). In addition, ubiquitinated protein aggregates, p62 and mitochondria with abnormal morphology accumulated in the tumor cells, indicating a block of selective autophagy. These tumors rely on autophagy and a block is beneficial in treatment. In contrast, a hallmark of neurodegenerative diseases are accumulated protein aggregates and dysfunctional mitochondria, suggesting that inhibited autophagy is the primary cause of disease etiology (Komatsu et al., 2006). Treatment therefore requires the reverse strategy of cancer therapy, an activation of autophagy. Regulation needs precise targets to avoid systemic side-effects.

 In yeast, Atg11 initiates selective, but not general, autophagy, rendering it a control-lever for certain types of autophagy. It was demonstrated that Atg11 can be activated to increase the rate of mitophagy without decreasing other forms of selective autophagy or non-selective autophagy in vegetative conditions (see Figure 32). Since the clearance of protein aggregates and dysfunctional mitochondria also relies on selective autophagy in mammalian cells, expectations are raised that autophagy could be modulated in a similar manner. However, this requires the identification of a regulable human homolog of Atg11. Using mitophagy as exemplary selective pathway reveals a high degree of diversification in higher eukaryotes in comparison to yeast, suggesting that Atg11 might have several homologs in mammalian cells. Mitophagy is employed tissue-specifically for the maturation of erythrocytes mediated by the receptor NIX (Schweers et al., 2007), degradation of paternal mitochondria in *C.elegans* oocytes mediated by an unknown receptor (Al Rawi et al., 2011), and for hypoxia-induced mitophagy mediated by FUNDC1 (Liu et al., 2012). The function of the recently identified mitochondria-specific receptor Bcl2-L13, the mammalian homolog of yeast Atg32 (Murakawa et al., 2015), is not yet known. Instead of employing a specific receptor, dysfunctional mitochondria can also be ubiquitinated to maintain mitochondrial homeostasis, a signal which is then recognized by autophagic adaptors. While autophagic adaptors like p62 mediate the interaction with Atg8-homologs directly, they can also be recognized by huntingtin (HTT), which interacts in addition with components of the Atg1/ULK1 kinase complex and the mitochondrial receptor NIX. Remarkably, the C-terminus of HTT shares structural features with Atg11 and, like Atg11, HTT needs to be activated to be functional in selective autophagy (Ochaba et al., 2014). Comparable to the Cvt pathway in yeast, it was suggested that HTT might be involved in its own autophagic clearance. HTT mutants were found to block this degradation, which results in protein aggregates and finally

causes Huntington Disease. The cargo-dependent activation of HTT is reminiscent of the cargo-dependent activation of Atg11 and therefore renders HTT a good candidate for a regulable Atg11 homolog. Structural studies of both yeast and mammalian Atg11 and its interacting cargo receptors might allow the identification of small peptides or chemicals able to induce or block selective autophagy of certain cargos. The targeted modulation of autophagy is a promising outlook for pharmacological intervention with reduced systemic side-effects.

4.11 Outlook

In this study recombinant Atg11 was found to be activated by the cargo receptor Atg32 to tether Atg9-vesicles in vitro and thereby initiate selective autophagy in *S.cerevisiae*. However, the switch from selective autophagy to non-selective autophagy, mediated by the tether Atg17, is not fully understood. It involves recruitment and activation of the respective tether by regulatory factors. While Atg17 is recruited by phosphorylated Atg29, its tethering activity is activated by Atg13 (Rao et al., 2016). Atg11, on the other hand, is activated by cargo, rendering the purpose of the observed interaction of Atg11 and Atg13 enigmatic. Atg13 is necessary for the recruitment of the essential Atg1 kinase to Atg17 (Kabeya et al., 2005). Directly tethering Atg1 to Atg11 might clarify if the sole purpose of Atg13 in selective autophagy is that of Atg1 recruitment. Although Atg11 and Atg17 are not functionally interchangeable, cooperation of both proteins suggests that switching between selective and non-selective autophagy is not fully deactivating the respectively alternate protein. It needs to be investigated which step of autophagy is mediated exclusively by one protein and in which manner they cooperate to amplify the autophagic response. In case of continuous cooperation increased colocalization of fluorescently tagged Atg11 and Atg17 could be observed at the PAS upon induction of autophagy, however, transient events of interaction cannot be captured due to too weak fluorescence. In that case, spatio-temporal regulation during the switch would need to be investigated at a single-molecule level.

A constant matter of discussion in the field of autophagy concerns the identity of the PAS. The PAS is defined as the perivacuolar site at which Atg proteins accumulate to promote the formation of the phagophore. Therefore the protein highest in the order of recruitment defines the location of the PAS. In non-selective autophagy Atg17 has been found to be the most upstream factor defining the location of Atg9 and the Atg1 kinase complex (Suzuki et al., 2007). This suggests that Atg11 would be the determining factor in selective autophagy. On the one hand, Atg11 is indeed required to recruit Atg9 in selective autophagy (He et al., 2006). On the other hand, the interaction of Atg11 with the core domain of Atg9 is sufficient to redistribute Atg11 to the cellular fraction containing Atg9^{core}. This indicates that Atg11 and Atg9 interact upstream of Atg1 kinase complex formation and are therefore together the main

determinant of PAS localization in selective autophagy. Taking into account that Atg11 is involved in mitochondrial fission prior to mitophagy (Mao et al., 2013b) and that Atg11 requires activation by cargo, it can be hypothesized that the selective PAS is initiated at a vacuolar-distant site and then transported to the perivacuolar location observed later on. However, the order of initiation and transport of the PAS together with cargo awaits further investigation.

A long-standing question also concerns how the cup-shaped precursor membrane is generated from Atg9-vesicles. After tethering of two vesicles by either Atg11 or Atg17, they need to fuse in a SNARE-mediated manner. SNARE-priming has been shown for Atg11 and Atg17 in late steps of autophagy, where they interact with the vacuolar SNARE Vam7 (Liu et al., 2016). However, autophagy-specific SNAREs involved in initial steps of phagophore assembly are not known yet in yeast. In vitro approaches testing sets of SNAREs for fusion of liposomes primed with autophagy-specific tethers will help to dissect SNAREs required for autophagy from SNAREs involved in general membrane trafficking and the generation of the Atg9-vesicle pool.

Special emphasis should be placed on structural studies in the future. It is not clear if Atg11 indeed acts as a dimer like shown for Atg17 and Atg11[N], or is activated by cargo interaction to expose a second Atg9 binding site within one protein moiety. However, Atg11 is flexible and prone to aggregation and degradation and therefore produces strong variation in structural data, rendering the distinguishing between monomers and dimers difficult. In addition, multivalent activation involves the simultaneous presence of several proteins within one sample and requires methods suitable for all of them. Nevertheless, extensive protocol optimization might allow the observation of a difference in the tether of two Atg9-vesicles depending on the use of Atg11 alone or Atg11 mixed with Atg32[SE] in e.g. single particle TEM. Fine-mapping of the cargo-receptor interaction with Atg11 requires crystal structures. C-terminal fragments of Atg11 are easier to handle than the full length protein and might be susceptible to co-crystallization.

Another direction of the project would be the direct translation to higher eukaryotes. Affinity capture MS of, for example, the newly identified mammalian homolog of yeast Atg32, Bcl2-L13 (Murakawa et al., 2015), will help to identify proteins unknown to be involved in selective autophagy in higher eukaryotes. While sequence alignments have helped to identify several possible homologs, their specific functions need to be dissected in the future. In vitro experiments will be necessary to confirm direct protein interactions and similar pathway induction and regulation as observed here in yeast. Importantly, mammalian ATG9 has not been linked to any autophagic tether yet, representing a substantial gap of knowledge. Therefore it remains to be investigated if tethering activity is coordinated with cargo

recruitment within one protein in mammalian cells. Possibly, functions are split up into individual proteins to increase the levels of regulation. This would allow fine-tuned stimulation of individual autophagic pathways by inducing them at the level of cargo-interaction.

Insights obtained in this study put Atg11 to the forefront of regulation of autophagy. Atg9 is at the center of the switch between selective and non-selective autophagy. Though spatially interchangeable, autophagy tethers are functionally restricted to mediate selective or non-selective autophagy and the switch is tightly regulated. Depending on the conditions and cargo, either Atg11 or Atg17 are activated to tether Atg9-vesicles to initiate autophagosome biogenesis, elongation and fusion with the vacuole. Discovery of regulatory proteins allows induction and regulation of the switch towards selective autophagy. Substantiating the results with crystal structures of protein interaction sites and identifying mammalian homologs of all proteins involved will be required for rendering pharmacological intervention in diverse human diseases achievable.

5 References

Al Rawi, S., Louvet-Vallee, S., Djeddi, A., Sachse, M., Culetto, E., Hajjar, C., Boyd, L., Legouis, R., and Galy, V. (2011). Postfertilization autophagy of sperm organelles prevents paternal mitochondrial DNA transmission. Science *334*, 1144-1147.

Angelova, M.I., and Dimitrov, D.S. (1986). Liposome Electroformation. Faraday Discuss *81*, 303-+.

Aoki, Y., Kanki, T., Hirota, Y., Kurihara, Y., Saigusa, T., Uchiumi, T., and Kang, D. (2011). Phosphorylation of Serine 114 on Atg32 mediates mitophagy. Mol Biol Cell *22*, 3206-3217.

Baba, M., Osumi, M., Scott, S.V., Klionsky, D.J., and Ohsumi, Y. (1997). Two distinct pathways for targeting proteins from the cytoplasm to the vacuole/lysosome. J Cell Biol *139*, 1687-1695.

Backues, S.K., and Klionsky, D.J. (2012). Atg11: a Rab-dependent, coiled-coil membrane protein that acts as a tether for autophagy. Autophagy *8*, 1275-1278.

Brocker, C., Engelbrecht-Vandre, S., and Ungermann, C. (2010). Multisubunit tethering complexes and their role in membrane fusion. Curr Biol *20*, R943-952.

Brown, P.H., Balbo, A., and Schuck, P. (2008). Characterizing protein-protein interactions by sedimentation velocity analytical ultracentrifugation. Curr Protoc Immunol *Chapter 18*, Unit 18 15.

Cao, X., Ballew, N., and Barlowe, C. (1998). Initial docking of ER-derived vesicles requires Uso1p and Ypt1p but is independent of SNARE proteins. Embo J *17*, 2156-2165.

Cebollero, E., van der Vaart, A., Zhao, M., Rieter, E., Klionsky, D.J., Helms, J.B., and Reggiori, F. (2012). Phosphatidylinositol-3-phosphate clearance plays a key role in autophagosome completion. Curr Biol *22*, 1545-1553.

Chan, T.F., Bertram, P.G., Ai, W., and Zheng, X.F. (2001). Regulation of APG14 expression by the GATA-type transcription factor Gln3p. J Biol Chem *276*, 6463-6467.

Chang, C.Y., and Huang, W.P. (2007). Atg19 mediates a dual interaction cargo sorting mechanism in selective autophagy. Mol Biol Cell *18*, 919-929.

Chen, Y.A., and Scheller, R.H. (2001). SNARE-mediated membrane fusion. Nat Rev Mol Cell Biol *2*, 98-106.

Cheong, H., Nair, U., Geng, J., and Klionsky, D.J. (2008). The Atg1 kinase complex is involved in the regulation of protein recruitment to initiate sequestering vesicle formation for nonspecific autophagy in Saccharomyces cerevisiae. Mol Biol Cell *19*, 668-681.

Cheong, H., Yorimitsu, T., Reggiori, F., Legakis, J.E., Wang, C.W., and Klionsky, D.J. (2005). Atg17 regulates the magnitude of the autophagic response. Mol Biol Cell *16*, 3438-3453.

Cuervo, A.M., and Wong, E. (2014). Chaperone-mediated autophagy: roles in disease and aging. Cell Res *24*, 92-104.

Darsow, T., Rieder, S.E., and Emr, S.D. (1997). A multispecificity syntaxin homologue, Vam3p, essential for autophagic and biosynthetic protein transport to the vacuole. J Cell Biol *138*, 517-529.

Diao, J., Liu, R., Rong, Y., Zhao, M., Zhang, J., Lai, Y., Zhou, Q., Wilz, L.M., Li, J., Vivona, S.*, et al.* (2015). ATG14 promotes membrane tethering and fusion of autophagosomes to endolysosomes. Nature *520*, 563-566.

Dove, S.K., Piper, R.C., McEwen, R.K., Yu, J.W., King, M.C., Hughes, D.C., Thuring, J., Holmes, A.B., Cooke, F.T., Michell, R.H.*, et al.* (2004). Svp1p defines a family of phosphatidylinositol 3,5-bisphosphate effectors. Embo J *23*, 1922-1933.

Farre, J.C., Burkenroad, A., Burnett, S.F., and Subramani, S. (2013). Phosphorylation of mitophagy and pexophagy receptors coordinates their interaction with Atg8 and Atg11. EMBO Rep *14*, 441-449.

Fasman, G.D. (1989). Practical Handbook of Biochemistry and Molecular Biology (Taylor & Francis).

Fujioka, Y., Suzuki, S.W., Yamamoto, H., Kondo-Kakuta, C., Kimura, Y., Hirano, H., Akada, R., Inagaki, F., Ohsumi, Y., and Noda, N.N. (2014). Structural basis of starvation-induced assembly of the autophagy initiation complex. Nat Struct Mol Biol *21*, 513-521.

Gammoh, N., Florey, O., Overholtzer, M., and Jiang, X. (2013). Interaction between FIP200 and ATG16L1 distinguishes ULK1 complex-dependent and -independent autophagy. Nat Struct Mol Biol *20*, 144-149.

Ge, L., Melville, D., Zhang, M., and Schekman, R. (2013). The ER-Golgi intermediate compartment is a key membrane source for the LC3 lipidation step of autophagosome biogenesis. Elife *2*, e00947.

Ghaemmaghami, S., Huh, W.K., Bower, K., Howson, R.W., Belle, A., Dephoure, N., O'Shea, E.K., and Weissman, J.S. (2003). Global analysis of protein expression in yeast. Nature *425*, 737-741.

He, C., Song, H., Yorimitsu, T., Monastyrska, I., Yen, W.L., Legakis, J.E., and Klionsky, D.J. (2006). Recruitment of Atg9 to the preautophagosomal structure by Atg11 is essential for selective autophagy in budding yeast. J Cell Biol *175*, 925-935.

Ho, Y., Gruhler, A., Heilbut, A., Bader, G.D., Moore, L., Adams, S.L., Millar, A., Taylor, P., Bennett, K., Boutilier, K.*, et al.* (2002). Systematic identification of protein complexes in Saccharomyces cerevisiae by mass spectrometry. Nature *415*, 180-183.

Hosokawa, N., Hara, T., Kaizuka, T., Kishi, C., Takamura, A., Miura, Y., Iemura, S., Natsume, T., Takehana, K., Yamada, N.*, et al.* (2009). Nutrient-dependent mTORC1 association with the ULK1-Atg13-FIP200 complex required for autophagy. Mol Biol Cell *20*, 1981-1991.

Huang, W.P., Scott, S.V., Kim, J., and Klionsky, D.J. (2000). The itinerary of a vesicle component, Aut7p/Cvt5p, terminates in the yeast vacuole via the autophagy/Cvt pathways. J Biol Chem *275*, 5845-5851.

References

Huh, W.K., Falvo, J.V., Gerke, L.C., Carroll, A.S., Howson, R.W., Weissman, J.S., and O'Shea, E.K. (2003). Global analysis of protein localization in budding yeast. Nature *425*, 686-691.

Hyttinen, J.M., Niittykoski, M., Salminen, A., and Kaarniranta, K. (2013). Maturation of autophagosomes and endosomes: a key role for Rab7. Biochim Biophys Acta *1833*, 503-510.

Ishihara, N., Hamasaki, M., Yokota, S., Suzuki, K., Kamada, Y., Kihara, A., Yoshimori, T., Noda, T., and Ohsumi, Y. (2001). Autophagosome requires specific early Sec proteins for its formation and NSF/SNARE for vacuolar fusion. Mol Biol Cell *12*, 3690-3702.

Itakura, E., Kishi-Itakura, C., and Mizushima, N. (2012). The hairpin-type tail-anchored SNARE syntaxin 17 targets to autophagosomes for fusion with endosomes/lysosomes. Cell *151*, 1256-1269.

Janke, C., Magiera, M.M., Rathfelder, N., Taxis, C., Reber, S., Maekawa, H., Moreno-Borchart, A., Doenges, G., Schwob, E., Schiebel, E.*, et al.* (2004). A versatile toolbox for PCR-based tagging of yeast genes: new fluorescent proteins, more markers and promoter substitution cassettes. Yeast *21*, 947-962.

Jiang, P., Nishimura, T., Sakamaki, Y., Itakura, E., Hatta, T., Natsume, T., and Mizushima, N. (2014). The HOPS complex mediates autophagosome-lysosome fusion through interaction with syntaxin 17. Mol Biol Cell *25*, 1327-1337.

Johansen, T., and Lamark, T. (2011). Selective autophagy mediated by autophagic adapter proteins. Autophagy *7*, 279-296.

Kabeya, Y., Kamada, Y., Baba, M., Takikawa, H., Sasaki, M., and Ohsumi, Y. (2005). Atg17 functions in cooperation with Atg1 and Atg13 in yeast autophagy. Mol Biol Cell *16*, 2544-2553.

Kakuta, S., Yamamoto, H., Negishi, L., Kondo-Kakuta, C., Hayashi, N., and Ohsumi, Y. (2012). Atg9 vesicles recruit vesicle-tethering proteins Trs85 and Ypt1 to the autophagosome formation site. J Biol Chem *287*, 44261-44269.

Kamada, Y., Funakoshi, T., Shintani, T., Nagano, K., Ohsumi, M., and Ohsumi, Y. (2000). Tor-mediated induction of autophagy via an Apg1 protein kinase complex. J Cell Biol *150*, 1507-1513.

Kamber, R.A., Shoemaker, C.J., and Denic, V. (2015). Receptor-Bound Targets of Selective Autophagy Use a Scaffold Protein to Activate the Atg1 Kinase. Mol Cell *59*, 372-381.

Kanki, T., Kurihara, Y., Jin, X., Goda, T., Ono, Y., Aihara, M., Hirota, Y., Saigusa, T., Aoki, Y., Uchiumi, T.*, et al.* (2013). Casein kinase 2 is essential for mitophagy. EMBO Rep *14*, 788-794.

Kanki, T., Wang, K., Cao, Y., Baba, M., and Klionsky, D.J. (2009). Atg32 is a mitochondrial protein that confers selectivity during mitophagy. Dev Cell *17*, 98-109.

Karsli-Uzunbas, G., Guo, J.Y., Price, S., Teng, X., Laddha, S.V., Khor, S., Kalaany, N.Y., Jacks, T., Chan, C.S., Rabinowitz, J.D.*, et al.* (2014). Autophagy is required for glucose homeostasis and lung tumor maintenance. Cancer Discov *4*, 914-927.

References

Kaufmann, A., Beier, V., Franquelim, H.G., and Wollert, T. (2014). Molecular mechanism of autophagic membrane-scaffold assembly and disassembly. Cell *156*, 469-481.

Kim, I., and Lemasters, J.J. (2011). Mitophagy selectively degrades individual damaged mitochondria after photoirradiation. Antioxid Redox Signal *14*, 1919-1928.

Kim, J., Kamada, Y., Stromhaug, P.E., Guan, J., Hefner-Gravink, A., Baba, M., Scott, S.V., Ohsumi, Y., Dunn, W.A., Jr., and Klionsky, D.J. (2001). Cvt9/Gsa9 functions in sequestering selective cytosolic cargo destined for the vacuole. J Cell Biol *153*, 381-396.

Kimura, S., Noda, T., and Yoshimori, T. (2008). Dynein-dependent movement of autophagosomes mediates efficient encounters with lysosomes. Cell Struct Funct *33*, 109-122.

Kirisako, T., Baba, M., Ishihara, N., Miyazawa, K., Ohsumi, M., Yoshimori, T., Noda, T., and Ohsumi, Y. (1999). Formation process of autophagosome is traced with Apg8/Aut7p in yeast. J Cell Biol *147*, 435-446.

Kirisako, T., Ichimura, Y., Okada, H., Kabeya, Y., Mizushima, N., Yoshimori, T., Ohsumi, M., Takao, T., Noda, T., and Ohsumi, Y. (2000). The reversible modification regulates the membrane-binding state of Apg8/Aut7 essential for autophagy and the cytoplasm to vacuole targeting pathway. J Cell Biol *151*, 263-276.

Kofinger, J., Ragusa, M.J., Lee, I.H., Hummer, G., and Hurley, J.H. (2015). Solution structure of the atg1 complex: implications for the architecture of the phagophore assembly site. Structure *23*, 809-818.

Komatsu, M., Waguri, S., Chiba, T., Murata, S., Iwata, J., Tanida, I., Ueno, T., Koike, M., Uchiyama, Y., Kominami, E.*, et al.* (2006). Loss of autophagy in the central nervous system causes neurodegeneration in mice. Nature *441*, 880-884.

Kondo-Okamoto, N., Noda, N.N., Suzuki, S.W., Nakatogawa, H., Takahashi, I., Matsunami, M., Hashimoto, A., Inagaki, F., Ohsumi, Y., and Okamoto, K. (2012). Autophagy-related protein 32 acts as autophagic degron and directly initiates mitophagy. J Biol Chem *287*, 10631-10638.

Kraft, C., Deplazes, A., Sohrmann, M., and Peter, M. (2008). Mature ribosomes are selectively degraded upon starvation by an autophagy pathway requiring the Ubp3p/Bre5p ubiquitin protease. Nat Cell Biol *10*, 602-610.

Kramer, L., and Ungermann, C. (2011). HOPS drives vacuole fusion by binding the vacuolar SNARE complex and the Vam7 PX domain via two distinct sites. Mol Biol Cell *22*, 2601-2611.

Lee, J.H., Yu, W.H., Kumar, A., Lee, S., Mohan, P.S., Peterhoff, C.M., Wolfe, D.M., Martinez-Vicente, M., Massey, A.C., Sovak, G.*, et al.* (2010). Lysosomal proteolysis and autophagy require presenilin 1 and are disrupted by Alzheimer-related PS1 mutations. Cell *141*, 1146-1158.

Lemasters, J.J. (2005). Selective mitochondrial autophagy, or mitophagy, as a targeted defense against oxidative stress, mitochondrial dysfunction, and aging. Rejuvenation Res *8*, 3-5.

References

Li, F., Chung, T., and Vierstra, R.D. (2014). AUTOPHAGY-RELATED11 plays a critical role in general autophagy- and senescence-induced mitophagy in Arabidopsis. Plant Cell *26*, 788-807.

Li, W.W., Li, J., and Bao, J.K. (2012). Microautophagy: lesser-known self-eating. Cell Mol Life Sci *69*, 1125-1136.

Lipatova, Z., Belogortseva, N., Zhang, X.Q., Kim, J., Taussig, D., and Segev, N. (2012). Regulation of selective autophagy onset by a Ypt/Rab GTPase module. Proc Natl Acad Sci U S A *109*, 6981-6986.

Liu, L., Feng, D., Chen, G., Chen, M., Zheng, Q., Song, P., Ma, Q., Zhu, C., Wang, R., Qi, W.*, et al.* (2012). Mitochondrial outer-membrane protein FUNDC1 mediates hypoxia-induced mitophagy in mammalian cells. Nat Cell Biol *14*, 177-185.

Liu, X., Mao, K., Yu, A.Y., Omairi-Nasser, A., Austin, J., 2nd, Glick, B.S., Yip, C.K., and Klionsky, D.J. (2016). The Atg17-Atg31-Atg29 Complex Coordinates with Atg11 to Recruit the Vam7 SNARE and Mediate Autophagosome-Vacuole Fusion. Curr Biol *26*, 150-160.

Loewith, R., and Hall, M.N. (2011). Target of rapamycin (TOR) in nutrient signaling and growth control. Genetics *189*, 1177-1201.

Lu, K., Psakhye, I., and Jentsch, S. (2014). Autophagic clearance of polyQ proteins mediated by ubiquitin-Atg8 adaptors of the conserved CUET protein family. Cell *158*, 549-563.

Lu, Y., Zhang, Z., Sun, D., Sweeney, S.T., and Gao, F.B. (2013). Syntaxin 13, a genetic modifier of mutant CHMP2B in frontotemporal dementia, is required for autophagosome maturation. Mol Cell *52*, 264-271.

Lynch-Day, M.A., Bhandari, D., Menon, S., Huang, J., Cai, H., Bartholomew, C.R., Brumell, J.H., Ferro-Novick, S., and Klionsky, D.J. (2010). Trs85 directs a Ypt1 GEF, TRAPPIII, to the phagophore to promote autophagy. Proc Natl Acad Sci U S A *107*, 7811-7816.

Maday, S., Wallace, K.E., and Holzbaur, E.L. (2012). Autophagosomes initiate distally and mature during transport toward the cell soma in primary neurons. J Cell Biol *196*, 407-417.

Mao, K., Chew, L.H., Inoue-Aono, Y., Cheong, H., Nair, U., Popelka, H., Yip, C.K., and Klionsky, D.J. (2013a). Atg29 phosphorylation regulates coordination of the Atg17-Atg31-Atg29 complex with the Atg11 scaffold during autophagy initiation. Proc Natl Acad Sci U S A *110*, E2875-2884.

Mao, K., Wang, K., Liu, X., and Klionsky, D.J. (2013b). The scaffold protein Atg11 recruits fission machinery to drive selective mitochondria degradation by autophagy. Dev Cell *26*, 9-18.

Mao, K., Wang, K., Zhao, M., Xu, T., and Klionsky, D.J. (2011). Two MAPK-signaling pathways are required for mitophagy in Saccharomyces cerevisiae. J Cell Biol *193*, 755-767.

Mari, M., Griffith, J., Rieter, E., Krishnappa, L., Klionsky, D.J., and Reggiori, F. (2010). An Atg9-containing compartment that functions in the early steps of autophagosome biogenesis. J Cell Biol *190*, 1005-1022.

Mathew, R., and White, E. (2011). Autophagy in tumorigenesis and energy metabolism: friend by day, foe by night. Curr Opin Genet Dev *21*, 113-119.

References
___

Mendl, N., Occhipinti, A., Muller, M., Wild, P., Dikic, I., and Reichert, A.S. (2011). Mitophagy in yeast is independent of mitochondrial fission and requires the stress response gene WHI2. J Cell Sci *124*, 1339-1350.

Mizushima, N. (2010). The role of the Atg1/ULK1 complex in autophagy regulation. Curr Opin Cell Biol *22*, 132-139.

Mochida, K., Ohsumi, Y., and Nakatogawa, H. (2014). Hrr25 phosphorylates the autophagic receptor Atg34 to promote vacuolar transport of alpha-mannosidase under nitrogen starvation conditions. FEBS Lett *588*, 3862-3869.

Mochida, K., Oikawa, Y., Kimura, Y., Kirisako, H., Hirano, H., Ohsumi, Y., and Nakatogawa, H. (2015). Receptor-mediated selective autophagy degrades the endoplasmic reticulum and the nucleus. Nature.

Monastyrska, I., He, C., Geng, J., Hoppe, A.D., Li, Z., and Klionsky, D.J. (2008). Arp2 links autophagic machinery with the actin cytoskeleton. Mol Biol Cell *19*, 1962-1975.

Monastyrska, I., Rieter, E., Klionsky, D.J., and Reggiori, F. (2009). Multiple roles of the cytoskeleton in autophagy. Biol Rev Camb Philos Soc *84*, 431-448.

Monastyrska, I., Shintani, T., Klionsky, D.J., and Reggiori, F. (2006). Atg11 directs autophagosome cargoes to the PAS along actin cables. Autophagy *2*, 119-121.

Morselli, E., Shen, S., Ruckenstuhl, C., Bauer, M.A., Marino, G., Galluzzi, L., Criollo, A., Michaud, M., Maiuri, M.C., Chano, T.*, et al.* (2011). p53 inhibits autophagy by interacting with the human ortholog of yeast Atg17, RB1CC1/FIP200. Cell Cycle *10*, 2763-2769.

Murakawa, T., Yamaguchi, O., Hashimoto, A., Hikoso, S., Takeda, T., Oka, T., Yasui, H., Ueda, H., Akazawa, Y., Nakayama, H.*, et al.* (2015). Bcl-2-like protein 13 is a mammalian Atg32 homologue that mediates mitophagy and mitochondrial fragmentation. Nat Commun *6*, 7527.

Nair, U., Jotwani, A., Geng, J., Gammoh, N., Richerson, D., Yen, W.L., Griffith, J., Nag, S., Wang, K., Moss, T.*, et al.* (2011). SNARE proteins are required for macroautophagy. Cell *146*, 290-302.

Nakatogawa, H., Ichimura, Y., and Ohsumi, Y. (2007). Atg8, a ubiquitin-like protein required for autophagosome formation, mediates membrane tethering and hemifusion. Cell *130*, 165-178.

Nakatogawa, H., Ohbayashi, S., Sakoh-Nakatogawa, M., Kakuta, S., Suzuki, S.W., Kirisako, H., Kondo-Kakuta, C., Noda, N.N., Yamamoto, H., and Ohsumi, Y. (2012). The autophagy-related protein kinase Atg1 interacts with the ubiquitin-like protein Atg8 via the Atg8 family interacting motif to facilitate autophagosome formation. J Biol Chem *287*, 28503-28507.

Nakatogawa, H., Suzuki, K., Kamada, Y., and Ohsumi, Y. (2009). Dynamics and diversity in autophagy mechanisms: lessons from yeast. Nat Rev Mol Cell Biol *10*, 458-467.

Nice, D.C., Sato, T.K., Stromhaug, P.E., Emr, S.D., and Klionsky, D.J. (2002). Cooperative binding of the cytoplasm to vacuole targeting pathway proteins, Cvt13 and Cvt20, to phosphatidylinositol 3-phosphate at the pre-autophagosomal structure is required for selective autophagy. J Biol Chem *277*, 30198-30207.

References

Noda, N.N., Ohsumi, Y., and Inagaki, F. (2010). Atg8-family interacting motif crucial for selective autophagy. FEBS Lett *584*, 1379-1385.

Noda, N.N., Satoo, K., Fujioka, Y., Kumeta, H., Ogura, K., Nakatogawa, H., Ohsumi, Y., and Inagaki, F. (2011). Structural basis of Atg8 activation by a homodimeric E1, Atg7. Mol Cell *44*, 462-475.

Noda, T., Fujita, N., and Yoshimori, T. (2009). The late stages of autophagy: how does the end begin? Cell Death Differ *16*, 984-990.

Noda, T., Kim, J., Huang, W.P., Baba, M., Tokunaga, C., Ohsumi, Y., and Klionsky, D.J. (2000). Apg9p/Cvt7p is an integral membrane protein required for transport vesicle formation in the Cvt and autophagy pathways. J Cell Biol *148*, 465-480.

Novak, I., Kirkin, V., McEwan, D.G., Zhang, J., Wild, P., Rozenknop, A., Rogov, V., Lohr, F., Popovic, D., Occhipinti, A*., et al.* (2010). Nix is a selective autophagy receptor for mitochondrial clearance. EMBO Rep *11*, 45-51.

Obara, K., Sekito, T., and Ohsumi, Y. (2006). Assortment of phosphatidylinositol 3-kinase complexes--Atg14p directs association of complex I to the pre-autophagosomal structure in Saccharomyces cerevisiae. Mol Biol Cell *17*, 1527-1539.

Ochaba, J., Lukacsovich, T., Csikos, G., Zheng, S., Margulis, J., Salazar, L., Mao, K., Lau, A.L., Yeung, S.Y., Humbert, S*., et al.* (2014). Potential function for the Huntingtin protein as a scaffold for selective autophagy. Proc Natl Acad Sci U S A *111*, 16889-16894.

Okamoto, K., Kondo-Okamoto, N., and Ohsumi, Y. (2009). Mitochondria-Anchored Receptor Atg32 Mediates Degradation of Mitochondria via Selective Autophagy. Dev Cell *17*, 87-97.

Okatsu, K., Saisho, K., Shimanuki, M., Nakada, K., Shitara, H., Sou, Y.S., Kimura, M., Sato, S., Hattori, N., Komatsu, M*., et al.* (2010). p62/SQSTM1 cooperates with Parkin for perinuclear clustering of depolarized mitochondria. Genes Cells *15*, 887-900.

Papinski, D., Schuschnig, M., Reiter, W., Wilhelm, L., Barnes, C.A., Maiolica, A., Hansmann, I., Pfaffenwimmer, T., Kijanska, M., Stoffel, I*., et al.* (2014). Early steps in autophagy depend on direct phosphorylation of Atg9 by the Atg1 kinase. Mol Cell *53*, 471-483.

Perna, M.G. (2014). In vitro reconstitution of the Atg1-kinase complex: Revealing the molecular mechanism of autophagy initiation. In PhD thesis (Munich, Technische Universität München).

Pfaffenwimmer, T., Reiter, W., Brach, T., Nogellova, V., Papinski, D., Schuschnig, M., Abert, C., Ammerer, G., Martens, S., and Kraft, C. (2014). Hrr25 kinase promotes selective autophagy by phosphorylating the cargo receptor Atg19. EMBO Rep *15*, 862-870.

Polson, H.E., de Lartigue, J., Rigden, D.J., Reedijk, M., Urbe, S., Clague, M.J., and Tooze, S.A. (2010). Mammalian Atg18 (WIPI2) localizes to omegasome-anchored phagophores and positively regulates LC3 lipidation. Autophagy *6*, 506-522.

Ragusa, M.J., Stanley, R.E., and Hurley, J.H. (2012). Architecture of the Atg17 complex as a scaffold for autophagosome biogenesis. Cell *151*, 1501-1512.

Rao, Y., Perna, M.G., Hofmann, B., Beier, V., and Wollert, T. (2016). The Atg1-kinase complex tethers Atg9-vesicles to initiate autophagy. Nat Commun *7*, 10338.

References

Rea, S.L., Majcher, V., Searle, M.S., and Layfield, R. (2014). SQSTM1 mutations--bridging Paget disease of bone and ALS/FTLD. Exp Cell Res *325*, 27-37.

Reggiori, F., Komatsu, M., Finley, K., and Simonsen, A. (2012). Autophagy: more than a nonselective pathway. Int J Cell Biol *2012*, 219625.

Reggiori, F., Monastyrska, I., Shintani, T., and Klionsky, D.J. (2005). The actin cytoskeleton is required for selective types of autophagy, but not nonspecific autophagy, in the yeast Saccharomyces cerevisiae. Mol Biol Cell *16*, 5843-5856.

Reggiori, F., Tucker, K.A., Stromhaug, P.E., and Klionsky, D.J. (2004). The Atg1-Atg13 complex regulates Atg9 and Atg23 retrieval transport from the pre-autophagosomal structure. Dev Cell *6*, 79-90.

Rieder, S.E., and Emr, S.D. (1997). A novel RING finger protein complex essential for a late step in protein transport to the yeast vacuole. Mol Biol Cell *8*, 2307-2327.

Sawa-Makarska, J., Abert, C., Romanov, J., Zens, B., Ibiricu, I., and Martens, S. (2014). Cargo binding to Atg19 unmasks additional Atg8 binding sites to mediate membrane-cargo apposition during selective autophagy. Nat Cell Biol *16*, 425-433.

Schneider, J.L., and Cuervo, A.M. (2014). Autophagy and human disease: emerging themes. Curr Opin Genet Dev *26*, 16-23.

Scholz, J., Besir, H., Strasser, C., and Suppmann, S. (2013). A new method to customize protein expression vectors for fast, efficient and background free parallel cloning. BMC Biotechnol *13*, 12.

Schweers, R.L., Zhang, J., Randall, M.S., Loyd, M.R., Li, W., Dorsey, F.C., Kundu, M., Opferman, J.T., Cleveland, J.L., Miller, J.L.*, et al.* (2007). NIX is required for programmed mitochondrial clearance during reticulocyte maturation. Proc Natl Acad Sci U S A *104*, 19500-19505.

Sekito, T., Kawamata, T., Ichikawa, R., Suzuki, K., and Ohsumi, Y. (2009). Atg17 recruits Atg9 to organize the pre-autophagosomal structure. Genes Cells *14*, 525-538.

Shintani, T., Huang, W.P., Stromhaug, P.E., and Klionsky, D.J. (2002). Mechanism of cargo selection in the cytoplasm to vacuole targeting pathway. Dev Cell *3*, 825-837.

Shpilka, T., Weidberg, H., Pietrokovski, S., and Elazar, Z. (2011). Atg8: an autophagy-related ubiquitin-like protein family. Genome Biol *12*, 226.

Simonsen, A., Cumming, R.C., Brech, A., Isakson, P., Schubert, D.R., and Finley, K.D. (2008). Promoting basal levels of autophagy in the nervous system enhances longevity and oxidant resistance in adult Drosophila. Autophagy *4*, 176-184.

Sou, Y.S., Waguri, S., Iwata, J., Ueno, T., Fujimura, T., Hara, T., Sawada, N., Yamada, A., Mizushima, N., Uchiyama, Y.*, et al.* (2008). The Atg8 conjugation system is indispensable for proper development of autophagic isolation membranes in mice. Mol Biol Cell *19*, 4762-4775.

Stanley, R.E., Ragusa, M.J., and Hurley, J.H. (2014). The beginning of the end: how scaffolds nucleate autophagosome biogenesis. Trends Cell Biol *24*, 73-81.

References

Stenmark, H. (2009). Rab GTPases as coordinators of vesicle traffic. Nat Rev Mol Cell Biol *10*, 513-525.

Stephan, J.S., Yeh, Y.Y., Ramachandran, V., Deminoff, S.J., and Herman, P.K. (2009). The Tor and PKA signaling pathways independently target the Atg1/Atg13 protein kinase complex to control autophagy. Proc Natl Acad Sci U S A *106*, 17049-17054.

Stromhaug, P.E., Reggiori, F., Guan, J., Wang, C.W., and Klionsky, D.J. (2004). Atg21 is a phosphoinositide binding protein required for efficient lipidation and localization of Atg8 during uptake of aminopeptidase I by selective autophagy. Mol Biol Cell *15*, 3553-3566.

Suzuki, K., Akioka, M., Kondo-Kakuta, C., Yamamoto, H., and Ohsumi, Y. (2013). Fine mapping of autophagy-related proteins during autophagosome formation in Saccharomyces cerevisiae. J Cell Sci *126*, 2534-2544.

Suzuki, K., Kirisako, T., Kamada, Y., Mizushima, N., Noda, T., and Ohsumi, Y. (2001). The pre-autophagosomal structure organized by concerted functions of APG genes is essential for autophagosome formation. Embo J *20*, 5971-5981.

Suzuki, K., Kondo, C., Morimoto, M., and Ohsumi, Y. (2010). Selective transport of alpha-mannosidase by autophagic pathways: identification of a novel receptor, Atg34p. J Biol Chem *285*, 30019-30025.

Suzuki, K., Kubota, Y., Sekito, T., and Ohsumi, Y. (2007). Hierarchy of Atg proteins in pre-autophagosomal structure organization. Genes Cells *12*, 209-218.

Takamura, A., Komatsu, M., Hara, T., Sakamoto, A., Kishi, C., Waguri, S., Eishi, Y., Hino, O., Tanaka, K., and Mizushima, N. (2011). Autophagy-deficient mice develop multiple liver tumors. Genes Dev *25*, 795-800.

Tan, D., Cai, Y., Wang, J., Zhang, J., Menon, S., Chou, H.T., Ferro-Novick, S., Reinisch, K.M., and Walz, T. (2013). The EM structure of the TRAPPIII complex leads to the identification of a requirement for COPII vesicles on the macroautophagy pathway. Proc Natl Acad Sci U S A *110*, 19432-19437.

Tanaka, C., Tan, L.J., Mochida, K., Kirisako, H., Koizumi, M., Asai, E., Sakoh-Nakatogawa, M., Ohsumi, Y., and Nakatogawa, H. (2014). Hrr25 triggers selective autophagy-related pathways by phosphorylating receptor proteins. J Cell Biol *207*, 91-105.

Ulgherait, M., Rana, A., Rera, M., Graniel, J., and Walker, D.W. (2014). AMPK modulates tissue and organismal aging in a non-cell-autonomous manner. Cell Rep *8*, 1767-1780.

Umekawa, M., and Klionsky, D.J. (2012). The Cytoplasm-to-Vacuole Targeting Pathway: A Historical Perspective. Int J Cell Biol *2012*, 142634.

Wang, C.W., Stromhaug, P.E., Shima, J., and Klionsky, D.J. (2002). The Ccz1-Mon1 protein complex is required for the late step of multiple vacuole delivery pathways. J Biol Chem *277*, 47917-47927.

Wang, J., Menon, S., Yamasaki, A., Chou, H.T., Walz, T., Jiang, Y., and Ferro-Novick, S. (2013). Ypt1 recruits the Atg1 kinase to the preautophagosomal structure. Proc Natl Acad Sci U S A *110*, 9800-9805.

Wei, H., Liu, L., and Chen, Q. (2015). Selective removal of mitochondria via mitophagy: distinct pathways for different mitochondrial stresses. Biochim Biophys Acta.

Wei, H., Wei, S., Gan, B., Peng, X., Zou, W., and Guan, J.L. (2011). Suppression of autophagy by FIP200 deletion inhibits mammary tumorigenesis. Genes Dev *25*, 1510-1527.

Winslow, A.R., and Rubinsztein, D.C. (2008). Autophagy in neurodegeneration and development. Biochim Biophys Acta *1782*, 723-729.

Xie, Z., Nair, U., and Klionsky, D.J. (2008). Atg8 controls phagophore expansion during autophagosome formation. Mol Biol Cell *19*, 3290-3298.

Yamaguchi, M., Noda, N.N., Nakatogawa, H., Kumeta, H., Ohsumi, Y., and Inagaki, F. (2010). Autophagy-related protein 8 (Atg8) family interacting motif in Atg3 mediates the Atg3-Atg8 interaction and is crucial for the cytoplasm-to-vacuole targeting pathway. J Biol Chem *285*, 29599-29607.

Yamamoto, H., Kakuta, S., Watanabe, T.M., Kitamura, A., Sekito, T., Kondo-Kakuta, C., Ichikawa, R., Kinjo, M., and Ohsumi, Y. (2012). Atg9 vesicles are an important membrane source during early steps of autophagosome formation. J Cell Biol *198*, 219-233.

Yorimitsu, T., and Klionsky, D.J. (2005). Atg11 links cargo to the vesicle-forming machinery in the cytoplasm to vacuole targeting pathway. Mol Biol Cell *16*, 1593-1605.

Youle, R.J., and Narendra, D.P. (2011). Mechanisms of mitophagy. Nat Rev Mol Cell Biol *12*, 9-14.

Yuga, M., Gomi, K., Klionsky, D.J., and Shintani, T. (2011). Aspartyl aminopeptidase is imported from the cytoplasm to the vacuole by selective autophagy in Saccharomyces cerevisiae. J Biol Chem *286*, 13704-13713.

6 Appendices

6.1 Abbreviations

AIM	Atg8-Interacting Motif
Ala, A	Alanine
ApeI	AminopeptidaseI
Asp, D	Aspartic acid
Atg	AuTophaGy-related
AUC	Analytical UltraCentrifugation
CD	Circular Dichroism
Cvt	Cytoplasm-to-vacuole targeting
cyt	cytoplasmic
D, Da	Dalton
DLS	Dynamic Light Scattering
DMSO	DiMethyl SulfOxide
DOL	Degree Of Labeling
DPPE	1,2-DiPalmitoyl-sn-glycero-3-PE
DTT	DiThioThreitol
FRAP	Fluorescence Recovery After Photobleaching
GAC	Giant ApeI Complex
GFP	Green Fluorescent Protein
Glu, E	Glutamic acid
Gly, G	Glycine
GUV	Giant Unilamellar Vesicle
His, H	Histidine
HT	High Tension
IMAC	Immobilized Metal ion Affinity Chromatography
IR	Ionizing Radiation
ITO	Indium Tin Oxide
LB	Lysogeny Broth
Leu	Leucine
LUV	Large Unilamellar Vesicle
M	Molar
MBP	Maltose-Binding Protein
min	Minutes
mt	mitochondrial
M_w	Molecular Weight
NHS	N-HydroxySuccinimide
Ni^{2+}-NTA	Nickel-NitriloTriAcetic acid
OD	Optical Density
Om45	45-kDa protein of the yeast mitochondrial Outer
PAS	Phagophore Assembly Site
PE	PhosphatidylEthanolamine
Pgk1	Phosphoglycerate kinase 1
Pho8	alkaline Phosphatase
PL	ProteoLiposome

POPE	1-Palmitoyl-2-Oleoyl-*sn*-glycero-3-PE
PVDF	Polyvinylidenfluorid
R_H	Hydrodynamic Radius
rpm	revolutions per minute
RT	room temperature
S	Svedberg
SEC	Size Exclusion Chromatography
Ser, S	Serine
SPR	Surface Plasmon Resonance
TB	Terrific Broth
RU	Resonance Units
TCEP	Tris(2-carboxyethyl) phosphine
Trp, W	Tryptophane
Ura	Uracil
β-ME	β-MercaptoEthanol
wt, WT	wild type

6.2   Index of Figures

6.3   Index of Tables

6.4 Acknowledgments

6.5 Curriculum Vitae

Nena Magdalena Matscheko

Nationality   Austrian

Date of birth   October 6, 1985

ACADEMIC EDUCATION

08/2011 – present	**PhD studies** at Ludwig Maximilians University, Munich, Germany
	Supervisor: Dr. T. Wollert, **Max Planck Institute of Biochemistry**
	(MPIB), Martinsried, Germany
01/2008 – 07/2008	International study program ERASMUS
	Universidad de Navarra, Pamplona, Spain
10/2004 – 09/2010	**Diploma studies: Molecular Biology**
	Focus on biochemistry, immunology and molecular medicine
	University of Vienna, Vienna, Austria
	Thesis title: *RNA transfer of Human Rhinovirus through Model Membranes*
06/2004	High school diploma (Matura): Gymnasium Rohrbach i.M., Austria

GRANTS / FELLOWSHIPS / PRIZES

03/2015	"**Best Poster prize**" selected by the keynote speakers of the Conference "**Interact 2015**", Munich, Germany
04/2012 – 08/2014	**PhD fellowship**, provided by Boehringer Ingelheim Fonds, Mainz, Germany
08/2011 – present	**International Max Planck Research School** for Molecular and Cellular Life Sciences (IMPRS-LS), Martinsried/Munich, Germany
01 – 06/2008	LLP/ERASMUS student **mobility grant**, financed by the European Union and Austrian BMWF/ BMUKK

PUBLICATIONS

Yijian Rao, **Nena Matscheko**, Thomas Wollert (2016). *Autophagy in the test tube: In vitro reconstitution of aspects of autophagosome biogenesis.* doi: 10.1111/febs.13661

Gerhard Bilek*, **Nena M. Matscheko*** et al. (2011). *Liposomal Nanocontainers as Models for Viral Infection: Monitoring Viral Genomic RNA Transfer through Lipid Membranes.*
doi: 10.1128/JVI.00329-11

*shared first-authors